Norges miljø- og
biovitenskapelige
universitet

Master's Thesis 2022 30 ECTS
Faculty of Chemistry, Biotechnology and Food Science

Pharmacological Tools to Study Transcriptional Addictions in Cancer

Hristo K. Iliev
Chemistry and Biotechnology, MSc

Acknowledgments

This project marks the end of my master's degree within Biotechnology and Applied Chemistry at the Faculty of Chemistry, Biotechnology and Food Science at the Norwegian University of Life Sciences. The practical aspect of the project was conducted with the collaboration of University Hospital of Oslo, Rikshospitalet, Department of Microbiology. The laboratory sessions began in January 2022 and ended in May, the same year.

During this period, I have been introduced to several cutting-edge methodologies, which have contributed to the overall development of my knowledge within the field of Biotechnology and Chemistry, with special focus on molecular- and cancer biology. The experience gained through this research project has definitely broaden my perspectives as future scientist. It was a pleasure for me to work in such a competent environment full of friendly minded professionals willing to share their knowledge.

I would like to thank my external supervisor Dr. Deo Prakash Pandey for his friendly attitude and for making me feel part of his research group. Thank you for the constant support during the investigation period and for answering my inquiries regarding the research.

I would also like to thank the Department of Microbiology and the Flow Cytometry group at Radium Hospitalet, especially to Silje Lier, Preeti Jain, Solveig Lund, Anja Kocijancic, Wygeya Balarajah, Idun Dale and Monica Bostad for the good laboratory advice and for the shown encouragement.

A big thanks to my internal supervisor Professor Harald Carlsen for good guidance through the investigation period and for reviewing the final written work.

Last, but certainly not least, I would like to thank my family, friends and fellow research students for the moral support and comfort and for cheering me up during this period.

Thank you all.

Norwegian University of Life Sciences

Faculty of Chemistry, Biotechnology and Food Science

Oslo, 14 June 2022

Hristo K. Iliev

Table of Contents

List of abbreviations

Abbreviations

ADP	Adenosine diphosphate
APC/C	Anaphase-promoting complex/cyclosome
ATM	Ataxia telangiectasia-mutated
ATP	Adenosine triphosphate
ATR	ATM-Rad3
Cdc6	Cell division cycle 6
CDK	Cyclin Dependent Kinase
CDKI	CDK inhibitor
ChK1	Checkpoint kinase 1
CKI	CDK inhibitors
CMG	Cdc45-MCM-GINS
CPSF	Cleavage and polyadenylation specificity factor
CSFF	Cleavage stimulation factor F
CTD	C-terminal domain
Cyc	Cyclin
DDK	Dbf4-Dependent Cdc7 Kinase
DMSO	Dimethyl sulfoxide
DNA	Deoxyribonucleic acid
DPE	Downstream promoter elements
DRB	5,6-Dichloro-1-β-D-RibofuranosylBenzimidazole
DSIF	DRB-sensitivity inducing factor

FACS	Fluorescence activated cell sorting
G0	Gap 0 phase
G1	Gap 1 phase
G2	Gap 2 phase|
GBM	Glioblastoma multifore
Gbp	Giga base pair
G-cells	Glioma cells
HeLa	Henrietta Lacks
IR	Infrared
M	Mitosis phase
MC	Mediator complex
MCM	Mini-chromosome maintenance
MiT	Microphthalmia
MPF	Mitosis promoting factor
mRNA	Messenger RNA
NE	Nuclear envelope
NELF	Negative elongation factor
NPC	Nuclear pore complex
ORC	Origin recognition complex
PAF1	Polymerase II-Associated Factor 1
PAS	Poly A-site
PBS	Phosphate buffered saline
PDL	Poly-D-lysine
PIC	Pre-initiation complex
Pol α	Polymerase alpha

Pre-LC	Pre-loading complex
Pre-RC	Pre-replication complex
PROTAC	Proteolysis targeting chimeras
Rb	Retinoblastoma
RNA	Ribonucleic acid
rRNA	Ribosomal RNA
S	DNA synthesis phase
S-CDK	S phase CDK
Ser	Serine
TAF	TBP-associated factor
TBP	TATA-box binding protein
TEF	Transcriptional elongation factor
TF	Transcription factor
TI	Trypsin inhibitor
Top II	Topoisomerase II
tRNA	Transfer RNA
TrypLe	Trypsin-like enzyme
TSS	Transcription start site
UV	Ultraviolet

Units of measurement

°C	Degrees celsius
%	Percentage
mg	Milligram
µg	Microgram
µL	Microlitre
µL/min	Microlitre per minute
µg/ml	Microgram per millilitre
M	Molar
mM	Millimolar
µM	Micromolar
nM	Nanomolar
ml	Millilitre
rcf	Relative centrifugal force
rpm	Revolution per minute
h	Hour
min	Minute
ms	millisecond
l	Liquid
cm	Centimeters
nm	Nanometers
V	Voltage

Abstract

Unfortunately, genetic diseases such as cancer are becoming more common among the global population, and only in 2020 approximately 19 million new cases were discovered, and 10 million lives were lost. With median overall survival of just over one year after diagnosis and with 1.6 % of all fatalities in 2020, brain and nervous system cancer represent one of the deadliest forms of this diseases. Moreover, 80 % of the malignancies occurring in the central nervous system are caused by gliomas, a type of tumour that originates from glial cells. Glioblastoma Multiforme (GBM) accounts for the most advanced and severe form of this cancer, with less than 5-10 % of people surviving longer than five years after diagnosis.

Foregoing studies indicate that genomic alternations leading to constitutive activation of CDK´s are a common factor for many cancer forms, including gliomas. For instance, brain cancer malignancies proliferate through the recruitment of several CDK´s early in G1 phase, and genomic instability in gliomas appears to be related to disturbances in S phase and in the transition between G2 and M phase. For this reason, numerous synthetically created CDK Inhibitors (CKI´s) have been studied in relation to cancer, with some of them making their way to the clinics. However, pre-clinical and clinical trials have generated mixed results over the past decades, giving a non-definite conclusion regarding the effectiveness of these therapeutics, especially on brain cancer.

In order to further elucidate the underlaying mechanisms that stimulate the aggressiveness of GBM in higher eukaryotes, different type of pharmacological tools targeting both transcriptional and cell cycle related CDK´s as well as drugs targeting ATR protein, human topoisomerase I and II and NF-κB activator were tested on two patient derived glioma cell lines (G7 and G144) and one control cell line (HeLa). Molecular techniques including cell viability assays and colony formation assays together with Fluorescence Activated Cell Sorting (FACS) were applied for this purpose.

The results depict that inhibition of cell cycle related CDK 1 and 2 by AUZ454, CR-8, NVP-2 and RO-3306 as well as inhibition of ATR protein, human topoisomerase I and II and NF-κB activator, did similarly affect proliferation of both HeLa and G-cells, with no statistically significant differences in neither colony formation nor cell viability assays. Likewise, targeting the transcriptional CDK´s 7 and 9 with LDC4297 and PROTAC CDK 9 Degrader-1, respectively, did not show any statistical difference. However, FACS analysis on G144 with the latter mentioned compounds resulted in cell cycle arrest at G2/M and G1 phase, respectively, enlightening the role of transcriptional CDK´s on the cell cycle. Similarly, results originating from the colony formation assay after inhibition of the transcriptional CDK´s 12 and 13 by THZ531 and SR-4835 did show a clear visual difference on the proliferation between the control cell line and G-cells. In addition, FACS analysis on G144 with SR-4835 did result in cell cycle arrest at M/G1 phase, once again elucidating the effect of transcriptional inhibitors on the cell cycle. Degradation of CDK 12 by BSJ-4-116 gave no statistically significant results.

Sammendrag

Genetiske sykdommer som kreft blir stadig mer vanlige blant den globale befolkningen, og bare i 2020 ble omtrent 19 millioner nye tilfeller oppdaget, og 10 millioner liv gikk tapt. Med median total overlevelse på litt over ett år etter diagnose og med 1,6 % av alle dødsfall i 2020, representerer hjernekreft en av de dødeligste formene for denne sykdommen. Dessuten, 80 % av malignitetene som oppstår i sentralnervesystemet forårsaket av gliomer, en type svulst som stammer fra gliaceller. Glioblastom (GBM) står for den mest avanserte og alvorlige formen av denne kreftformen, med mindre enn 5-10 % av menneskene som overlever lenger enn fem år etter diagnosen.

Foregående studier indikerer at genomiske endringer som fører til konstitutiv aktivering av CDK-er er en vanlig faktor for mange kreftformer, inkludert gliomer. Maligniteter i hjernekreft proliferer gjennom rekruttering av flere CDK-er tidlig i G1-fasen, og genomisk ustabilitet i gliomer ser ut til å være relatert til forstyrrelser i S-fasen og i overgangen mellom G2- og M-fasen. Av denne grunn har en rekke syntetiske CDK-hemmere (CDKI-er) blitt studert i sammenheng med kreftutvikling, med noen av dem som har allerede blitt implementert i behandlingsprogrammer verden rundt. Derimot, prekliniske og kliniske studier har generert blandede resultater de siste tiårene, noe som gir en ikke-klar konklusjon angående effektiviteten av disse medikamentene, spesielt ved behandling av hjernekreft.

For å ytterligere belyse de underliggende mekanismene som stimulerer aggressiviteten til GBM i høyere eukaryoter, forskjellige typer farmakologiske verktøy rettet mot både transkripsjonelle og cellesyklusrelaterte CDK-er samt inhibitorer rettet mot ATR-protein, human topoisomerase I og II og NF-κB aktivator ble testet på to pasientavledede gliomcellelinjer (G7 og G144) og en kontrollcellelinje (HeLa). Molekylære teknikker inkludert cellelevedyktighetsanalyser og kolonidannelsesanalyser sammen med fluorescensaktivert cellesortering (FACS) ble brukt for dette formålet.

Resultatene viser at inhibering av cellesyklusrelatert CDK 1 og 2 av AUZ454, CR-8, NVP-2 og RO-3306 samt hemming av ATR-protein, human topoisomerase I og II og NF-KB-aktivator, påvirket proliferasjonen av både HeLa- og G-celler på samme vis, uten statistisk signifikante forskjeller i verken kolonidannelse eller cellelevedyktighetsanalyser. Likeledes, inhibering av transkripsjonelle CDK-er 7 og 9 med henholdsvis LDC4297 og PROTAC CDK 9 Degrader-1, viste heller ingen statistisk forskjell. Derimot, FACS-analyse på G144 med de sistnevnte forbindelsene resulterte i cellesyklusstans ved henholdsvis G2/M og G1-fasen, noe som opplyser rollen til transkripsjonelle CDK-er på cellesyklusen. Likeledes, resultater fra kolonidannelsesanalysen etter inhibering av de transkripsjonelle CDK-ene 12 og 13 ved hjelp av THZ531 og SR-4835 viste en klar visuell forskjell på proliferasjonen mellom kontrollcellelinjen og G-celler. I tillegg resulterte FACS-analyse på G144 med SR-4835 i cellesyklusstans ved M/G1-fase, noe som igjen belyste effekten av transkripsjonshemmere på cellesyklusen. Nedbrytning av CDK 12 ved hjelp av BSJ-4-116 ga ingen statistisk signifikante resultater.

1. Introduction

Since the sequencing of cancer genomes over the last one and half decade, it has become quite clear that cancer cells harbour mutations which alter their epigenetic state and transcriptional program. As a result, there has been a great push to develop novel therapeutic strategies against epigenetic and transcriptional mechanisms. A study performed by Mohammad et. al. [1] has shown that the enzymatic activity of the Polycomb repressor group can be targeted to inhibit glioma growth in paediatric patients. The idea of targeting transcriptional Cyclin-Dependent Kinases (CDK´s) to treat cancer is not new, but the progress in the field has been hindered by the fact that the first generation of inhibitors were not target specific. However, over the last few years, a new set of inhibitors have been developed, increasing the investigation of new drugs that present the potential to selectively inhibit proliferation of cancer cells, especially gliomas. This is easily reflected in the number of clinical trials using inhibitors of transcriptional CDK´s started the last half decade [2]. The current study provides an insight into this topic by taking in consideration the "normal" functioning of the transcriptional program in cells and its dysregulation in cancer, more specifically in gliomas.

1.1 The eukaryotic cell cycle and cyclins

In multicellular organisms, the cell cycle is referred as the process leading to cell division or cytokinesis [3]. This mechanism promotes tissue growth and differentiation as well as cell maintenance in mature organisms. Giving its importance, the cell cycle has evolved to be a strictly regulated system involving several stages. The four main steps in the eukaryotic version of this process includes Gap1 phase (G1), DNA Synthesis phase (S), Gap2 phase (G2) and Mitosis phase (M) [4]. These are illustrated in Figure 1.1. The transition from G0 to G1 phase, also described as induction of cell proliferation, occurs only when all necessary signalling proteins, growth and transcription factors as well as membrane receptors are synchronized in a regulated manner at a given time of the cell's lifespan [4]. When the critical cell size is achieved, expression and synthesis of Cyclin D (Cyc D), a protein pertaining to the cyclin family, is initiated [4]. Several isoforms of cyclin have been discovered and studied during the last decades, with the vast majority of

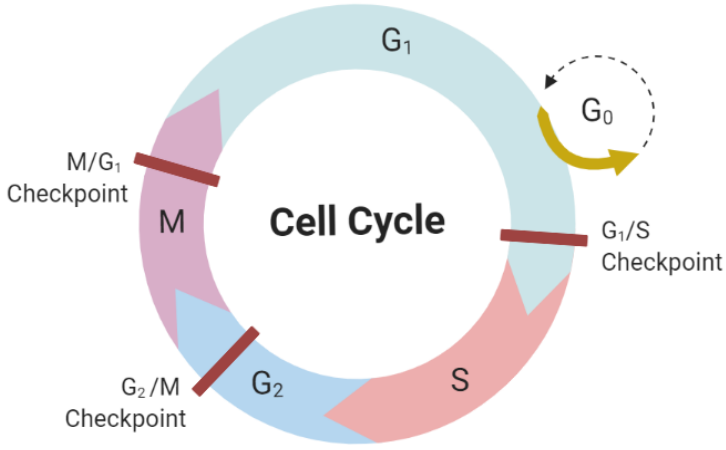

Figure 1.1 The eukaryotic cell cycle. The illustration shows a schematic representation of the four main steps in the eukaryotic cell cycle, thus G1-phase, S-phase, G2-phase and M-phase. The corresponding checkpoints are also shown in the transition between G1 and S phase, G2 and M phase as well as the exit checkpoint in late M phase. Created with BioRender.com.

them acting as regulatory subunits in Cyclin-Dependent Kinases (CDK´s), a type of enzymes pertaining to the serine/threonine protein family [5]. In humans, this subgroup of kinases assemble with their cyclic partners (appendix A) and function as regulators of both the cell cycle and the transcriptional machinery [5]. For instance, Cyc D1 type interacts with the catalytic site of CDK 4 and CDK 6, forming a complex which leads to the partial phosphorylation of the Retinoblastoma tumour suppressor protein (Rb-protein) [6]. The latter is bound to E2 transcriptional Factor (E2F), which plays an important role in the transition from G1 to S phase [7]. This occurs as the partial phosphorylation of Rb-protein makes it loosens its grip on E2F, allowing the transcription of Cyclin E (Cyc E) gene to take place [7]. As concentration of Cyc E increases, CDK 2, one of the catalytic partners of Cyc E, becomes active and fully phosphorylates the Rb-protein, leading to its total loss of function [8]. The Cyc E - CDK 2 complex also phosphorylates $p27^{kip1}$, a protein pertaining to the universal CDK Inhibitor family (CDKI) [9]. This in turn leads to the degradation of $p27^{kip1}$ and together with E2F promotes expression of Cyclin A (Cyc A). The expression of Cyc A and its interaction with CDK 2 triggers the cell to enter S phase, hence proceeding with DNA replication [10]. Nevertheless, this step is tightly regulated by the checkpoint control p53 protein, which in turn is induced by the detection of DNA damage (G1/S checkpoint in Figure 1.1) [11]. If DNA damage is detected, the cell proliferation enters in a temporal arrest and remains in this state until correction of the error. In the case where the error is severe and cannot be repaired, p53 may induce programmed cell death or apoptosis [11]. However, in a study performed by Deckbar et. al. [12] it has been shown that the arrest of the cell cycle at this stage is limited and dosage-dependent, suggesting that more errors are passed to daughter cells than previously thought. It is also important to remark that during G1 phase the cell is metabolically active, allowing its continuous growth, but DNA replication does not take place until its entrance in S phase [10]. Moreover, Cyc A remains in the nucleus of the cell regulating the initiation/completion of DNA replication. This assures that DNA replication occurs only once per cell cycle, thus avoiding overgrowth. The underlying mechanisms involved in the regulation of DNA replication during S phase are further covered in section 1.2.

Given the successful duplication of DNA during S phase, the cell further proceeds to G2 phase before entering the mitotic cycle. The progress through this stage is dependent on the binding of Cyc A to CDK 1, a complex that activates the transcriptional factors NF-Y, FoxM1 and B-Myb [13]. These regulate the transcription of Cyclin B (Cyc B), which together with CDK 1 form the Mitosis-Promoting Factor (MPF) [13]. As the name suggests, MPF plays an essential role for mitotic entry and during the mitotic cycle, and is thereby tightly controlled by a swich-like mechanisms including transcription as well as degradation of Cyc B via Anaphase-Promoting Complex/Cyclosome (APC/C) [13]. Interestingly, the cellular location of the Cyc B - CDK 1 complex changes as the cell cycle advances through G2 phase, moving from the cytoplasm to the nucleus. This process is mediated by Importin-β protein, and the counteractive shuttle by the export protein CRM1 [13]. The relocation of MPF emphasizes its

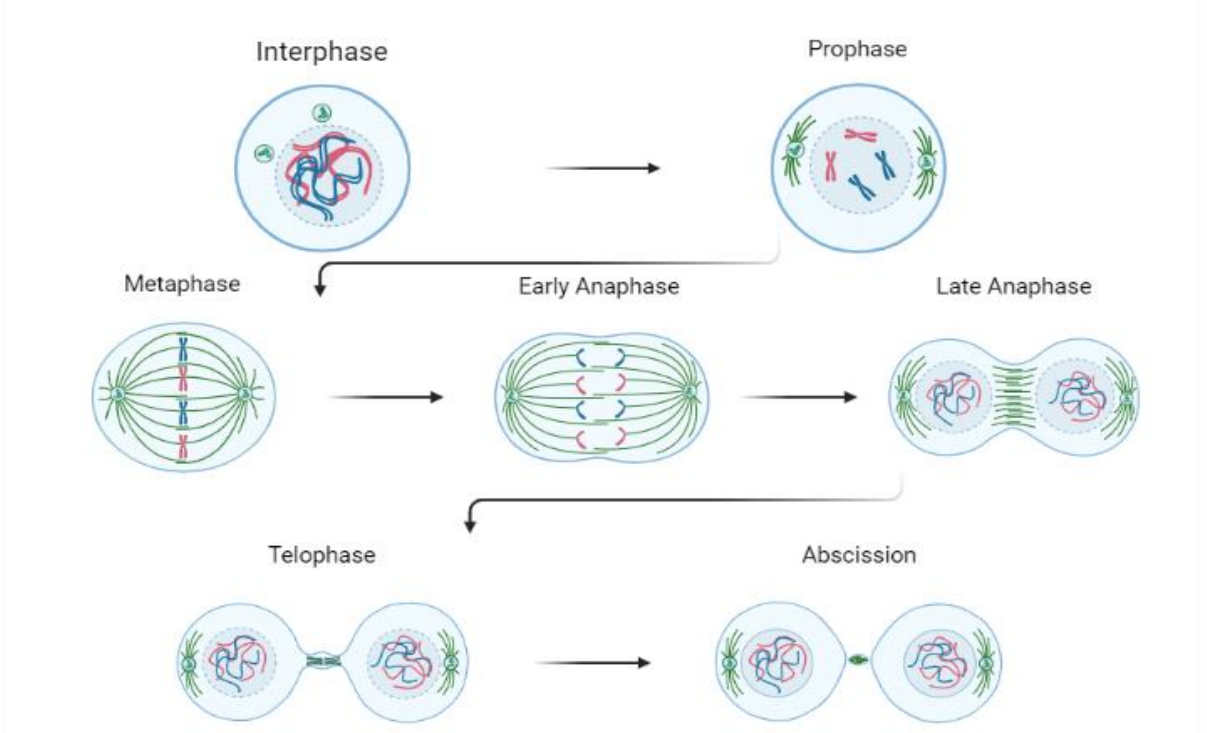

Figure 1.2 Interphase and mitotic cycle. The picture highlights the details involved in cell division through the mitotic cycle. As depicted, the DNA is duplicated during the interphase followed by the condensation of the chromatin reticulum and the formation of the spindle-microtubule (green-coloured) polymers in the prophase. Assuming their most compacted state, the chromosomes of the cell line up at the centre of the spindle during the metaphase and are separated by degradation of cohesin due to separase activity in early anaphase. In addition, the kinetochore microtubules are shortened during early anaphase, causing the gradual attraction of the chromosomes towards the poles of the spindle in late anaphase. Mitosis ends when the chromosomes reach the poles during telophase. This stimulates the formation of the new nuclear membrane and the condensation of the chromosomes into their interphase conformation. Division of the cytoplasm or cytokinesis (abscission in illustration) marks the completion of the two new daughter cells. Created with BioRender.com.

importance during mitosis, especially in mechanisms involving generation of the mitotic spindle, chromosome condensation and nuclear envelope breakdown [14]. In addition, the duplicated DNA is "proof-read" in late S and G2 phase, assuring that no replication errors will be transmitted over the two nascent cells. This process activates a complex machinery involving several sensors, transducers and effectors which regulate mitotic entry and/or cellular arrest at this stage of the cell cycle [15]. For instance, proteins sensing DNA damage such as Ataxia Telangiectasia-Mutated kinase (ATM) and ATM-Rad3 related kinases (ATR) mediate the phosphorylation of several transducers as for example Checkpoint Kinase 1 (ChK1), which in turn is responsible for the activation of multiple components involved in the nuclear re-localization of CDK 1 [16].

As Cyc B concentration increases, G2 phase is left behind leading to the entry of the first out four subphases composing the mitotic cycle, namely prophase. It is important to remark that the accepted common designation describing the three previous phases, thus G1, S and G2 phase is referred as interphase. Figure 1.2 illustrates this, as well as a detailed map of the different stages during the mitotic cycle. During prophase, polymers of tubulin also referred as microtubules are formed and start migrating towards opposite poles surrounding the Nuclear Envelope (NE) [14].

Simultaneously, centrosome migration starts by a dynein-dependent manner, which in turn is also associated with the tearing of the NE and its rupture. This occurs as dynein, a cytoplasmic motor microtubule protein, associates with the NE during late G2 phase, and stays attached during mitosis. As prophase advances, nuclear compartmentalization is gradually lost, mainly due to NE disintegration, which in turn leads to the first step in the formation of the mitotic spindle [14]. Consequentially, Nuclear Pore Complexes (NPCs) and their components, such as nucleoporins, are dispersed into the cytoplasm playing and important role in the assembly of the kinetochores and later in the regulation of nuclear re-organization [14]. The kinetochores are attached to the centromere of each chromosome and make a bridge with the centrosomes to form the mature mitotic spindle [14]. Composed of several regulatory, structural and motor proteins, the kinetochore is central for the coordination of chromatid displacement in late metaphase, as separase starts degrading the cohesin proteins holding the chromatid sisters together. This is preceded by the condensation of the chromosomes and their alignment at the centre of the mitotic spindle, creating the metaphase plate, during early metaphase [14]. Given that tension has been established by the pulling of the kinetochores and that cohesin proteins have been successfully degraded, the microtubules start shortening in early anaphase, and are gradually displaced towards the poles in the late stage of this phase [14]. The mitotic cycle ends when the chromosomes reach their corresponding poles during telophase, stimulating the re-assembly of the NE by recruitment and interactions between chromatin, nuclear membrane, NCPs and nucleoporins [14]. This process culminates with cytokinesis or the division of the two nascent cells. Interestingly, the dramatic changes that occur during M-phase last less than one hour, while interphase may take up to twenty-three hours to complete. The two new cells will eventually enter either G1 or G0 phase and undergo the same sequence of events as their progenitor cell.

1.2 Regulation of DNA replication

The survival and proliferation of progeny cells, as described above, is completely dependent on the successful passage of genetic information from their parent cell. Naturally, this process has evolved to be a complex interplay between spatial organization and time-dependent coordination, ensuring that the specific demands of multicellularity are being met at every single developmental stage. Even though we do not have a complete picture of all the mechanisms involved in DNA replication, our understanding has significantly advanced during the last decades, equipping us with better tools to approach genetic disorders such as cancer. For instance, it is well known that eukaryotic replication initiates at multiple genomic loci or origins located along the genome in question, and that their number varies depending on genome size and internal organization. Moreover, the number of active origins is essential for replication to occur in a biologically manageable timescale for the specific organism. In humans, it is estimated that around 30 000 – 50 000 origins are activated during the duplication of the 3 Gbp long genome [17], emphasizing the complexity of this process.

The decision to replicate DNA starts during the transition from M to G1 phase, where the accumulation of external signals, as the ones mentioned in section 1.1, stimulate the synthesis of S phase proteins and prepare the cell´s DNA for duplication [18]. The first step is led by the binding of the Origin Recognition Complex (ORC), a replication-initiator complex composed of six different subunits (Orc1-Orc6), to their sequence specific origins [19]. ORC serves as a platform for the soon to be formed pre-Replication Complex (pre-RC) as well as recruiter of the necessary replication factors composing this protein machinery [10]. The Cell division cycle 6 (Cdc6) protein as well as the DNA replication factor Cdt1 are the first to be recruited by the ORC and act as licensing agents allowing further gathering of replicative factors during G1 phase [20]. The completion of pre-RC is successful only when the latter mentioned manage to recruit the Mini-Chromosome Maintenance (MCM) complex, which in turn is composed of six protein subunits (MCM2-MCM7), forming a hexamer around the origin DNA [17]. Several studies [17-20] indicate that the MCM complex functions as a helicase, unwinding the double stranded DNA and thereby facilitating its orchestrated duplication. In addition, it is important to remark that two, if not more, helicases are loaded per replication origins, allowing bi-directional replication of DNA [18]. However, the double hexamer is inactive and does not proceed with chromosomal unwinding until entrance in S phase, where CDK activity is increased [21]. It is believed that loading and activation of helicase are timely separated in order to avoid re-replication of the DNA in the same S phase, an occurrence that could lead to sever aberrations during cell proliferation and even cellular death. A study performed by Nguyen et. al. [22] describes one of the possible mechanisms involved in the prevention of re-replication by directly targeting one of the licensing factors, namely Cdc6. According to the study, phosphorylation of Cdc6 by B-type CDK´s Clb-Cdc28 leads to the degradation of the licencing factor and thereby blocks the formation of pre-RC. In addition, the transcriptional activator Swi5, responsible for the expression of Cdc6, is also phosphorylated and thereby prevented from entering the nucleus [22]. Moreover, the study also points that Clb-Cdc28 may play a role in the nuclear export of MCM complex, leading to their removal until next round with DNA replication. Interestingly, several of the ORC´s subunits do present CDK phosphorylation sites, indicating that these may also be an *in vivo* target for Clb-Cdc28 and thus prevent the assembly of pre-RC [22]. While the specific mechanisms of action may vary from eukaryote to eukaryote, the regulative role of cyclin-dependent kinases involved in DNA replication remains essential throughout different organisms [19]. This emphasizes their importance in diseases such as cancer, where cell growth and proliferation are severely dysregulated. Equally important is the role of the second licencing factor or Cdt1 in ensuring faithful control of the replicative process. In both S and G2 phase, a Cdt1 inhibitor named Geminin binds to the licencing factor and prevents its interaction with the MCM complex, thus repressing the completion of pre-RC [18]. Alternatively, Cdt1 is phosphorylated by CDK 2 or CDK 4 and thereby targeted for degradation in an E3-ubiquitin-ligase dependent manner [23].

As mentioned above, the double hexamer is not active until entrance in S phase, where complementary proteins bind to it and enhance the bi-directional unwinding of DNA. Specifically, two S phase kinases, Dbf4-Dependent Cdc7 Kinase (DDK) and S phase Cyclin Dependent Kinase (S-CDK) contribute to its activation by phosphorylating the MCM4 and MCM6 subunits of the MCM complex and recruiting the necessary co-activators to form the pre-Loading Complex (pre-LC) [18]. Cdc45 is one of two essential factors implicated in helicase activation and together with his partner creates the base for faithful DNA unwinding [24]. The phosphorylation of the MCM subunits by DDK stimulates Cdc45 interaction with the complex assuring the first step in the activation process [18]. The second essential factor, GINS, is a tetrameric protein (Sld5-Psf1-Psf2-Psf3) and its S-CDK-dependent assembly with MCM and Cdc45 gives rise to the formation of the CMG complex [25]. Both activating factors are reliant on other proteins to properly perform their function. In humans, Treslin, RecQ4, TopBP1 and Polymerase ε (Pol ε) are some of the key players regulating CMG association and formation of the replication fork [18, 26]. The presence of Pol ε in the CMG complex assures that there is a replicative factor involved in the activation of the helicase and thus initiation of DNA unwinding [26]. Finally, the partition of the double hexamer is triggered by MCM10 association to the MCM complex during S phase and consequent recruitment of Polymerase α (Pol α) [27]. This marks the initiation of *de novo* DNA synthesis by the replisome complex and the formation of the "replication bubble" [18].

1.2.1 Topoisomerase´s role in DNA organization

As DNA unwinding is being carried by the helicase complex, a new cellular challenge starts forming a few base pairs downstream the replication forks. Indeed, helicase activity gives rise to supercoiling of the double stranded DNA structure [28], creating an obstacle for faithful DNA replication, transcription or simply chromatin re-organization. This topological problem is solved by a family of enzymes referred as topoisomerases, which in turn also affect gene activity during these processes [29]. Their mechanism of action involves the insertion of a temporary single- or double-strand break on the phosphate backbone of the DNA, the break being dependent on the type of topoisomerase being active at the given cellular stage. Type I topoisomerases are responsible for the insertion of single-strand breaks, while type II topoisomerases work by inserting a double-strand break induced by ATP hydrolysis [30]. In addition, a variety of isomers for both type I and II are found in nature, Table 1.1 illustrating the human variants.

Interestingly, the mammalian isomers of Topoisomerase II (Top II) have evolved to control different cellular processes, as Top II-α is involved in DNA replication and mitosis, while Top II-β is active during transcription [28]. Naturally, proteins involved in such essential pathways are an attractive target for different type of cancer therapies, and indeed several topoisomerase poisons have been utilized in the fight against this diseases [31]. In the current study, several inhibitors targeting Top II will be further reviewed, with special emphasis on drugs interfering with the transcriptional program in glioma cells.

Table 1.1. Human isomers of topoisomerase. The table illustrates the different types of topoisomerases found in human cells. This is an adaptation of Champoux et. al. [30].

Isomer	Type
Topoisomerase I	IB
Topoisomerase I (mitochondrial)	IB
Topoisomerase II alpha	IIA
Topoisomerase II beta	IIA
Topoisomerase III alpha	IA
Topoisomerase III beta	IA

1.3 Transcription and transcriptional regulation

The transcriptional program in higher eukaryotes is a highly dynamic and complex process which involves several steps before its completion. Similarly to DNA replication, this pathway is tightly regulated by the cellular machinery in order to satisfy the exact demands of the cell at every developmental stage. In this process a single-stranded RNA or transcript is synthetized by using one of the DNA strands, also referred as sense strand, as a template [32]. Genes needed for a specific function in a given tissue will commence transcription when the necessary internal and/or external stimuli have triggered a set of reactions leading to the activation/deactivation of transcriptional regulators such as enhancer or silencers. The later mentioned may in turn influence other transcriptional regulators which facilitate commencement of transcription by for example attachment of a DNA-binding protein or RNA polymerase itself to a target sequence called promoter [32]. As Brown points out in his book [32], attachment of a DNA-binding protein serves as a platform for further recruitment of factors involved in transcription, analogously to the ORC role in forming the pre-replication complex (section 1.2). Due to the high variance in sequence, the eukaryotic promoters and regulatory regions are not as well defined as the bacterial ones and, with a few exceptions, no consensus sequences are established in the literature for these specific genomic locations. In addition, some eukaryotic genes dispone of multiple promoters, often referred as alternative promoters, increasing the overall level of complexity in the transcriptional process [33]. However, the polymerases involved in transcription have evolved in a specific manner recognizing different patterns or elements along the eukaryotic genome [32]. For this reason, the sequence to which RNA polymerase will bind is often referred as the core promoter or basal promoter while the remaining components receive their names depending on their specific position in regard to the core promoter [32]. For instance, the promoters of RNA polymerase II can be prolongated for several kilobases upstream of the Transcription Start Site (TSS) and in addition in-

clude Downstream Promoter Elements (DPE) as depicted in Figure 1.3. Indeed, the structural difference between the RNA polymerases and the sequential variation at the initiation site defines which genes are transcribed by which polymerase [34]. In vertebrates, RNA polymerase I is responsible for the transcription of genes that encode most of the ribosomal RNAs (rRNAs), while RNA polymerase III transcribes most of the genes for transfer RNAs (tRNAs) and other small regulatory RNA molecules [34]. RNA polymerase II is thereby left with one central role, namely transcription of genes that code for messenger RNA (mRNA), which in turn serve as templates for protein synthesis [32]. Although the main function of RNA polymerase II is the transcription of protein-coding genes, this enzyme is also responsible for transcribing many non-coding genes, some of them being involved in transcriptional regulation [35]. Interestingly, RNA polymerases cannot solely carry out the transcription process, but are much dependent on other factors that partially regulate this complex machinery [32].

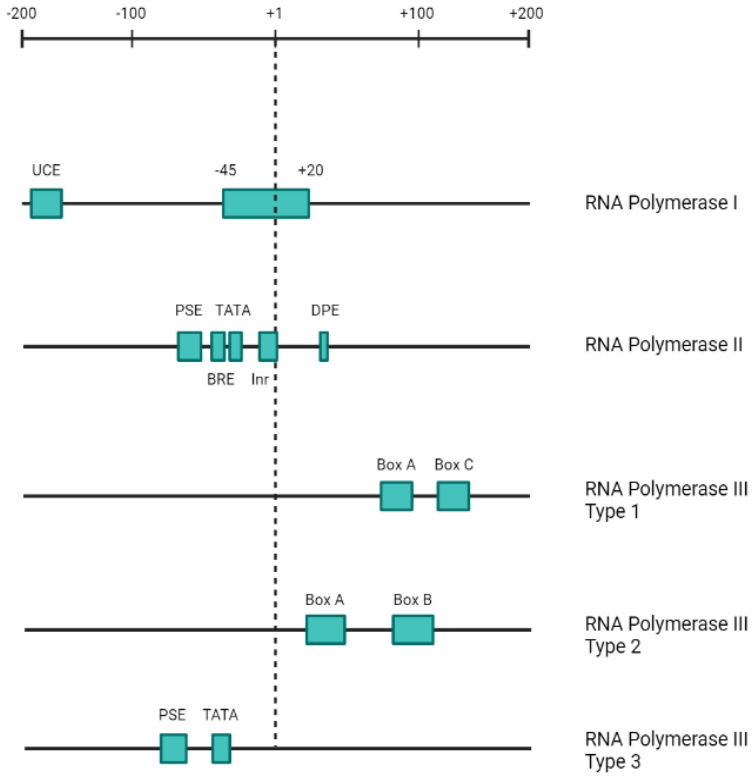

Figure 1.3 Sequential differences between eukaryotic promoters. The illustration eludes the different DNA structures recognized by the RNA polymerases and the relative positioning in bp of the elements in regard to the core promoter. The Upstream Control Element (UCE), the Proximal Sequence Element (PSE), the B Response Element (BRE), the Initiator (Inr) as well as DPE, TATA-box and Box A, B and C are all represented in the figure. This is an adaptation from [30]. Created with Biorander.com.

Given the important role of RNA polymerase II, this protein has been widely studied in relation to many diseases including cancer, and several therapies targeting this enzyme have successfully been implemented in the clinics [36]. How DNA transcription is regulated by RNA polymerase II and what the implications of this process are for cellular integrity will be in-depth analysed in the following section.

1.3.1 RNA polymerase II as transcriptional regulator

As mentioned earlier, eukaryotic transcription is a well-orchestrated interplay between several regulatory factors and genomic regions as well as the different type of polymerases acting on the DNA molecules. The **initiation** step in RNA polymerase II-based transcription starts by the binding of the general Transcription Factor II D (TF-II D) to the TATA element in the promoter region which is situated around 30 nucleotides (nt) upstream to the TSS [37]. The TF-II D complex is composed of the TATA-box Binding Protein (TBP), which is in turn the domain facilitating the interaction between the TATA

element and the TF, and the TBP-Associated Factors (TAFs) [37]. The binding of TBP to the TATA element causes the bending of the DNA helix by 80 ° [38], promoting further recruitment of TFs such as TF-II A and TF-II B. TF-II A will stabilize the Pre-Initiation Complex (PIC), also referred as closed complex, by interacting with the TBP domain of TF-II D, upstream the initiation site, and further enhance its binding to the TATA element in the promoter region [39]. TF-II A also serves as a coactivator for some transcriptional activators and plays an important role in excluding repressors to bind to the TBP domain [38]. On the other hand, TF-II B binds the TBP domain downstream to the TATA element and stimulates recruitment of RNA polymerase II on the promoter region [35]. However, RNA polymerase II is not capable of binding to this region by its own, and an additional TF is necessary to complete this step. Indeed, TF-II F interacts with both TBP domain and TF-II B and stimulates the coupling of RNA polymerase to the complex [40]. In addition, the general TF-II F assures that RNA polymerase II does not start transcribing the DNA outside the promoter region until the completion of PIC [41]. Finally, TF-II E binds to the promoter region downstream the initiation site and enhances recruitment of TF-II H, which dispones of ATPase activity and functions as helicase melting the promoter region [42]. This marks the transition from PIC to open complex and exit from the initiation stage. However, in order to create the transcriptional bubble, one of the subunits of TF-II H, namely the cyclin activating kinase-subcomplex formed by CDK 7, MAT 1 and cyclin H needs to activate RNA polymerase II by phosphorylating the C-Terminal Domain (CTD) of this enzyme [43]. In this case, Serine (Ser) 5 and 7 at the CTD region of RNA polymerase II become phosphorylated by CDK 7, thus enhancing promoter escape by interrupting the interaction between the Mediator Complex (MC) and PIC [43].

It is important to remark that the assembly of PIC happens partially before binding to the promoter region as depicted by Greber et. al. [44]. In addition, gene-specific transcriptional factors, enhancers, chromatin remodelers as well as other transcriptional co-activator such as MC do play an important role in the initiation stage of this process. This occurs as some of the forehead cited elements facilitate the interaction of RNA polymerase II with the promoter region and thereby stimulate a faster proceeding of the transcriptional process at this stage of the cycle [45]. Figure 1.4 illustrates the complexity of this mechanism.

Following phosphorylation of RNA polymerase II, **elongation** is the next phase to takes place in transcription [32]. As in the initiation step, several proteins participate in elongation, with them being referred as Transcriptional Elongation Factors or TF-Es. In addition to that, elongation can be separated into early elongation, where the necessary components for the process are being recruited, and productive elongation, where the transcript is being actively synthetized [46]. Moreover, a key regulatory event called promoter-proximal pausing occurs in early elongation, around 30-50 nt downstream the TSS, and involves promotor-associated TFs as well as RNA Polymerase II-Associated Factor 1 (PAF1), Negative Elongation Factor (NELF) and 5,6-Dichloro-1-β-D-RibofuranosylBenzimidazole

(DRB)-Sensitivity Inducing Factor (DSIF) [47]. NELF and DSIF have been shown to stabilize the pause complex but are not required for the pausing itself [47]. As elongation proceeds, TF-Eb, a member of the MicrophThalmia family (MiT) composed of Cyc T1 and CDK 9, is recruited to RNA polymerase II, phosphorylating serine residues at the CTD of the protein [48]. This event leads to NELF

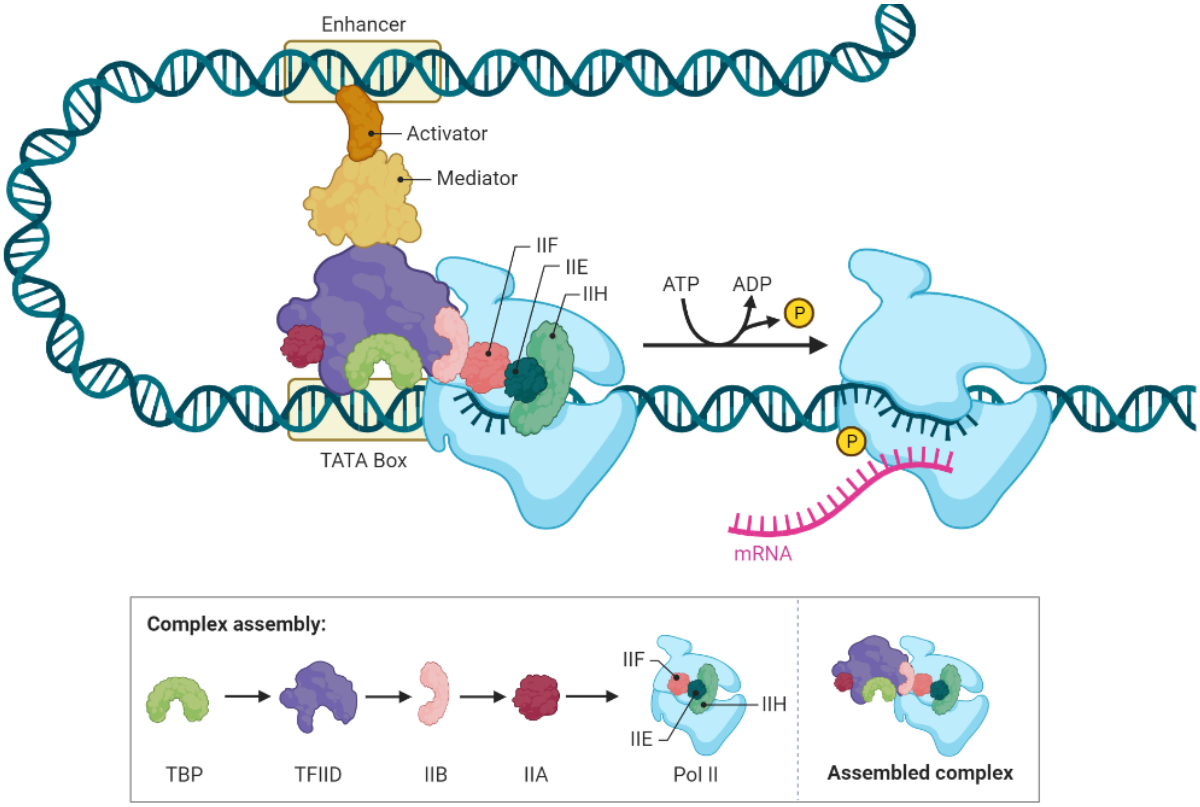

Figure 1.4 The transcriptional machinery. The illustration shows the different elements participating in the initiation stage of eukaryotic transcription as well as the mechanism involved in the activation of RNA polymerase II. Proteins such as enhancer, activator, MC as well as all general TFs and RNA polymerase II are depicted in the figure. The TATA-box region as well as Adenosine Tri-Phosphate (ATP), Adenosine Di-Phosphate (ADP) and Phosphate (P) molecules are also illustrated. The box below graphically describes the assembly of PIC, which partially occurs before associating with the targe DNA. Created with BioRender.com.

release from the complex and thereby enhances promoter escape of RNA polymerase II as well as entrance into productive elongation [48]. However, most of the time, TF-Eb remains inactive in the cytosol and nuclear translocation occurs only when the protein is unphosphorylated. Thus, the regulative role of TF-Eb in transcription is part of an elaborated pathway involving several elements [49].

On the other hand, during productive elongation, activity of TF-II S stimulates arrested RNA polymerase II (mainly due to nucleosome hindrance) to cleave the nascent transcript, generating a new 3´ end in the pre-mRNA being synthetized and thereby resuming transcription [50]. Thus, TF-II S increases the rate of transcription by several means through its interaction with RNA polymerase II [51]. In addition, the processivity factor Spt4/5 also plays an important role in the kinetics of the transcriptional process by interfering with the mechanical movement of RNA polymerase II through the nucleosome [52]. It is believed that this mechanism partially solves the hindrance problem caused by histone-DNA

interactions in the nucleosomes, and thereby facilitates further DNA transcription by RNA polymerase II [52].

It is important to remark that the first RNA processing event occurs during elongation and is referred as 5´capping [53]. During this process, the terminal γ-phosphate of the 5´-end nt is removed by RNA triphosphatase, while guanylyl transferase adds a new phosphate, which in turn is attached to the nucleobase guanine [53]. Guanine is then methylated by the enzyme methyl transferase, and gives rise to the 5´-cap structure involved in the recruitment of mRNA on the ribosome for the initiation of translation [54].

Termination of transcription is entered when RNA polymerase II reaches the end of the targeted gene, also referred as terminator sequence. This process has several cellular functions such as regulation of gene expression through premature termination of transcription, promotion of RNA 3´-end processing and recycling of RNA polymerase [55]. During termination, the CTD of RNA polymerase II interacts with two proteins, namely Cleavage Stimulation Factor F (CSTF) and Cleavage and Polyadenylation Specificity Factor (CPSF). As the name depicts, the CSTF cleaves the pre-mRNA and disassociates from the complex, leaving CPSF bound to the transcript [56]. The later recruits Poly A polymerase, which adds about 200 adenine residues at the 3´-end of the transcript and thereby forms the so called Poly A tail at the Poly A-Site (PAS) [56]. Poly A binding protein is then recruited to the tail and stimulates CPSF release and simultaneously prevents degradation of the Poly A tail by sterically hindering exonucleases targeting adenine residues [57]. Different mechanisms may lead to transcriptional termination, depending on the phosphorylation status of RNA polymerase II CTD and its interaction with surrounding termination factors [55]. However, only two CTD-dependent termination models have been well defined during the last decades, these being the allosteric and the torpedo model [56]. The former proposes that RNA polymerase II recognizes PAS and thereby induces a conformational change in the active site of the polymerase, leading to its disassociation from the complex [56]. The later proposes that the nascent transcript is still being synthetized even after cleavage at PAS through a mechanism involving the enzyme 5´- 3´ exoribonuclease 2 [56].

It is clear now that CDK-mediated phosphorylation is a key regulatory process involved in both DNA replication and DNA transcription and one of the main drivers of the cell cycle in eukaryotic species. Naturally, it is of immense importance to understand how this mechanisms function in healthy organisms as well as in the pathological ones. The following chapters focus on dysregulation of the transcriptional machinery with special emphasis on cancer disease.

1.4 Brain cancer and gliomas

Single impairments such as genomic point mutations occur spontaneously in every type of cell under unfavourable conditions and are usually of no considerable importance. However, if not rectified on time, these events may enhance major changes within the genome or other essential cellular compo-

nents and even result in the development of diseases such as cancer. For instance, point mutations in the DNA binding region of p53 have been shown to affect glioma progression and prognosis [58]. In addition, factors such as high radiation levels, specially ionizing and ultraviolet (UV) radiation, nitric oxides, nitrous acids, oxygen radicals and increased heat intensify the rate at which such impairments occur [59]. Unfortunately, genetic diseases as cancer are becoming more common among the global population, and only in 2020 approximately 19 million new cases were discovered and 10 million lives were lost [60]. With median overall survival of just over one year after diagnosis and with 1.6 % of all fatalities in 2020, brain and nervous system cancer represent one of the deadliest forms of this diseases [60]. Moreover, 80 % of the malignancies occurring in the central nervous system are caused by gliomas, a type of tumour that originates from glial cells [61]. As with many other cancers, the risk of developing glioma increases with age, life style, viral infections, exposure to radiation and harmful chemicals, as well as familiar record of this disease [61]. Depending on the type of cells involved in the tumour, gliomas can be classified as astrocytoma, oligoastrocytoma and oligodendroglioma [61], as shown in Table 1.2.

Table 1.2. Histological classification of gliomas. The table illustrates the grading of the different type of gliomas according to their severity and developmental stage as depicted by the world health organization. This is an adaptation from [61].

Histological grading	Astrocytoma	Oligoastrocytoma	Oligodendroglioma
Grade I	Pilocytic astrocytoma	NA	NA
Grade II	Diffuse astrocytoma	Oligoastrocytoma	Oligodendroglioma
Grade III	Anaplastic astrocytoma	Anaplastic oligoastrocytoma	Anaplastic oligodendroglioma
Grade IV	Glioblastoma multiforme	NA	NA

1.4.1 Glioblastoma

As it can be observed from Table 1.2, Glioblastoma Multiforme (GBM) accounts for the most advanced and severe form of this diseases, with less than 5-10 % of people surviving longer than five years after diagnosis [60]. As the term “multiforme” suggests, the histopathology of these tumours is extremely variable. In addition, existing therapies fail to successfully reduce the burden of the diseases, and even after surgical removal followed by chemotherapy (usually with Temozolomide) and radiotherapy, the cancer tends to recure in the vast majority of the cases [62]. This is partially due to the ability of glioblastoma cells to adopt stem cell states, facilitating tumour recurrence [63]. Therefore, it is of vital importance to find new therapies that can approach the diseases in a more specific manner

and extend the life expectancy of patients suffering from this illness. The following chapter describes in-depth the transcriptional dysregulation in gliomas, with special focus on transcriptional regulators such as CDK´s.

1.5 Transcriptional dysregulation in gliomas and therapeutical strategies

As discussed earlier through sections 1.1-1.3, CDK´s and their correspondent cyclin partners are of crucial importance in cellular processes such as cell cycle, transcription, and mRNA processing. Several studies [64-66] point that genomic alternations leading to constitutive activation of CDK´s are a common factor for many cancer forms, including gliomas. Usually, brain cancer malignancies proliferate through the recruitment of several CDK´s early in G1 phase, and genomic instability in gliomas appears to be related to disturbances in S phase and in the transition between G2 and M phase [2]. In addition, both natural occurring or synthetically created CDK Inhibitors (CKI´s) play an important role in progression of this diseases, as they act as breaks to control cell cycle progression or other processes in which CDK´s are involved [67]. In fact, some CKI´s are currently in clinical use for treatment of certain types of malignancies, as for example breast cancer [68]. However, pre-clinical and clinical trials have generated mixed results over the past decades, giving a non-definite conclusion regarding the effectiveness of these therapeutics, especially on brain cancer [2]. Despite this fact, the effort to advance the understanding and development of effective inhibitors targeting this type of cancer has never been bigger [2]. For instance, the recent discovery of a covalent CDK 7 inhibitor, THZ1, by Meng et. al. [69] is a clear example of this. This molecule appears to affect cancer proliferation by arresting the cell cycle at G2 phase, a phenomenon derived from disturbed transcriptional cycle and disabled CDK activation [70]. Moreover, THZ1 seems to affect mRNA processing by disrupting nuclear Cajal body and nuclear speckle formation [70]. On the other hand, well established CDK inhibitors such as Abemaciclib and Palbociclib, which selectively target CDK 4/6, have been actively used in certain types of breast cancers during the past few years [71]. This emphasizes once again the importance to develop highly selective inhibitors in order to actually reach the patients.

Lately, a new set of promising drugs referred as PROteolysis TArgeting Chimeras (PROTAC´s) has been emerging in the scientific community, given hope to function on therapeutically relevant targets, including previously considered “undruggable” ones [63]. The underlaying mechanism of this technology takes advantage of the natural protein turnover machinery of the cell, namely the proteasome. Since the discovery of this technology by Sakamoto et. al. [72], the ubiquitin system, especially E3 ubiquitin ligases have been employed in the development of small molecules aiming to degrade a broad range of cellular factors, including CDK´s [73]. This is accomplished by designing a heterobifunctional compound composed of two active domains and a linker molecule. One of the active domains, also referred as “warhead”, aims to target the protein of interest, while the second active domain, usually a small molecule capable of recruiting E3 ligase, triggers ubiquitination of the target compound and thereby initiates proteasomal degradation of the protein [72]. As it is unnecessary for

“warheads” to occupy druggable binding sites which modulate protein function, this type of drugs can exploit all surface binding sites on the protein of interest, giving them an advantage over traditional occupancy-based inhibitors as the ones mentioned above. One example of this technology is a highly selective PROTAC CDK 9 degrader discovered by Qiu et. al. [73]. As discussed earlier, CDK 9 plays an important role in transcriptional elongation, and new evidence [74] suggests that this enzyme is of particular value in therapeutical strategies targeting several forms of cancer. This emphasizes the importance of the technology developed my Sakamoto et. al. and its potential in the fight against cancer.

Recently, a study lead by Zhang et. al. [75] did show that some circular RNAs (circRNAs) have the ability to generate regulatory peptides that may interfere with key molecular pathways, including transcription. For instance, an analogous peptide of the long intergenic non-coding protein RNA p53-induced transcript (LINC-PINT) has shown a suppressive function in the proliferation of GBM, both *in vitro* and *in vivo* [75]. Interestingly, this peptide and PAF1 interact and disable the expression of several oncogenes. The study shows that expression of this regulatory peptide is reduced in GBM, compared to healthy tissue.

Similarly, proteins containing a bromodomain have been widely studied in cancer research and their dysregulation has been associated to several types of malignancies [76]. For instance, the deregulation of bromodomain protein 4, which binds to acetylated lysine residues of histone tails and recruits TF-Eb, has been directly associated to glioma growth and proliferation [77]. As this protein stimulates initiation of transcription, it is an important therapeutical target and indeed several inhibitors have made their way to the clinics during the last years [77].

1.6 Aim of study

Earlier, Pandey´s group has focused on a family of transcriptional CDK´s which were ascribed the functional role of CDK´s less than a decade ago and are indeed still not well characterized in present day. In this project, we will expand our analyses to a few more inhibitors. For the cancer model, we will focus on Glioblastoma Multiforme (GBM). These are tumours of central nervous system, and with median overall survival of just over one year after diagnosis [60], represent one of the deadliest cancer forms that affect mankind.

We will investigate and characterize the effect of a few small inhibitors of transcription and replication on glioma cells. For this, molecular techniques such as proliferation and clonogenic assays as well as fluorescence activated cell sorting will be employed in the duration of the project. Studying the effect of these drugs through such techniques could shed light to the *in vivo* role of the above-mentioned proteins in relation to brain cancer proliferation, more specifically in GBM, and give an insight into their effect on the cell cycle. Hopefully, through this project, we may elucidate the underlaying mechanisms that stimulate the aggressiveness of GBM, and thereby facilitate the development of new treatment strategies or improve existing therapies that efficiently work against this dreadful disease.

2. Materials and methods

2.1 Cell culture

Three cell lines were used in this project, these being Henrietta Lacks (HeLa) Kyoto cells, an immortal human cell line derived from cervical cancer cells in 1951 [78], and two glioma cells referred as G7 and G144 cells. The later were originally obtained by Pollard et. al. [79]. Both cell lines were used in the treatments performed at the department, with HeLa representing a control for the experiments.

2.1.1 Thawing

The cells were collected from the N_2 (l) cryogenic container and rapidly thawed at 37 °C for approximately 5-10 min. The aliquot was transferred to a 15 ml Falcon® tube containing 10 ml PBS buffer and spined down at 1 200 rpm for 3 min. The supernatant was discarded, and the cell pellet re-suspended in the corresponding pre-warmed medium (appendix B). The cell suspension was plated on the chosen dish size (appendix B) and incubated at 37 °C with 5 % constant supply of CO_2.

2.1.2 Coating for glioma cell culturing

For adherent monolayer Neural Stem Cells (NSC), thus G7 and G144 cells, the plates to be used were coated in advance with 5 µg/ml Poly-D-Lysine (PDL, MerckMillipore) in 1X Phosphate-Buffered Saline (PBS, Gibco) for 1 h at 37 °C and with 5 µg/ml laminin [80] in 1X PBS solution for at least 3 h. The coating agent was discarded, and the cells plated in their according medium.

2.1.3 Cell cultivation

The cell cultivation part was performed in regard to the experiments to be conducted. Several types of plates were used and are described in detail in Table B.1 (appendix B). HeLa cells were cultivated in "HeLa" medium while G7 and G144 cells were grown in NSC medium. For a detailed description of the media see appendix B. The physical growing parameters were equal for all cell lines, as mentioned in section 2.11. When approx. 80 % confluency was observed by using an inverted laboratory microscope (Leica DM IL), the cells were passed to a new dish as described in the following section.

2.1.4 Cell splitting and seeding

Periodical splitting is required in order to maintain exponential growth of the different cell cultures. The optimal passage of HeLa cells was set up to two days while glioma cells were passed every third day. This was performed by first aspiring the medium with Vacuboy (Integra) and second by washing the plate with 1X PBS buffer (Table B.1, appendix B). The washing reagent was discarded, and the cells were detached from the plate by usage of a trypsin-like enzyme (TrypLE™ (Gibco)) according to Table B.1 (appendix B). The plate was gently shacked by tapping and incubated at 37 °C for 2-3 min. The reaction was stopped by the addition of a Trypsin Inhibitor in 1X PBS solution (PBS+TI), where 100 mg TI were added to 500 ml 1X PBS buffer (Table B.1, appendix B). The cell suspension was transferred to a 15 ml Falcon® tube and centrifugated at 1 200 rpm for 5 min in a Megafuge 1.0 tab-

letop centrifuge (Heraeus Instruments). The supernatant was discarded, and the cell pellet re-suspended in the corresponding medium by gently pipetting. The cells were prepared for counting by making a 1:1 solution with Trypan Blue staining 0.4 % followed by the addition of 10 µl Trypan/cell solution into a counter cell (Invitrogen, Thermo Fisher Scientific). The counter cell was disposed into the Countess II FL (Invitrogen, Thermo Fisher Scientific) for reading, and the cell concentration was adjusted by diluting with the corresponding medium (Table B.1, appendix B). The cell suspension was plated again in the chosen containers and incubated according to the standard parameters described above.

2.2 Pharmacological treatments

The cells were treated with several drugs mainly targeting different type of CDK isoforms, ATM and ATR as well as topoisomerase I and II and NF-κB activator (Table 2.1). The treatments were performed by first preparing the 96-well plates to be used in the experiments. For the G7 and G144 plates coating was conducted according to section 2.1.2 and Table B.1. Following coating, 10 000 cells per well were seeded for both G7 and G144, while the number for HeLa was set to 3 000 cells per well (section 2.1.4 and Table B.1). Stock solutions of the drugs were prepared by dissolving them in Dimethyl Sulfoxide (DMSO, Sigma Aldrich®) to a final concentration of 10 mM. A three-fold serial dilution was prepared in 1.5 ml Eppendorf® tubes with a high of 20 µM (0.2 % DMSO) and a low of 0.01 µM (0.001 % DMSO). The corresponding medium was used for the serial dilution following appendix B. 50 µl of each dilution were applied to their corresponding wells (three replicates per dilution) to give a final volume of 100 µl, this resulting in a high of 10 µM (0.1 % DMSO) and a low of 0.003 µM (0.0003 % DMSO). 0.1 % DMSO in corresponding medium was used as control and pure medium as blank. The treatment was performed for 72 h under incubation temperature of 37 °C and constant flow of 5 % CO_2. Appendix C illustrates the details described above. The seeding as well as the drug treatment were performed both manually using a multichannel pipette by Thermo Fisher and by taking advantage of an Open-Source Lab Robot (Opentrons System and Software, MTU59619).

2.2.1 Cell viability assays

The viability experiments were conducted by taking advantage of the reducing capabilities of live cells in culture. PrestoBlue reagents (Invitrogen, Thermo Fisher Scientific) were utilized as signalling dye compounds for the construction of IC_{50} curves, where relative fluorescence was plotted against drug concentration. This was done by the addition of 10 µl per well PrestoBlue cell viability reagent to the treated 96-well plates and succeeded by incubation at 37 °C and constant flow of 5 % CO_2 for about 10-30 min. The relative fluorescence signals were measured by using a multimode plate reader (VICTOR Nivo™, PerkinElmer) and the data processed with GraphPad Prism 9 software. The plate reader was set to shake the samples for 10 sec. previous to end-point analysis with an excitation filter of 530/30 nm and emission filter of 600/10 nm. The measurement time was set to 100 millisecond (ms) per sample.

Table 2.1. Pharmacological tools. The table illustrates the drugs used in the experiments during this project and their respective function. It is important to remark that some drugs such as CR-8 do act as both transcriptional and cell cycle inhibitors by targeting multifunctional cyclins as for example Cyc K.

Pharmacological tool	Function
ATR inhibitor 2	ATR inhibitor
AUZ454	Type II CDK 2 inhibitor
AZ20	Selective inhibitor of ATR
BSJ-4-116	CDK 12 degrader (PROTAC)
CR-8	CDK 1, CDK 2, CDK 5, CDK 7 and CDK 9 inhibitor
Doxorubicin (hydrochloride)	Human DNA topoisomerase I and II inhibitor
DRB	CDK 9 inhibitor
Etoposide	Topoisomerase II inhibitor
LDC4297	Selective CDK 7 inhibitor
NVP-2	CDK 9 as well as CDK 1, CDK 2 and CDK 16 inhibitor
PROTAC CDK9 Degrader-1	CDK9 degrader (PROTAC)
RO-3306	CDK 1 inhibitor
SR-4835	Selective and ATP competitive dual inhibitor of CDK 12/CDK 13
THZ531	Covalent inhibitor of CDK 12 and CDK 13
Triptolide	NF-κB activation inhibitor

2.3 Clonogenic assay

The cell lines were exposed to an additional experiment involving long-term drug treatment. HeLa cells were treated for one week while G-cells were treated for two weeks. During this period colonies were formed, allowing an easier analysis of the dose-response effect in the different cell lines. The following sections describe the details of this assay.

2.3.1 Cell culture preparation, pharmacological treatments, and crystal violet staining

The plates used for the glioma experiments were coated similarly as described in section 2.1.2. Following coating, the cells were seeded in their respective plates by taking advantage of the protocol specified in section 2.1.4. The cell cultures were prepared using 6-well plates containing approximately 8 000 – 10 000 cells per well for the G7 and G144 lines and around 2 000 – 3 000 cells per well for HeLa. The cells were incubated for approximately 24 h at standard parameters, as described in section 2.1.1, before proceeding with the drug treatment stage of the experiment. Five different drug concentrations diluted in the corresponding media (section 2.1.3) were used, these being 2 µM (0.04 % DMSO), 1 µM, 0.5 µM, 0.2 µM and 0.1 µM (0.001 % DMSO). 0.04 % DMSO in corresponding media was used as a positive control. For each drug concentration duplicates were employed, thus two 6-well plates were used for one drug. A detailed illustration of the set up can be found in Table C.2, appendix C. In order to obtain colonies, the cells were incubated for a period of 14/(7) days where no parameter was regulated. The medium was discarded using Vacuboy (Integra), and the colonies were stained by incubating for 20 min with crystal violet staining reagent. The reagent was removed, and the cells gently submerged in a water container for washing. The plates were air dried overnight and visually analysed.

2.4 Flow cytometry

The effect of the anti-cancer compounds on cell cycle was studied by taking advantage of Fluorescence Activated Cell Sorting (FACS) analysis preceded by methanol fixation of the cells. Only G144 cells were used in this experiment with treatments of 6 and 24 h. The following sections delineate the procedures involved in this part of the project.

2.4.1 Cell culture preparation, drug treatment, and cell staining

The plates used for the glioma experiment were coated similarly as described in section 2.1.2. Following coating, the cells were seeded in their respective plates by taking advantage of the protocol specified in section 2.1.4. The cell cultures were prepared using 6-well plates containing approximately 300 000 and 500 000 cells for treatments to be done in two-days' time or next day, respectively. Two different drug concentrations diluted in the corresponding media (section 2.1.3) were used, these being 3 µM (0.06 % DMSO) and 1 µM (0.02 % DMSO). 0.06 % DMSO in corresponding media was used as a positive control for both time points. For each drug concentration duplicates were employed, thus two 6-well plates were used for one drug (one plate for each time point). A detailed illustration of the set

up can be found in Table C.3, appendix C. The treated plates were incubated at 37 °C and constant flow of 5 % CO_2 for 6 and 24 h. The cells were harvested by gently removing the media and adding Tryp-LE (Table B.1, appendix B). After detachment, the cells were collected with 1 ml cold PBS+TI, transferred to 1.5 ml Eppendorf tubes and centrifugated at 500 rcf for 5 min. The supernatant was discarded by decantation and the remaining liquid removed with a pipette. The cell pellet was resuspended in 100 µl PBS+Live/Dead™ Fixable Near-IR stain (Invitrogen, Thermo Fisher Scientific, 0.5 µl stain reagent in 1 ml cold PBS) and incubated in dark at room temperature for 15 min. 1 ml cold PBS buffer was added to the solutions and centrifugated at 500 rcf for 5 min. The supernatant was discarded by decantation. This step was repeated twice. The cells were fixed in 1 ml ice-cold methanol (-20 °C) and the samples stored in -20 °C for further analysis.

Previous to cell measuring, 3 ml PBS was added to each sample and centrifugated at 1 700 rpm for 3 min. The supernatant was removed, and the cell pellet resuspended in 400 µl 1.5 µg/ml Hoechst (Invitrogen, Thermo Fisher Scientific) in PBS and incubated at room temperature for 30 min. Alternatively, the cells were incubated at 4 °C overnight. The samples were filtered in a cell strainer cap 30 min previous to Flow Cytometry analysis and stored in sterile round bottom polystyrene FACS tubes.

2.4.2 Cell measuring and data analysis

The cells were analysed by taking advantage of an BD™ LSR II Flow Cytometer operating with UV, 405, 488 and 633 nanometre (nm) line lasers. For this experiment, a UV laser (355 nm) as well as a low energy red laser (633 nm) were employed in order to excite the fluorophores incorporated in the cell samples. A bandpass filter of 450/50 nm was employed for UV excitation, while a bandpass filter of 780/60 nm and a longpass dichroic filter of 735 nm were used for the near IR excitation. 20 min previous to analysis, the instrument was turned on in order to warm-up the lasers and stabilize them. The flow chamber was primed in order to remove undesirable air bubbles or other impurities. The FACS tubes were positioned in the instrument one by one, and the samples run at low (12 µl/min) to high (60 µl/min) flow rate depending on the number of events detected per second. The voltage (V) parameters for forward and side scattering as well as for Live/Dead and Hoechst stain were adjusted to 260, 230, 500 and 227 V, respectively. Several graphs recording different type of 2D data were employed in order to gather the necessary information for the experiments. This was done using the BD FACSDiva™ software. Post-analysis of the data was performed using FlowJo™ v10 software.

3. Results

3.1 Cell viability and clonogenic assays

All three cell lines used in the cell viability and clonogenic experiments were grown in their corresponding medium and seeded accordantly to section 2.2 and appendix B. The pharmacological tools, as described in Table 2.1, were employed in the experiments and IC_{50} curves were constructed using the fluorescence data originating from the multimode plate reader after incubation with PrestoBlue reagent. For this, the plate reader was set to perform an end-point analysis with an excitation filter of 530/30 nm and emission filter of 600/10 nm. The measurement time was set to 100 millisecond (ms) per sample. The collected data was processed with GraphPad Prism 9 software, normalizing the samples to the positive control (DMSO), and using a variable slope model as depicted in equation I.

$$Y = \frac{100}{1+10^{(LogIC50-X)\times HillSlope}} \qquad \text{(I)}$$

Here Y is the normalized relative fluorescence and X depicts the Log-value of the concentration used in the experiment.

The non-parametrical Mann-Whitney test was employed in order to reveal any statistically significant difference in the drug response between HeLa and glioma cells, with the results shown in Table 3.1. The confidence interval was set to 95 %.

The results originating from the clonogenic assay were visually analysed. The following subsections describe in detail the results obtained from all pharmacological treatments performed in the study.

3.1.1 Cell cycle and transcriptional CDK inhibitors and degraders

In order to shed light to the mechanism lying back transcriptional and cell cycle dysregulation in glioma cells, more specifically those involving CDK-dependent regulation, colony formation and cell proliferation experiments were performed using several pharmacological tools targeting CDK 1, CDK 2, CDK 5, CDK 7, CDK 9 and CDK 12/13. Five different concentrations were employed on HeLa, G7 and G144 cells for the clonogenic assay, these being 2 µM, 1 µM, 0.5 µM, 0.2 µM and 0.1 µM.

Figure 3.1 A illustrates the results obtained from the colony formation experiment after 14 days (7 days for HeLa) treatment with AUZ454, a type II CDK 2 inhibitor. The experiment was performed in duplicates, with the control shown in the further left well on the picture followed by the highest AUZ454 concentration of 2 µM and down to 0.1 µM (from left to right). No parameters were changed during the 14/(7) days incubation period. On the other hand, Figure 3.1 B illustrates the results obtained from the cell viability assay after 72 h treatment with AUZ454. The IC_{50} curves for HeLa, G7 and G144 are shown as pink, violet and blue, respectively. Eight different concentrations were employed in this experiment, these being 10 µM, 3 µM, 1 µM, 0.3 µM, 0.1 µM, 0.03 µM, 0.01 µM and 0.003 µM. The Log-values of these concentrations are shown in the x-axis of panel B. The relative

fluorescent units are shown in percentage (y-axis) after normalization with DMSO. The IC_{50}-values for HeLa, G7 and G144 were measured to be 5.9 x 10^{-7}, 2.3 x 10^{-6} and 9.2 x 10^{-7} M, respectively. Their correspondent R^2-values were calculated to be 0.918 for HeLa, 0.963 for G7 and 0.930 for G144.

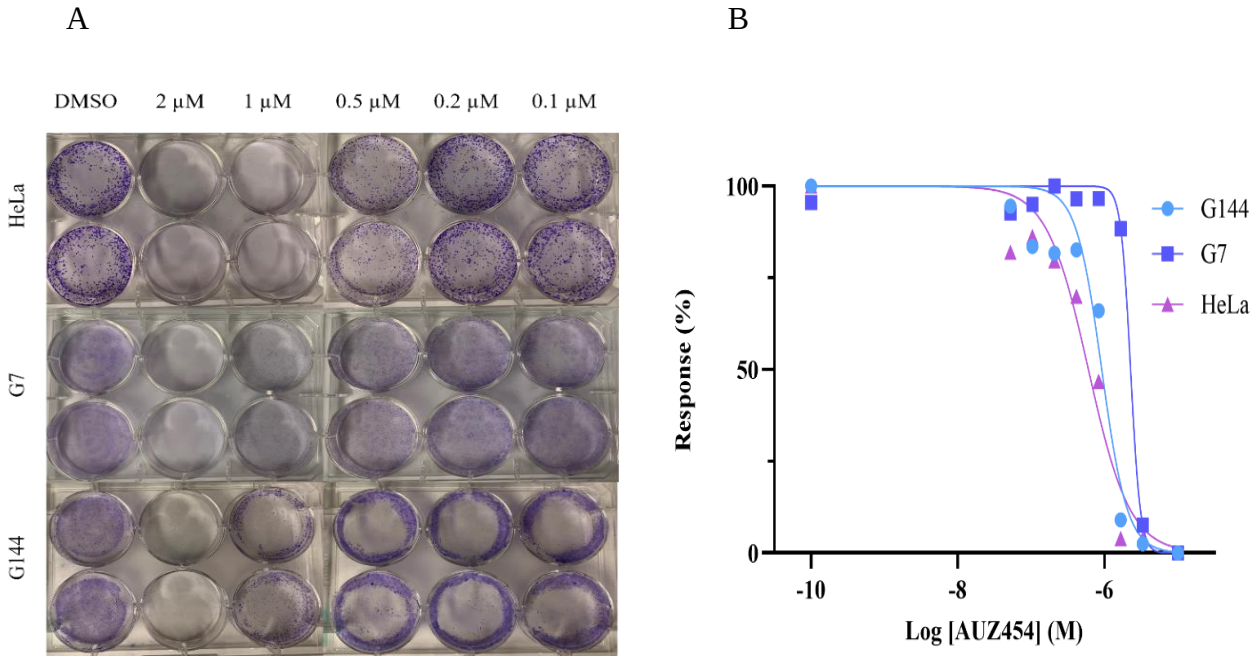

Figure 3.1 (A) Clonogenic assay for AUZ454. The picture illustrates the plates used in the colony formation experiments with Hela on the upper panel, G7 in the middle and G144 on the bottom panel. The experiment was performed in duplicates with 0.04 % DMSO as control (further left well) and with a two-fold decreasing concentration of 2, 1, 0.5, 0.2 and 0.1 µM AUZ454 (from left to right). **(B) Cell viability assay for AUZ454.** The plot shows the IC_{50} curves constructed after treatment with AUZ454 for HeLa, G7 and G144 cell lines. Three-fold dilutions spanning between 10 µM and 0.005 µM were used in the experiment. 10^{-10} was used to normalize with DMSO. The IC_{50}-values for HeLa, G7 and G144 were measured to be 5.9 x 10^{-7}, 2.3 x 10^{-6} and 9.2 x 10^{-7} M, respectively. Their correspondent R^2-values were 0.918 for HeLa, 0.963 for G7 and 0.930 for G144.

Figure 3.2 A illustrates the results obtained from the colony formation experiment after 14/(7) days treatment with BSJ-4-116, a CDK 12 degrader. The experiment was performed in duplicates, with the control shown in the further left well on the picture followed by the highest BSJ-4-116 concentration of 2 µM and down to 0.1 µM (from left to right). No parameters were changed during the 14/(7) days incubation period.

On the other hand, Figure 3.2 B illustrates the results obtained from the cell viability assay after 72 h treatment with BSJ-4-116. The IC_{50} curves for HeLa, G7 and G144 are shown as pink, violet and blue, respectively. Eight different concentrations were employed in this experiment, these being 10 µM, 3 µM, 1 µM, 0.3 µM, 0.1 µM, 0.03 µM, 0.01 µM and 0.003 µM. The Log-values of these concentrations are shown in the x-axis of panel B. The relative fluorescent units are shown in percentage (y-axis) after normalization with DMSO. The IC_{50}-values for HeLa, G7 and G144 were measured to be 6.8 x 10^{-8}, 4.1 x 10^{-7} and 2.3 x 10^{-7} M, respectively. Their correspondent R^2-values were 0.991 for HeLa, 0.970 for G7 and 0.989 for G144.

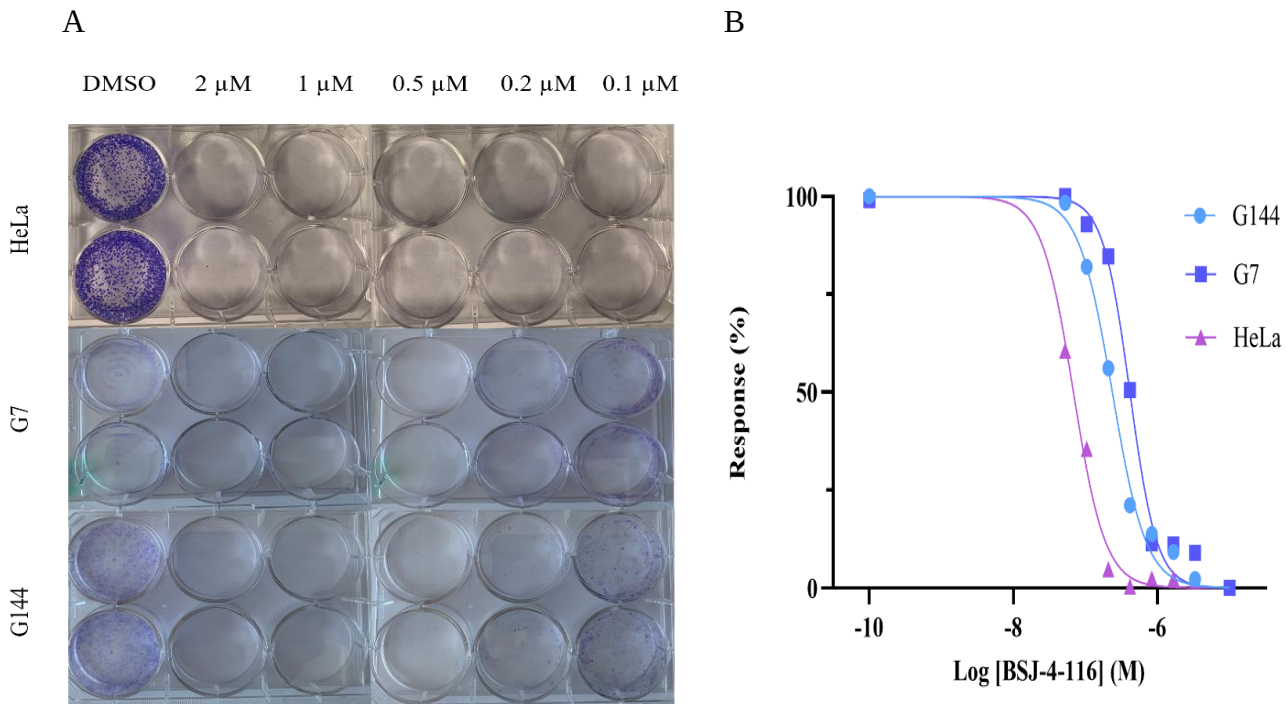

Figure 3.2 (A) Clonogenic assay for BSJ-4-116. The picture illustrates the plates used in the colony formation experiments with Hela on the upper panel, G7 in the middle and G144 on the bottom panel. The experiment was performed in duplicates with 0.04 % DMSO as control (further left well) and with a two-fold decreasing concentration of 2, 1, 0.5, 0.2 and 0.1 µM BSJ-4-116 (from left to right). **(B) Cell viability assay for BSJ-4-116.** The plot shows the IC_{50} curves constructed after treatment with BSJ-4-116 for HeLa, G7 and G144 cell lines. Three-fold dilutions spanning between 10 µM and 0.005 µM were used in the experiment. 10^{-10} was used to normalize with DMSO. The IC_{50}-values for HeLa, G7 and G144 were measured to be 6.8 x 10^{-8}, 4.1 x 10^{-7} and 2.3 x 10^{-7} M, respectively. Their correspondent R^2-values were 0.991 for HeLa, 0.970 for G7 and 0.989 for G144.

Figure 3.3 A illustrates the results obtained from the colony formation experiment after 14/(7) days treatment with CR-8, a CDK 1, CDK 2, CDK 5, CDK 7 and CDK 9 inhibitor. The experiment was performed in duplicates, with the control shown in the further left well on the picture followed by the highest CR-8 concentration of 2 µM and down to 0.1 µM (from left to right). No parameters were changed during the 14/(7) days incubation period.

On the other hand, Figure 3.3 B illustrates the results obtained from the cell viability assay after 72 h treatment with CR-8. The IC_{50} curves for HeLa, G7 and G144 are shown as pink, violet and blue, respectively. Eight different concentrations were employed in this experiment, these being 10 µM, 3 µM, 1 µM, 0.3 µM, 0.1 µM, 0.03 µM, 0.01 µM and 0.003 µM. The Log-values of these concentrations are shown in the x-axis of panel B. The relative fluorescent units are shown in percentage (y-axis) after normalization with DMSO. The IC_{50}-values for HeLa, G7 and G144 were measured to be 1.7 x 10^{-7}, 3.3 x 10^{-7} and 1.2 x 10^{-7} M, respectively. Their correspondent R^2-values were calculated to be 0.987 for HeLa, 0.990 for G7 and 0.941 for G144.

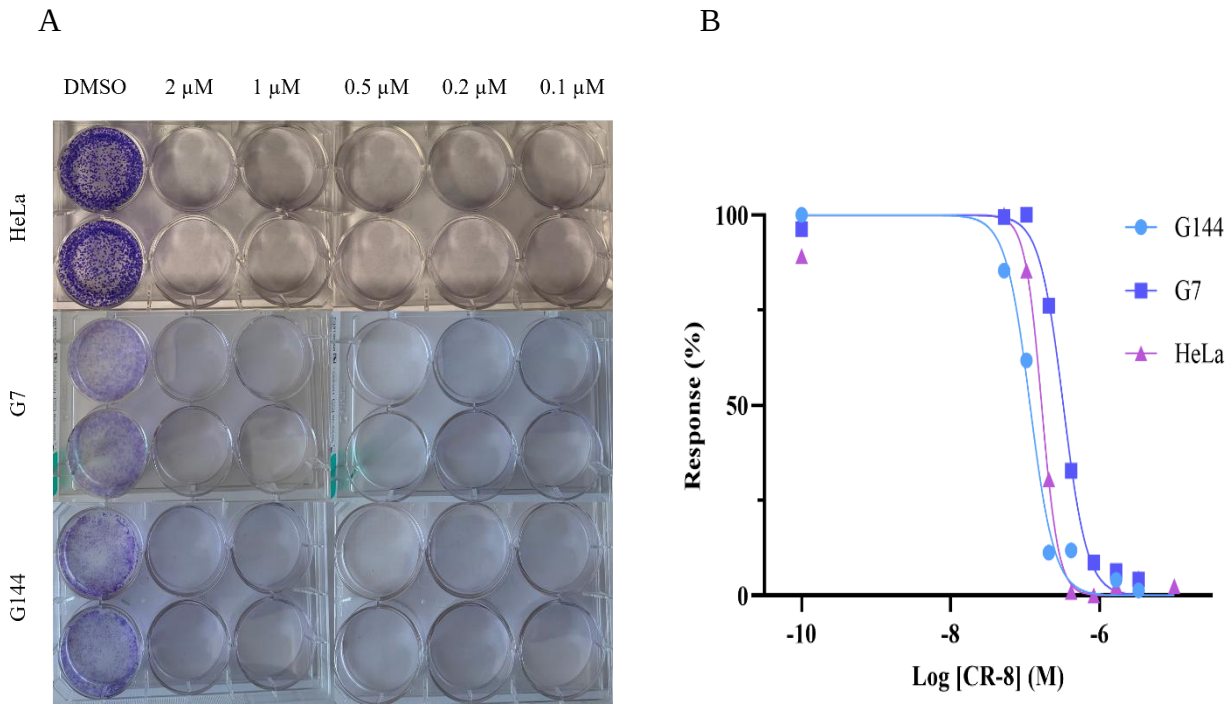

Figure 3.3 (A) Clonogenic assay for CR-8. The picture illustrates the plates used in the colony formation experiments with Hela on the upper panel, G7 in the middle and G144 on the bottom panel. The experiment was performed in duplicates with 0.04 % DMSO as control (further left well) and with a two-fold decreasing concentration of 2, 1, 0.5, 0.2 and 0.1 µM CR-8 (from left to right). **(B) Cell viability assay for CR-8.** The plot shows the IC_{50} curves constructed after treatment with CR-8 for HeLa, G7 and G144 cell lines. Three-fold dilutions spanning between 10 µM and 0.005 µM were used in the experiment. 10^{-10} was used to normalize with DMSO. The IC_{50}-values for HeLa, G7 and G144 were measured to be 1.7 x 10^{-7}, 3.3 x 10^{-7} and 1.2 x 10^{-7} M, respectively. Their correspondent R^2-values were 0.987 for HeLa, 0.990 for G7 and 0.941 for G144.

Figure 3.4 A illustrates the results obtained from the colony formation experiment after 14/(7) days treatment with LDC4297, a CDK 7 inhibitor. The experiment was performed in duplicates, with the control shown in the further left well on the picture followed by the highest LDC4297 concentration of 2 µM and down to 0.1 µM (from left to right). No parameters were changed during the 14/(7) days incubation period.

On the other hand, Figure 3.4 B illustrates the results obtained from the cell viability assay after 72 h treatment with LDC4297. The IC_{50} curves for HeLa, G7 and G144 are shown as pink, violet and blue, respectively. Eight different concentrations were employed in this experiment, these being 10 µM, 3 µM, 1 µM, 0.3 µM, 0.1 µM, 0.03 µM, 0.01 µM and 0.003 µM. The Log-values of these concentrations are shown in the x-axis of panel B. The relative fluorescent units are shown in percentage (y-axis) after normalization with DMSO. The IC_{50}-values for HeLa, G7 and G144 were measured to be 2.0 x 10^{-7}, 6.0 x 10^{-7} and 9.7 x 10^{-7} M, respectively. Their correspondent R^2-values were calculated to be 0.985 for HeLa, 0.950 for G7 and 0.881 for G144.

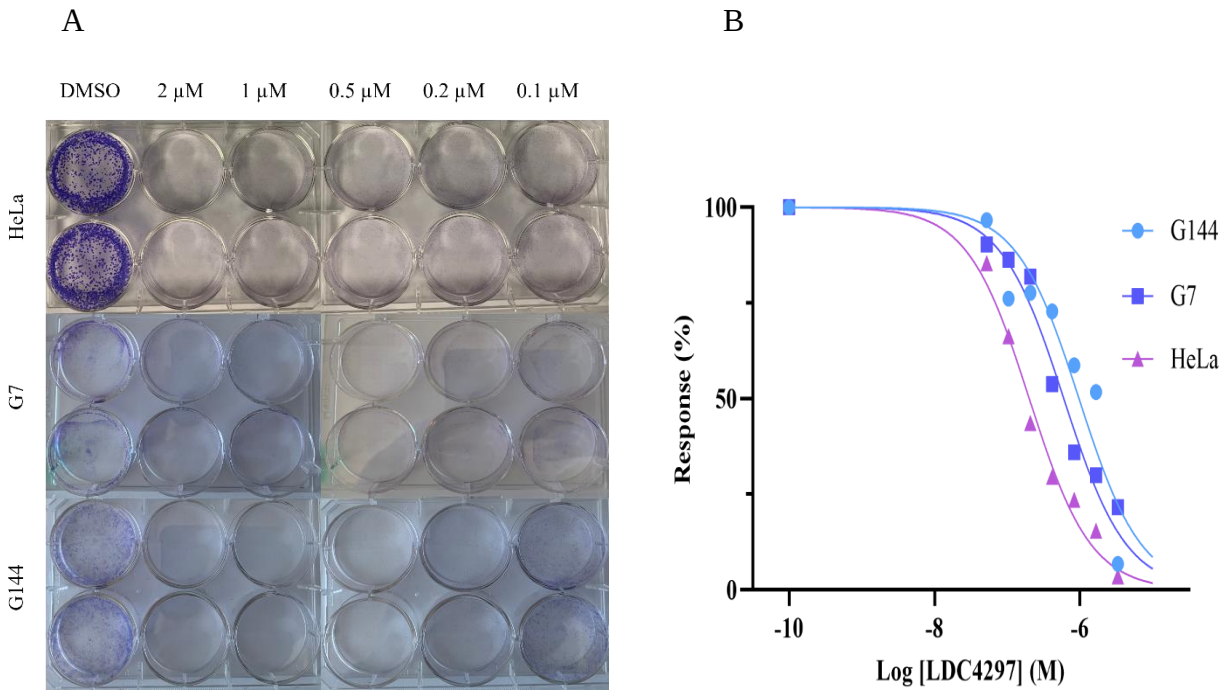

Figure 3.4 (A) Clonogenic assay for LDC4297. The picture illustrates the plates used in the colony formation experiments with Hela on the upper panel, G7 in the middle and G144 on the bottom panel. The experiment was performed in duplicates with 0.04 % DMSO as control (further left well) and with a two-fold decreasing concentration of 2, 1, 0.5, 0.2 and 0.1 µM LDC4297 (from left to right). **(B) Cell viability assay for LDC4297.** The plot shows the IC_{50} curves constructed after treatment with LDC4297 for HeLa, G7 and G144 cell lines. Three-fold dilutions spanning between 10 µM and 0.005 µM were used in the experiment. 10^{-10} was used to normalize with DMSO. The IC_{50}-values for HeLa, G7 and G144 were measured to be 2.0 x 10^{-7}, 6.0 x 10^{-7} and 9.7 x 10^{-7} M, respectively. Their correspondent R^2-values were 0.985 for HeLa, 0.950 for G7 and 0.881 for G144.

Figure 3.5 A illustrates the results obtained from the colony formation experiment after 14/(7) days treatment with NVP-2, CDK 9, as well as CDK 1, CDK 2 and CDK 16 inhibitor. The experiment was performed in duplicates, with the control shown in the further left well on the picture followed by the highest NVP-2 concentration of 2 µM and down to 0.1 µM (from left to right). No parameters were changed during the 14/(7) days incubation period.

On the other hand, Figure 3.5 B illustrates the results obtained from the cell viability assay after 72 h treatment with NVP-2. The IC_{50} curves for HeLa, G7 and G144 are shown as pink, violet and blue, respectively. Eight different concentrations were employed in this experiment, these being 10 µM, 3 µM, 1 µM, 0.3 µM, 0.1 µM, 0.03 µM, 0.01 µM and 0.003 µM. The Log-values of these concentrations are shown in the x-axis of panel B. The relative fluorescent units are shown in percentage (y-axis) after normalization with DMSO. The IC_{50}-values for HeLa, G7 and G144 were measured to be 4.9 x 10^{-8}, 1.2 x 10^{-7} and 7.0 x 10^{-8} M, respectively. Their correspondent R^2-values were calculated to be 0.994 for HeLa, 0.934 for G7 and 0.948 for G144.

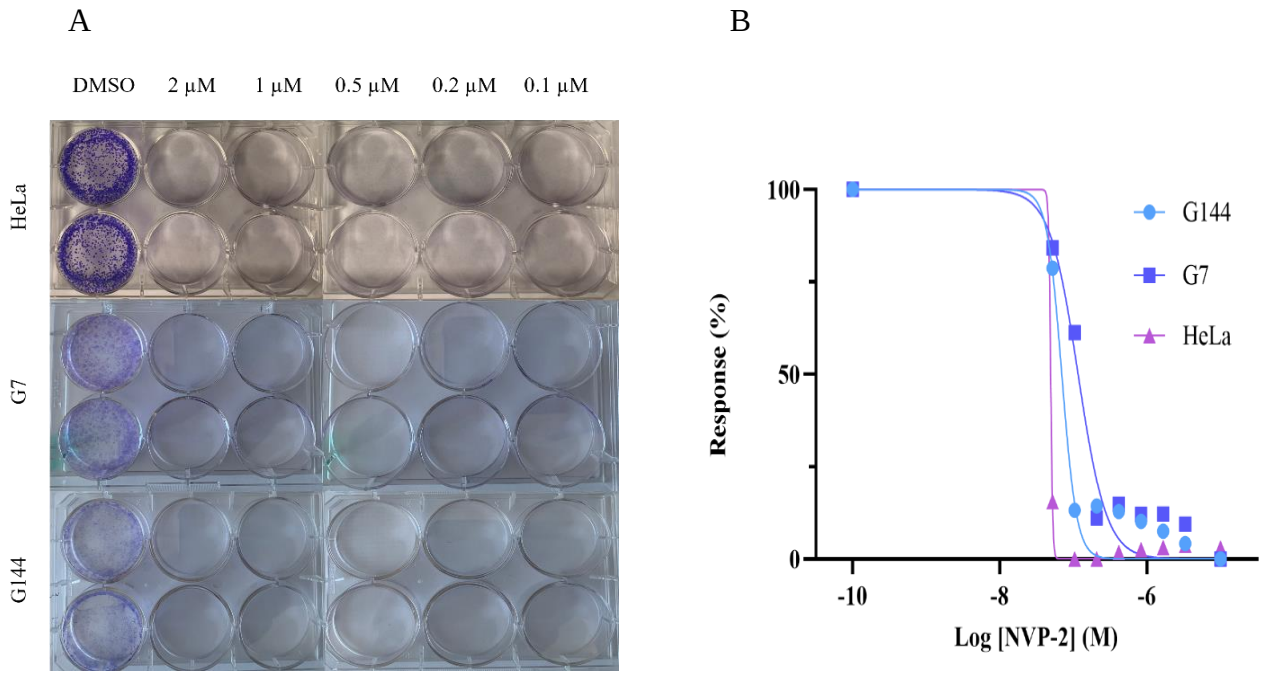

Figure 3.5 (A) Clonogenic assay for NVP-2. The picture illustrates the plates used in the colony formation experiments with Hela on the upper panel, G7 in the middle and G144 on the bottom panel. The experiment was performed in duplicates with 0.04 % DMSO as control (further left well) and with a two-fold decreasing concentration of 2, 1, 0.5, 0.2 and 0.1 µM NVP-2 (from left to right). **(B) Cell viability assay for NVP-2.** The plot shows the IC_{50} curves constructed after treatment with NVP-2 for HeLa, G7 and G144 cell lines. Three-fold dilutions spanning between 10 µM and 0.005 µM were used in the experiment. 10^{-10} was used to normalize with DMSO. The IC_{50}-values for HeLa, G7 and G144 were measured to be 4.9 x 10^{-8}, 1.2 x 10^{-7} and 7.0 x 10^{-8} M, respectively. Their correspondent R^2-values were 0.994 for HeLa, 0.934 for G7 and 0.948 for G144.

Figure 3.6 A illustrates the results obtained from the colony formation experiment after 14/(7) days treatment with PROTAC CDK9 Degrader-1. The experiment was performed in duplicates, with the control shown in the further left well on the picture followed by the highest PROTAC CDK9 Degrader-1 concentration of 2 µM and down to 0.1 µM (from left to right). No parameters were changed during the 14/(7) days incubation period.

On the other hand, Figure 3.6 B illustrates the results obtained from the cell viability assay after 72 h treatment with PROTAC CDK9 Degrader-1. The IC_{50} curves for HeLa, G7 and G144 are shown as pink, violet and blue, respectively. Eight different concentrations were employed in this experiment, these being 10 µM, 3 µM, 1 µM, 0.3 µM, 0.1 µM, 0.03 µM, 0.01 µM and 0.003 µM. The Log-values of these concentrations are shown in the x-axis of panel B. The relative fluorescent units are shown in percentage (y-axis) after normalization with DMSO. The IC_{50}-values for HeLa, G7 and G144 were measured to be 4.2 x 10^{-6}, 1.4 x 10^{-6} and 4.4 x 10^{-6} M, respectively. Their correspondent R^2-values were calculated to be 0.710 for HeLa, 0.990 for G7 and 0.893 for G144.

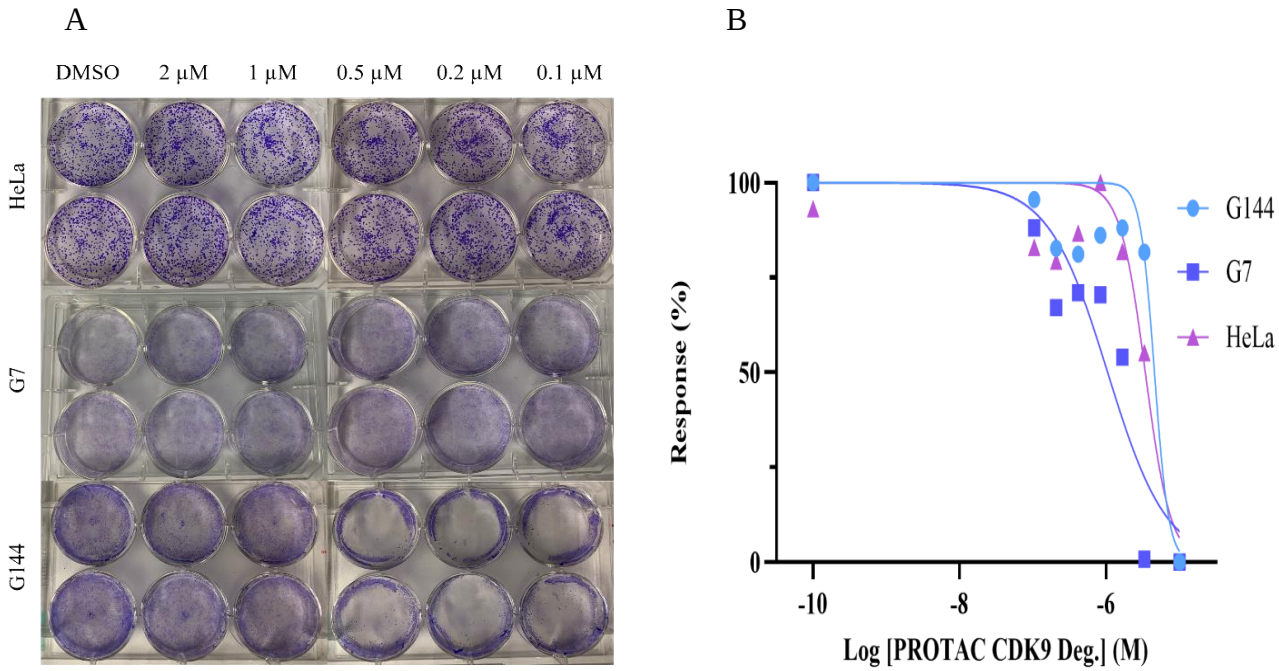

Figure 3.6 (A) Clonogenic assay for PROTAC CDK9 Degrader-1. The picture illustrates the plates used in the colony formation experiments with Hela on the upper panel, G7 in the middle and G144 on the bottom panel. The experiment was performed in duplicates with 0.04 % DMSO as control (further left well) and with a two-fold decreasing concentration of 2, 1, 0.5, 0.2 and 0.1 µM PROTAC CDK9 Degrader-1 (from left to right). **(B) Cell viability assay for PROTAC CDK9 Degrader-1.** The plot shows the IC_{50} curves constructed after treatment with PROTAC CDK9 Degrader-1 for HeLa, G7 and G144 cell lines. Three-fold dilutions spanning between 10 µM and 0.005 µM were used in the experiment. 10^{-10} was used to normalize with DMSO. The IC_{50}-values for HeLa, G7 and G144 were measured to be 4.2 x 10^{-6}, 1.4 x 10^{-6} and 4.4 x 10^{-6} M, respectively. Their correspondent R^2-values were 0.710 for HeLa, 0.990 for G7 and 0.893 for G144.

Figure 3.7 A illustrates the results obtained from the colony formation experiment after 14/(7) days treatment with RO-3306, a CDK 1 inhibitor. The experiment was performed in duplicates, with the control shown in the further left well on the picture followed by the highest RO-3306 concentration of 2 µM and down to 0.1 µM (from left to right). No parameters were changed during the 14/(7) days incubation period.

On the other hand, Figure 3.7 B illustrates the results obtained from the cell viability assay after 72 h treatment with RO-3306. The IC_{50} curves for HeLa, G7 and G144 are shown as pink, violet and blue, respectively. Eight different concentrations were employed in this experiment, these being 10 µM, 3 µM, 1 µM, 0.3 µM, 0.1 µM, 0.03 µM, 0.01 µM and 0.003 µM. The Log-values of these concentrations are shown in the x-axis of panel B. The relative fluorescent units are shown in percentage (y-axis) after normalization with DMSO. The IC_{50}-values for HeLa, G7 and G144 were measured to be 2.1 x 10^{-6}, 2.4 x 10^{-6} and 3.1 x 10^{-6} M, respectively. Their correspondent R^2-values were calculated to be 0.871 for HeLa, 0.959 for G7 and 0.988 for G144.

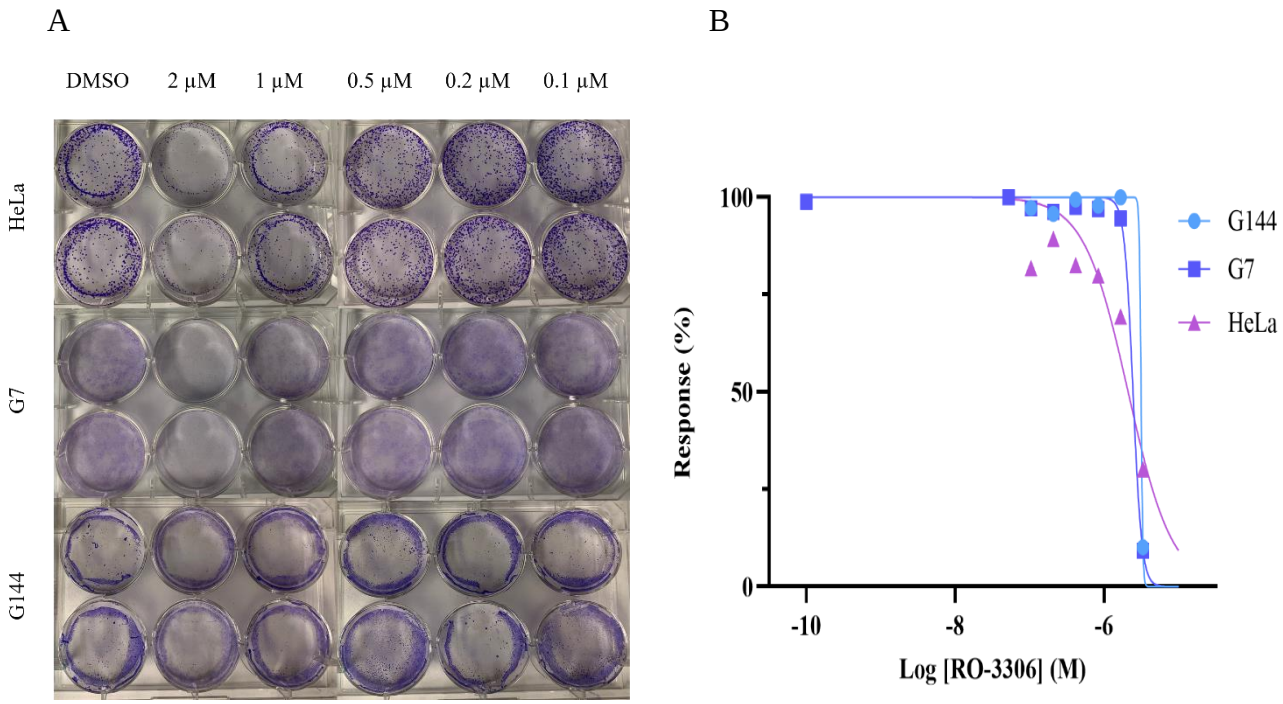

Figure 3.7 (A) Clonogenic assay for RO-3306. The picture illustrates the plates used in the colony formation experiments with Hela on the upper panel, G7 in the middle and G144 on the bottom panel. The experiment was performed in duplicates with 0.04 % DMSO as control (further left well) and with a two-fold decreasing concentration of 2, 1, 0.5, 0.2 and 0.1 µM RO-3306 (from left to right). **(B) Cell viability assay for RO-3306.** The plot shows the IC_{50} curves constructed after treatment with RO-3306 for HeLa, G7 and G144 cell lines. Three-fold dilutions spanning between 10 µM and 0.005 µM were used in the experiment. 10^{-10} was used to normalize with DMSO. The IC_{50}-values for HeLa, G7 and G144 were measured to be 2.1 x 10^{-6}, 2.4 x 10^{-6} and 3.1 x 10^{-6} M, respectively. Their correspondent R^2-values were 0.871 for HeLa, 0.959 for G7 and 0.988 for G144.

Figure 3.8 A illustrates the results obtained from the colony formation experiment after 14/(7) days treatment with SR-4835, a CDK 12/13 inhibitor. The experiment was performed in duplicates, with the control shown in the further left well on the picture followed by the highest SR-4835 concentration of 2 µM and down to 0.1 µM (from left to right). No parameters were changed during the 14/(7) days incubation period.

On the other hand, Figure 3.8 B illustrates the results obtained from the cell viability assay after 72 h treatment with SR-4835. The IC_{50} curves for HeLa, G7 and G144 are shown as pink, violet and blue, respectively. Eight different concentrations were employed in this experiment, these being 10 µM, 3 µM, 1 µM, 0.3 µM, 0.1 µM, 0.03 µM, 0.01 µM and 0.003 µM. The Log-values of these concentrations are shown in the x-axis of panel B. The relative fluorescent units are shown in percentage (y-axis) after normalization with DMSO. The IC_{50}-values for HeLa and G7 were measured to be 2.8 x 10^{-7} and 2.4 x 10^{-7} M, respectively. Their correspondent R^2-values were calculated to be 0.993 for HeLa and 0.988 for G7. Despite the efforts, no IC_{50} curve was obtained for SR-4835 treated G144 cells.

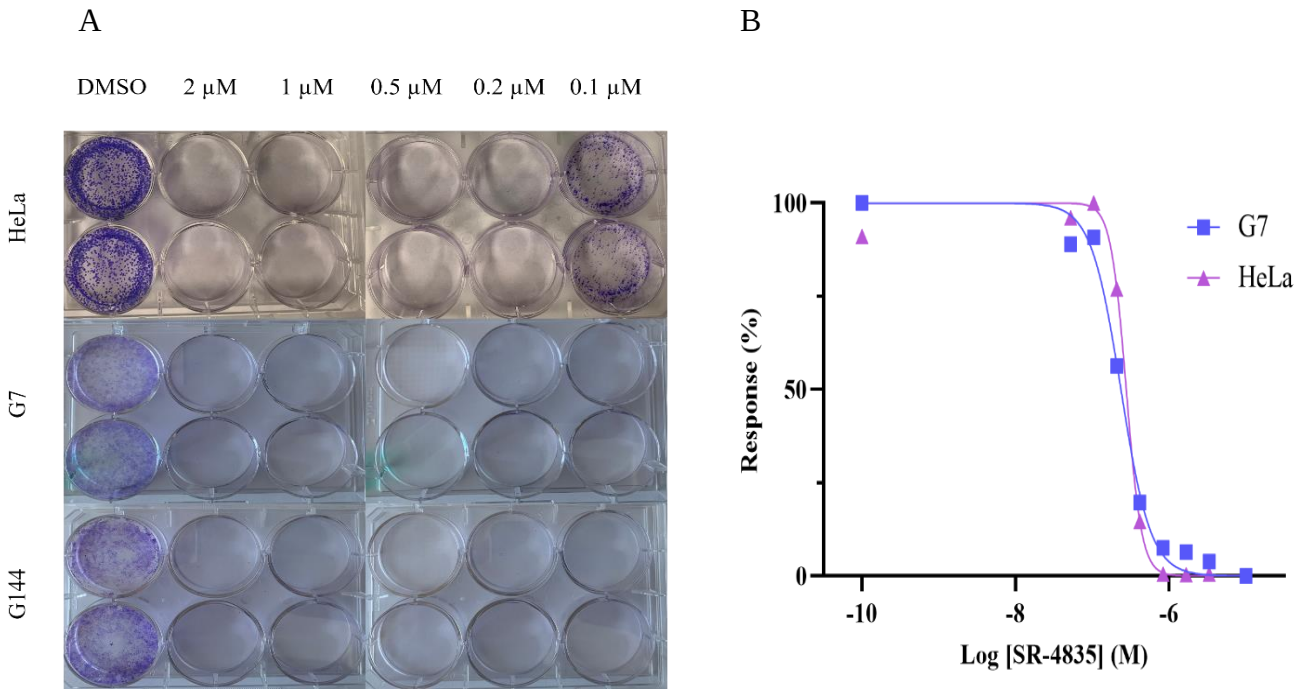

Figure 3.8 (A) Clonogenic assay for SR-4835. The picture illustrates the plates used in the colony formation experiments with Hela on the upper panel, G7 in the middle and G144 on the bottom panel. The experiment was performed in duplicates with 0.04 % DMSO as control (further left well) and with a two-fold decreasing concentration of 2, 1, 0.5, 0.2 and 0.1 µM SR-4835 (from left to right). **(B) Cell viability assay for SR-4835.** The plot shows the IC_{50} curves constructed after treatment with SR-4835 for HeLa, G7 and G144 cell lines. Three-fold dilutions spanning between 10 µM and 0.005 µM were used in the experiment. 10^{-10} was used to normalize with DMSO. The IC_{50}-values for HeLa and G7 were measured to be 2.8 x 10^{-7} and 2.4 x 10^{-7} M, respectively. Their correspondent R^2-values were 0.993 for HeLa and 0.988 for G7. Data for G144 is not shown.

Figure 3.9 A illustrates the results obtained from the colony formation experiment after 14/(7) days treatment with THZ531, a covalent CDK 12/13 inhibitor. The experiment was performed in duplicates, with the control shown in the further left well on the picture followed by the highest THZ531 concentration of 2 µM and down to 0.1 µM (from left to right). No parameters were changed during the 14/(7) days incubation period.

On the other hand, Figure 3.9 B illustrates the results obtained from the cell viability assay after 72 h treatment with THZ531. The IC_{50} curves for HeLa, G7 and G144 are shown as pink, violet and blue, respectively. Eight different concentrations were employed in this experiment, these being 10 µM, 3 µM, 1 µM, 0.3 µM, 0.1 µM, 0.03 µM, 0.01 µM and 0.003 µM. The Log-values of these concentrations are shown in the x-axis of panel B. The relative fluorescent units are shown in percentage (y-axis) after normalization with DMSO. The IC_{50}-values for HeLa, G7 and G144 were measured to be 9.4 x 10^{-7}, 9.7 x 10^{-7} and 2.2 x 10^{-7} M, respectively. Their correspondent R^2-values were calculated to be 0.985 for HeLa, 0.914 for G7 and 0.962 for G144.

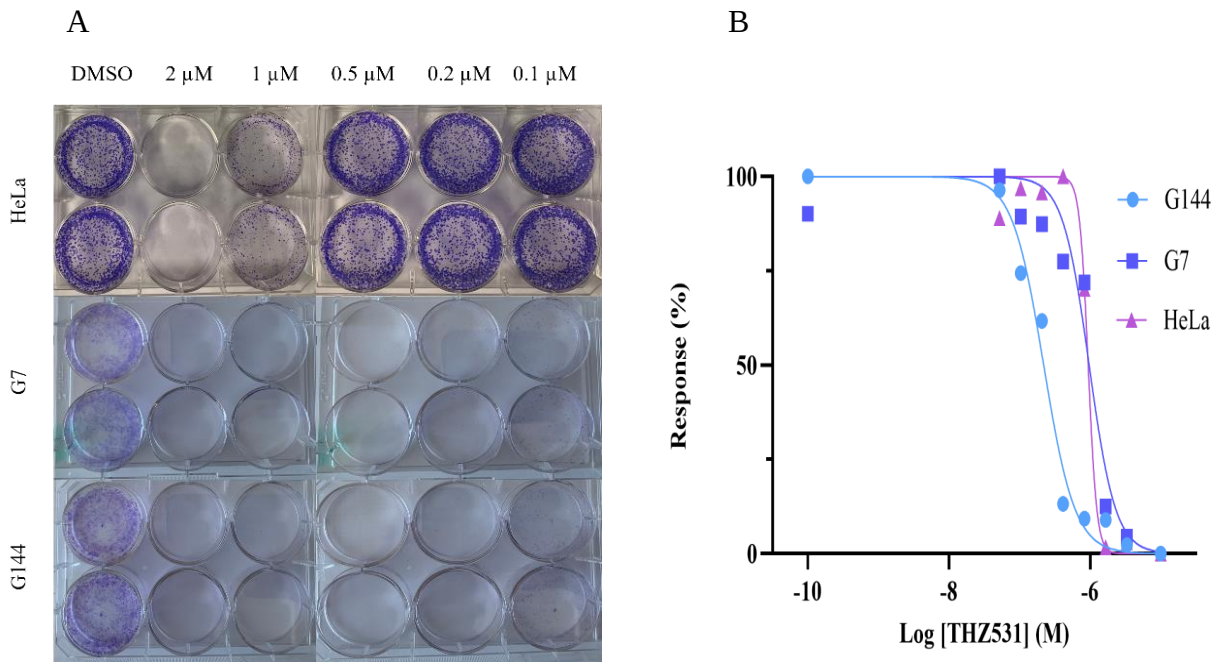

Figure 3.9 (A) Clonogenic assay for THZ531. The picture illustrates the plates used in the colony formation experiments with Hela on the upper panel, G7 in the middle and G144 on the bottom panel. The experiment was performed in duplicates with 0.04 % DMSO as control (further left well) and with a two-fold decreasing concentration of 2, 1, 0.5, 0.2 and 0.1 µM THZ531 (from left to right). **(B) Cell viability assay for THZ531.** The plot shows the IC_{50} curves constructed after treatment with THZ531 for HeLa, G7 and G144 cell lines. Three-fold dilutions spanning between 10 µM and 0.005 µM were used in the experiment. 10^{-10} was used to normalize with DMSO. The IC_{50}-values for HeLa, G7 and G144 were measured to be 9.4 x 10^{-7}, 9.7 x 10^{-7} and 2.2 x 10^{-7} M, respectively. Their correspondent R^2-values were 0.985 for HeLa, 0.914 for G7 and 0.962 for G144.

Table 3.1 summarizes the results from the cell viability experiments, illustrating the IC_{50}-values as well as the R^2 and p-values for HeLa, G7 and G144 after treatment with cell cycle and transcriptional CDK inhibitors and degraders.

Table 3.1. IC_{50}, R^2 and p-values for the cell viability experiment using cell cycle and transcriptional CDK inhibitors and degraders. The table summarizes the cell viability experiment for all three cell lines. The IC_{50}-values as well as the R^2-values are indicated in the table. In addition, the p-values from the Mann-Whitney test are shown, with glioma cells tested against HeLa.

Cell line / **Drug**	**G7**			**G144**			**HeLa**	
	IC50	***R²***	***p-value***	***IC50***	***R²***	***p-value***	***IC50***	***R²***
AUZ454	2.3 x 10^{-6}	0.96	0.079	9.2 x 10^{-7}	0.93	0.62	5.9 x 10^{-7}	0.92
BSJ-4-116	4.1 x 10^{-7}	0.97	0.12	2.3 x 10^{-7}	0.99	0.50	6.8 x 10^{-8}	0.99
CR-8	3.3 x 10^{-7}	0.99	0.40	1.2 x 10^{-7}	0.94	0.95	1.7 x 10^{-7}	0.99
LDC4297	6.0 x 10^{-7}	0.95	0.40	9.7 x 10^{-7}	0.88	0.35	2.0 x 10^{-7}	0.99

NVP-2	1.2×10^{-7}	0.93	0.080	7.0×10^{-8}	0.95	0.097	4.9×10^{-8}	0.99
PROTAC CDK9 Degrader-1	1.4×10^{-6}	0.99	0.40	4.4×10^{-6}	0.89	0.60	4.2×10^{-6}	0.71
RO-133	2.4×10^{-6}	0.96	0.17	3.1×10^{-6}	0.99	0.35	2.1×10^{-6}	0.87
SR-4835	2.4×10^{-7}	0.99	0.82	NA	NA	NA	2.8×10^{-7}	0.99
THZ531	9.7×10^{-7}	0.91	0.99	2.2×10^{-7}	0.96	0.73	9.4×10^{-7}	0.99

3.1.2 ATR protein, human topoisomerase I & II and NF-κB activation inhibitors

In addition, drugs targeting ATR protein, human topoisomerase I and II and NF-κB activator were tested on all cell lines used in the study. This included well characterized drugs such as Doxorubicin, Etoposide and Triptolide.

Figure 3.10 A illustrates the results obtained from the colony formation experiment after 14/(7) days treatment with ATR inhibitor 2. The experiment was performed in duplicates, with the control shown in the further left well on the picture followed by the highest ATR inhibitor 2 concentration of 2 µM and down to 0.1 µM (from left to right). No parameters were changed during the 14/(7) days incubation period.

On the other hand, Figure 3.10 B illustrates the results obtained from the cell viability assay after 72 h treatment with ATR inhibitor 2. The IC_{50} curves for HeLa, G7 and G144 are shown as pink, violet and blue, respectively. Eight different concentrations were employed in this experiment, these being 10 µM, 3 µM, 1 µM, 0.3 µM, 0.1 µM, 0.03 µM, 0.01 µM and 0.003 µM. The Log-values of these concentrations are shown in the x-axis of panel B. The relative fluorescent units are shown in percentage (y-axis) after normalization with DMSO. The IC_{50}-values for HeLa, G7 and G144 were measured to be 3.9×10^{-7}, 7.9×10^{-7} and 1.2×10^{-6} M, respectively. Their correspondent R^2-values were calculated to be 0.985 for HeLa, 0.976 for G7 and 0.971 for G144.

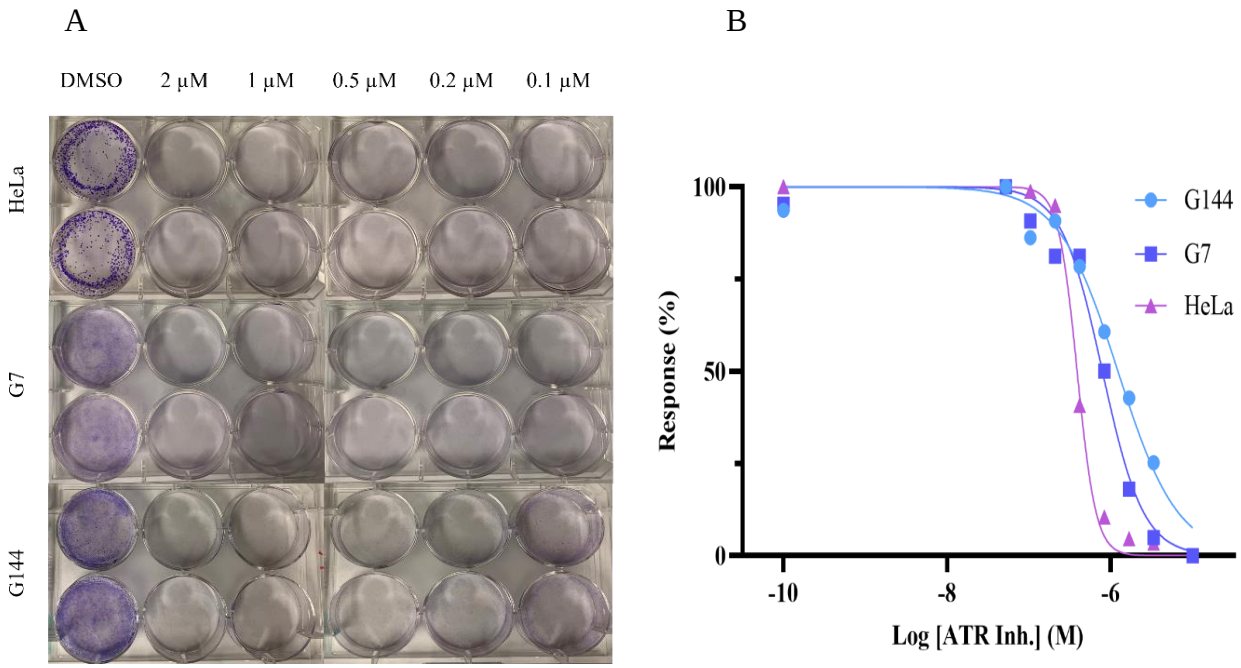

Figure 3.20 (A) Clonogenic assay for ATR inhibitor 2. The picture illustrates the plates used in the colony formation experiments with Hela on the upper panel, G7 in the middle and G144 on the bottom panel. The experiment was performed in duplicates with 0.04 % DMSO as control (further left well) and with a two-fold decreasing concentration of 2, 1, 0.5, 0.2 and 0.1 µM ATR inhibitor 2 (from left to right). **(B) Cell viability assay for ATR inhibitor 2.** The plot shows the IC_{50} curves constructed after treatment with ATR inhibitor 2 for HeLa, G7 and G144 cell lines. Three-fold dilutions spanning between 10 µM and 0.005 µM were used in the experiment. 10^{-10} was used to normalize with DMSO. The IC_{50}-values for HeLa, G7 and G144 were measured to be 3.9 x 10^{-7}, 7.9 x 10^{-7} and 1.2 x 10^{-6} M, respectively. Their correspondent R^2-values were 0.985 for HeLa, 0.976 for G7 and 0.971 for G144.

Figure 3.11 A illustrates the results obtained from the colony formation experiment after 14/(7) days treatment with AZ20, an ATR and mTOR inhibitor. The experiment was performed in duplicates, with the control shown in the further left well on the picture followed by the highest AZ20 concentration of 2 µM and down to 0.1 µM (from left to right). No parameters were changed during the 14/(7) days incubation period.

On the other hand, Figure 3.11 B illustrates the results obtained from the cell viability assay after 72 h treatment with AZ20. The IC_{50} curves for HeLa, G7 and G144 are shown as pink, violet and blue, respectively. Eight different concentrations were employed in this experiment, these being 10 µM, 3 µM, 1 µM, 0.3 µM, 0.1 µM, 0.03 µM, 0.01 µM and 0.003 µM. The Log-values of these concentrations are shown in the x-axis of panel B. The relative fluorescent units are shown in percentage (y-axis) after normalization with DMSO. The IC_{50}-values for HeLa, G7 and G144 were measured to be 8.2 x 10^{-7}, 5.6 x 10^{-7} and 1.2 x 10^{-6} M, respectively. Their correspondent R^2-values were calculated to be 0.987 for HeLa, 0.974 for G7 and 0.963 for G144.

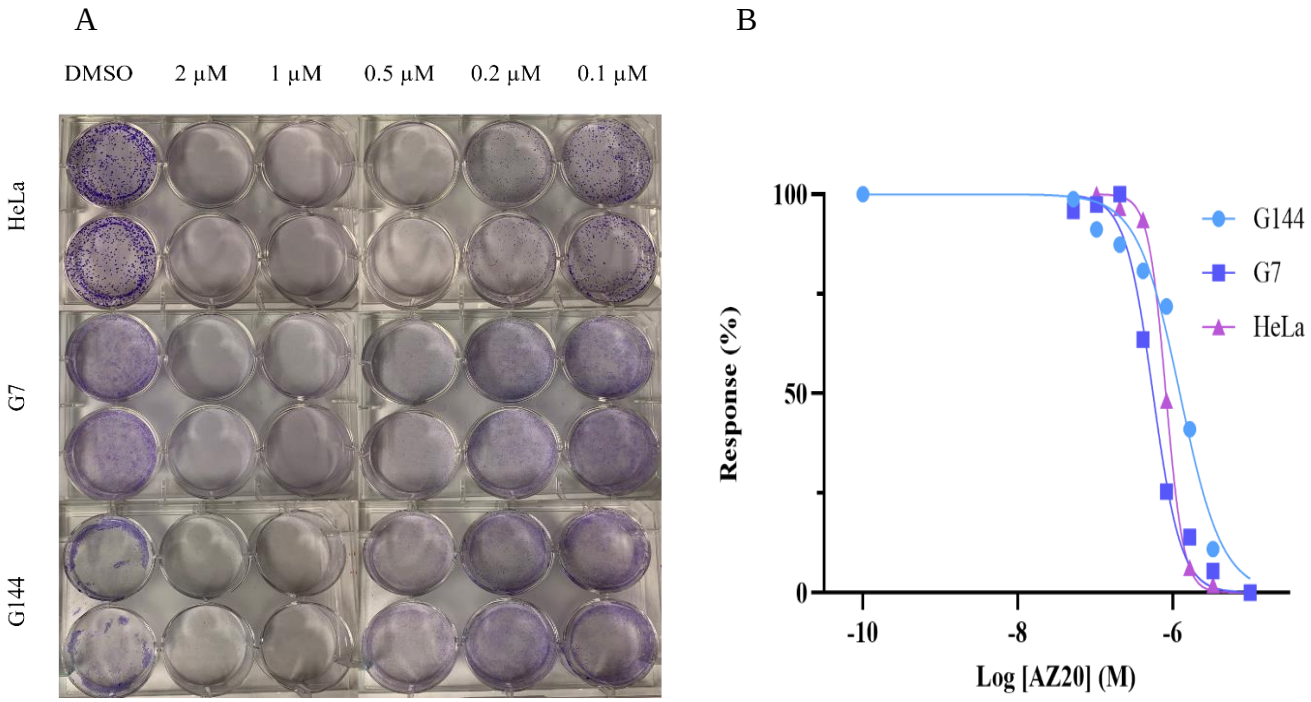

Figure 3.31 (A) Clonogenic assay for AZ20. The picture illustrates the plates used in the colony formation experiments with Hela on the upper panel, G7 in the middle and G144 on the bottom panel. The experiment was performed in duplicates with 0.04 % DMSO as control (further left well) and with a two-fold decreasing concentration of 2, 1, 0.5, 0.2 and 0.1 µM AZ20 (from left to right). **(B) Cell viability assay for AZ20.** The plot shows the IC_{50} curves constructed after treatment with AZ20 for HeLa, G7 and G144 cell lines. Three-fold dilutions spanning between 10 µM and 0.005 µM were used in the experiment. 10^{-10} was used to normalize with DMSO. The IC_{50}-values for HeLa, G7 and G144 were measured to be 8.2 x 10^{-7}, 5.6 x 10^{-7} and 1.2 x 10^{-6} M, respectively. Their correspondent R^2-values were 0.987 for HeLa, 0.974 for G7 and 0.963 for G144.

Figure 3.12 A illustrates the results obtained from the colony formation experiment after 14/(7) days treatment with Doxorubicin, an inhibitor of human topoisomerase I and II. The experiment was performed in duplicates, with the control shown in the further left well on the picture followed by the highest Doxorubicin concentration of 2 µM and down to 0.1 µM (from left to right). No parameters were changed during the 14/(7) days incubation period.

On the other hand, Figure 3.12 B illustrates the results obtained from the cell viability assay after 72 h treatment with Doxorubicin. The IC_{50} curves for HeLa, G7 and G144 are shown as pink, violet and blue, respectively. Eight different concentrations were employed in this experiment, these being 10 µM, 3 µM, 1 µM, 0.3 µM, 0.1 µM, 0.03 µM, 0.01 µM and 0.003 µM. The Log-values of these concentrations are shown in the x-axis of panel B. The relative fluorescent units are shown in percentage (y-axis) after normalization with DMSO. The IC_{50}-values for HeLa, G7 and G144 were measured to be 8.3 x 10^{-8}, 4.0 x 10^{-7} and 3.8 x 10^{-7} M, respectively. Their correspondent R^2-values were calculated to be 0.994 for HeLa, 0.947 for G7 and 0.962 for G144.

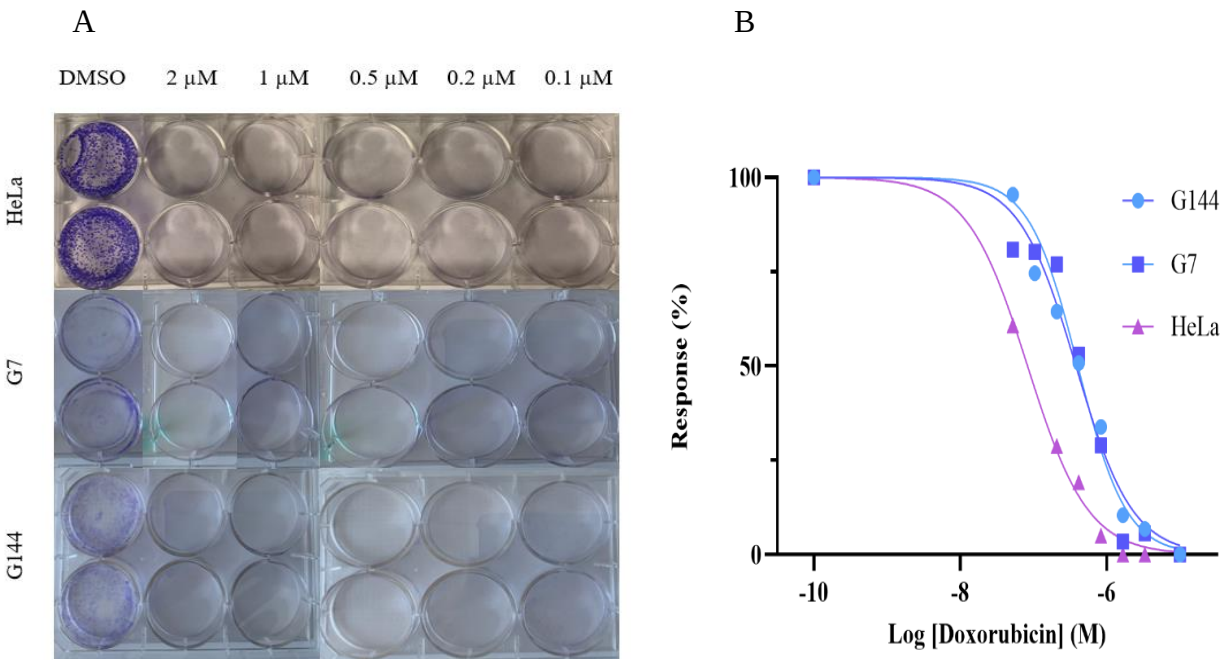

Figure 3.42 (A) Clonogenic assay for Doxorubicin. The picture illustrates the plates used in the colony formation experiments with Hela on the upper panel, G7 in the middle and G144 on the bottom panel. The experiment was performed in duplicates with 0.04 % DMSO as control (further left well) and with a two-fold decreasing concentration of 2, 1, 0.5, 0.2 and 0.1 µM Doxorubicin (from left to right). **(B) Cell viability assay for Doxorubicin.** The plot shows the IC_{50} curves constructed after treatment with Doxorubicin for HeLa, G7 and G144 cell lines. Three-fold dilutions spanning between 10 µM and 0.005 µM were used in the experiment. 10^{-10} was used to normalize with DMSO. The IC_{50}-values for HeLa, G7 and G144 were measured to be 8.3 x 10^{-8}, 4.0 x 10^{-7} and 3.8 x 10^{-7} M, respectively. Their correspondent R^2-values were 0.994 for HeLa, 0.947 for G7 and 0.962 for G144.

Figure 3.13 A illustrates the results obtained from the colony formation experiment after 14/(7) days treatment with Etoposide, an inhibitor of topoisomerase II. The experiment was performed in duplicates, with the control shown in the further left well on the picture followed by the highest Etoposide concentration of 2 µM and down to 0.1 µM (from left to right). No parameters were changed during the 14/(7) days incubation period.

On the other hand, Figure 3.13 B illustrates the results obtained from the cell viability assay after 72 h treatment with Etoposide. The IC_{50} curves for HeLa, G7 and G144 are shown as pink, violet and blue, respectively. Eight different concentrations were employed in this experiment, these being 10 µM, 3 µM, 1 µM, 0.3 µM, 0.1 µM, 0.03 µM, 0.01 µM and 0.003 µM. The Log-values of these concentrations are shown in the x-axis of panel B. The relative fluorescent units are shown in percentage (y-axis) after normalization with DMSO. The IC_{50}-values for HeLa, G7 and G144 were measured to be 6.0 x 10^{-7}, 3.4 x 10^{-7} and 1.1 x 10^{-6} M, respectively. Their correspondent R^2-values were calculated to be 0.988 for HeLa, 0.975 for G7 and 0.955 for G144.

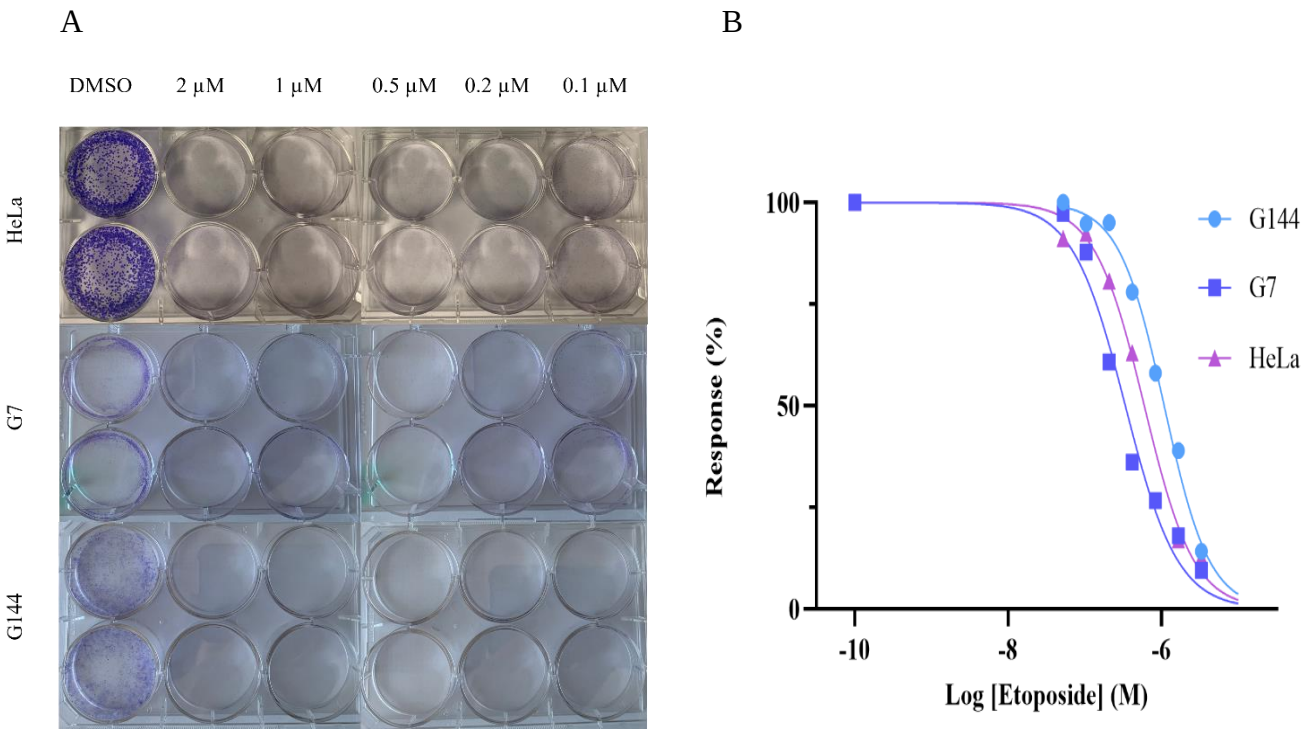

Figure 3.53 (A) Clonogenic assay for Etoposide. The picture illustrates the plates used in the colony formation experiments with Hela on the upper panel, G7 in the middle and G144 on the bottom panel. The experiment was performed in duplicates with 0.04 % DMSO as control (further left well) and with a two-fold decreasing concentration of 2, 1, 0.5, 0.2 and 0.1 µM Etoposide (from left to right). **(B) Cell viability assay for Etoposide.** The plot shows the IC_{50} curves constructed after treatment with Etoposide for HeLa, G7 and G144 cell lines. Three-fold dilutions spanning between 10 µM and 0.005 µM were used in the experiment. 10^{-10} was used to normalize with DMSO. The IC_{50}-values for HeLa, G7 and G144 were measured to be 6.0 x 10^{-7}, 3.4 x 10^{-7} and 1.1 x 10^{-6} M, respectively. Their correspondent R^2-values were 0.988 for HeLa, 0.975 for G7 and 0.955 for G144.

Figure 3.14 A illustrates the results obtained from the colony formation experiment after 14/(7) days treatment with Triptolide, a NF-κB activation inhibitor. The experiment was performed in duplicates, with the control shown in the further left well on the picture followed by the highest Triptolide concentration of 2 µM and down to 0.1 µM (from left to right). No parameters were changed during the 14/(7) days incubation period.

On the other hand, Figure 3.14 B illustrates the results obtained from the cell viability assay after 72 h treatment with Triptolide. The IC_{50} curves for HeLa, G7 and G144 are shown as pink, violet and blue, respectively. Eight different concentrations were employed in this experiment, these being 10 µM, 3 µM, 1 µM, 0.3 µM, 0.1 µM, 0.03 µM, 0.01 µM and 0.003 µM. The Log-values of these concentrations are shown in the x-axis of panel B. The relative fluorescent units are shown in percentage (y-axis) after normalization with DMSO. The IC_{50}-values for HeLa, G7 and G144 were measured to be 3.0 x 10^{-8}, 1.5 x 10^{-7} and 1.2 x 10^{-7} M, respectively. Their correspondent R^2-values were calculated to be 0.999 for HeLa, 0.973 for G7 and 0.975 for G144.

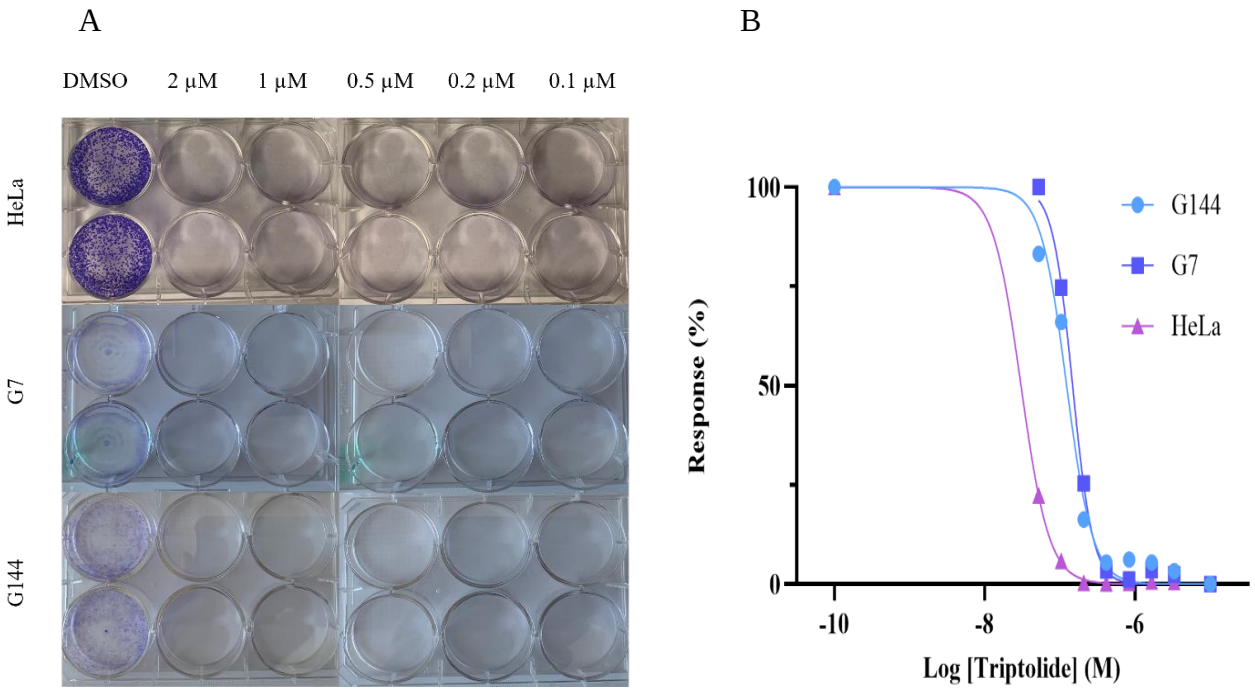

Figure 3.64 (A) Clonogenic assay for Triptolide. The picture illustrates the plates used in the colony formation experiments with Hela on the upper panel, G7 in the middle and G144 on the bottom panel. The experiment was performed in duplicates with 0.04 % DMSO as control (further left well) and with a two-fold decreasing concentration of 2, 1, 0.5, 0.2 and 0.1 µM Triptolide (from left to right). **(B) Cell viability assay for Triptolide.** The plot shows the IC_{50} curves constructed after treatment with Triptolide for HeLa, G7 and G144 cell lines. Three-fold dilutions spanning between 10 µM and 0.005 µM were used in the experiment. 10^{-10} was used to normalize with DMSO. The IC_{50}-values for HeLa, G7 and G144 were measured to be 3.0 x 10^{-8}, 1.5 x 10^{-7} and 1.2 x 10^{-7} M, respectively. Their correspondent R^2-values were 0.999 for HeLa, 0.973 for G7 and 0.975 for G144.

Table 3.2 summarizes the results from the cell viability experiments, illustrating the IC_{50}-values as well as the R^2 and p-values for HeLa, G7 and G144 after treatment with ATR inhibitor 2 as well as human topoisomerase I and II and NF-κB activator inhibitors.

Table 3.2. IC_{50}, R^2 and p-values for the cell viability experiment using ATR, human topoisomerase I & II and NF-κB activator inhibitors. The table summarizes the cell viability experiment for all three cell lines. The IC_{50}-values as well as the R^2-values are indicated in the table. In addition, the p-values from the Mann-Whitney test are shown, with glioma cells tested against HeLa.

Cell line / Drug	G7			G144			HeLa	
	IC50	***R²***	***p-value***	***IC50***	***R²***	***p-value***	***IC50***	***R²***
ATR inhibitor 2	7.9 x 10^{-7}	0.98	0.63	1.2 x 10^{-6}	0.97	0.63	3.9 x 10^{-7}	0.99
AZ20	5.6 x 10^{-7}	0.97	0.81	1.2 x 10^{-6}	0.96	0.78	8.2 x 10^{-7}	0.99
Doxorubicin (hydrochloride)	4.0 x 10^{-7}	0.95	0.25	3.8 x 10^{-7}	0.96	0.21	8.3 x 10^{-8}	0.99
Etoposide	3.4 x 10^{-7}	0.98	0.77	1.1 x 10^{-6}	0.96	0.90	6.0 x 10^{-7}	0.99
Triptolide	1.5 x 10^{-7}	0.97	0.21	1.2 x 10^{-7}	0.98	0.17	3.0 x 10^{-8}	0.99

3.2 Fluorescence-activated cell sorting analysis

In order to study the effect of the pharmacological tools on the cell cycle, fluorescence-activated cell sorting analysis was performed for glioma cells, more specifically for G144 cells. These were grown in their corresponding medium and seeded accordantly to section 2.2 and appendix B, thus approximately 300 000 (24 h treatment) and 500 000 (6 h treatment) cells for treatments to be done in two-days' time or next day, respectively. Only nine of the pharmacological tools described in Table 2.1 were employed in the FACS experiment, these being BSJ-4-116, CR-8, DRB, LDC4297, NVP-2, PROTAC CDK9 Degrader-1, SR-4835, THZ531 and Triptolide. A BD™ LSR II Flow Cytometer operating with UV, 405, 488 and 633 nm line lasers was utilized in the experiment. In addition, a bandpass filter of 450/50 nm was employed for UV excitation, while a bandpass filter of 780/60 nm and a longpass dichroic filter of 735 nm were used for the near IR excitation. The samples were run at low flow rate of 12 µl/min and the voltage for forward and side scattering as well as for Live/Dead and Hoechst stain were adjusted to 260, 230, 500 and 227 V, respectively. The data was acquired by usage of the BD FACSDiva™ software, while the post-analysis was performed using FlowJo™ v10 software and Microsoft 365® Excel.

Figure 3.15 A illustrates the overlap Hoechst signal between DMSO (orange) and 3 µM LDC4297 (blue) treated cells originating from the 24 h FACS experiment. 9243 and 8633 single cells were analysed for DMSO and 3 µM LDC4297, respectively. In addition, the analysed single cells were quantified accordantly to their cellular stage, thus categorizing them into G1, S and G2+M phase. This is depicted in Figure 3.15 panel B, where control cells (DMSO) indicate a distribution of 55, 36 and 9 % for G1, S and G2+M phase, respectively. The distribution for 3 µM LDC4297 treated cells was calculated to be 48, 28 and 23 % for G1, S and G2+M phase, respectively.

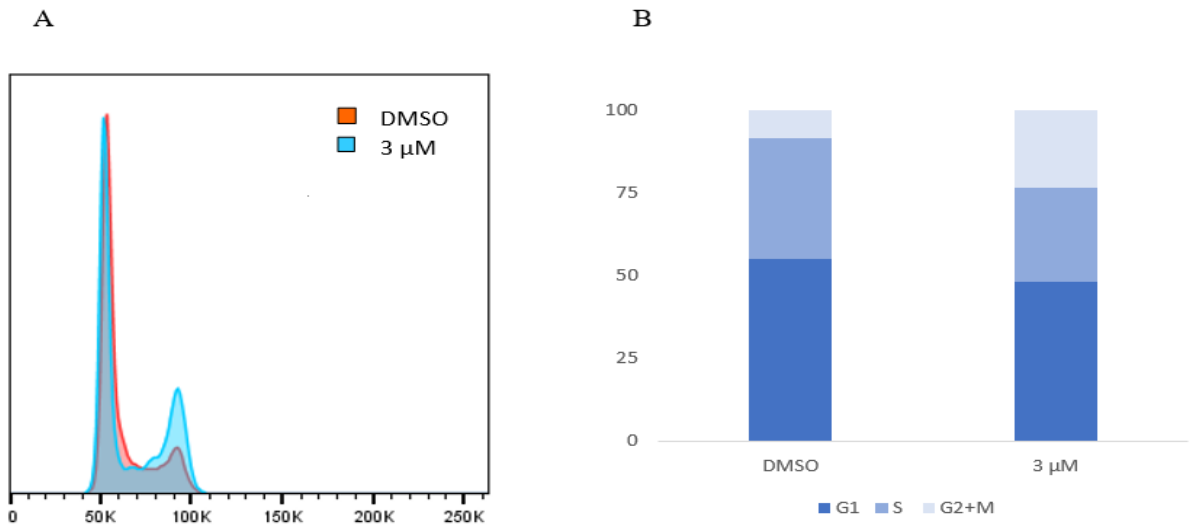

Figure 3.15 (A) Cell cycle analysis by FACS for 24 h LDC4297 treated cells. The figure illustrates the results obtained from the FACS experiment performed after treatment of G144 cells with LDC4297. The overlap Hoechst signal for DMSO and 3 µM treatment are shown, where 9243 and 8633 single cells were analysed, respectively. **(B) Quantification of cell cycle for 24 h LDC4297 treated cells.** The diagram depicts the distribution of the cell cycle for both DMSO and 3 µM treatment in percentage. The analysis was done by FlowJo analytical software and Microsoft 365® Excel.

Figure 3.16 A illustrates the overlap Hoechst signal between DMSO (orange) and 3 µM PROTAC CDK 9 Degrader-1 (blue) treated cells originating from the 24 h FACS experiment. 3923 and 9181 single cells were analysed for DMSO and 3 µM PROTAC CDK 9 Degrader-1, respectively. In addition, the analysed single cells were quantified accordantly to their cellular stage, thus categorizing them into G1, S and G2+M phase. This is depicted in Figure 3.16 panel B, where control cells (DMSO) indicate a distribution of 50, 40 and 10 % for G1, S and G2+M phase, respectively. The distribution for 3 µM PROTAC CDK 9 Degrader-1 treated cells was calculated to be 73, 21 and 7 % for G1, S and G2+M phase, respectively.

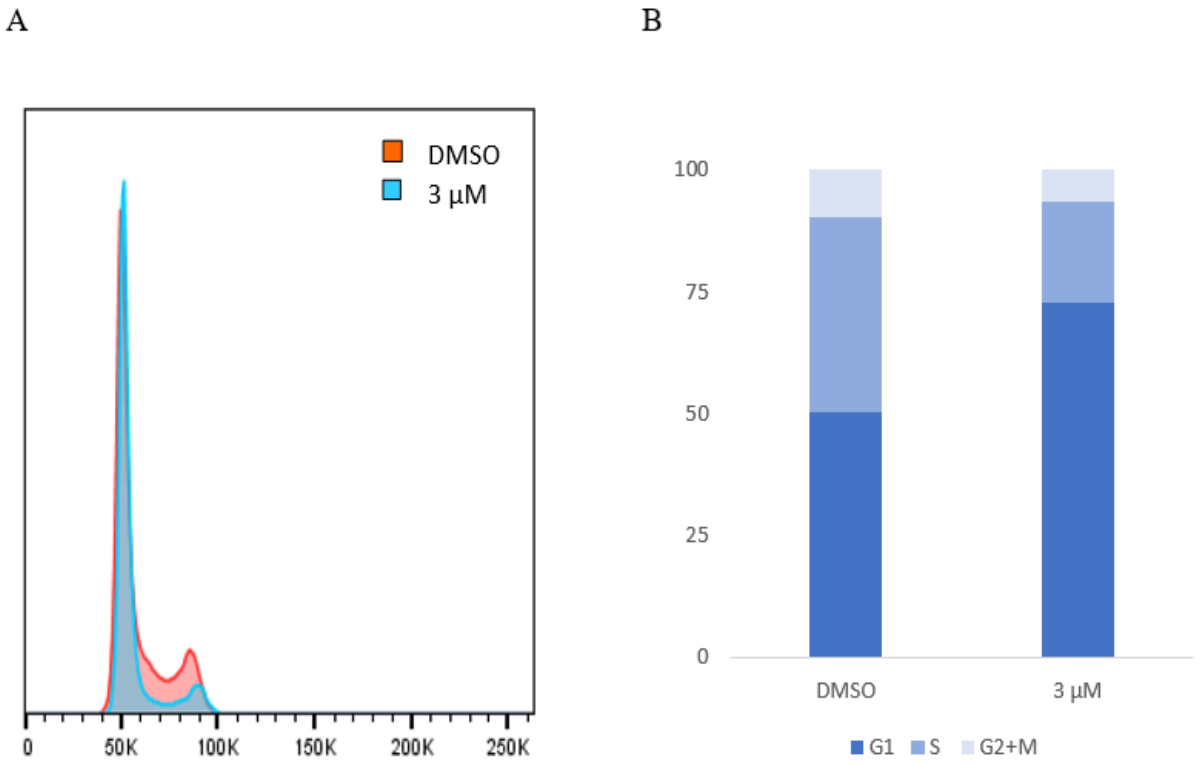

Figure 3.16 (A) Cell cycle analysis by FACS for 24 h PROTAC CDK 9 Degrader-1 treated cells. The figure illustrates the results obtained from the FACS experiment performed after treatment of G144 cells with PROTAC CDK 9 Degrader-1. The overlap Hoechst signal for DMSO and 3 µM treatment are shown, where 3923 and 9181 single cells were analysed, respectively. **(B) Quantification of cell cycle for 24 h PROTAC CDK 9 Degrader-1 treated cells.** The diagram depicts the distribution of the cell cycle for both DMSO and 3 µM treatment in percentage. The analysis was done by FlowJo analytical software.

Figure 3.17 A illustrates the overlap Hoechst signal between DMSO (orange) and 3 µM SR-4835 (blue) treated cells originating from the 24 h FACS experiment. 9243 and 8633 single cells were analysed for DMSO and 3 µM SR-4835, respectively. In addition, the analysed single cells were quantified accordantly to their cellular stage, thus categorizing them into G1, S and G2+M phase. This is depicted in Figure 3.17 panel B, where control cells (DMSO) indicate a distribution of 51, 40 and 9 % for G1, S and G2+M phase, respectively. The distribution for 3 µM SR-4835 treated cells was calculated to be 52, 24 and 24 % for G1, S and G2+M phase, respectively.

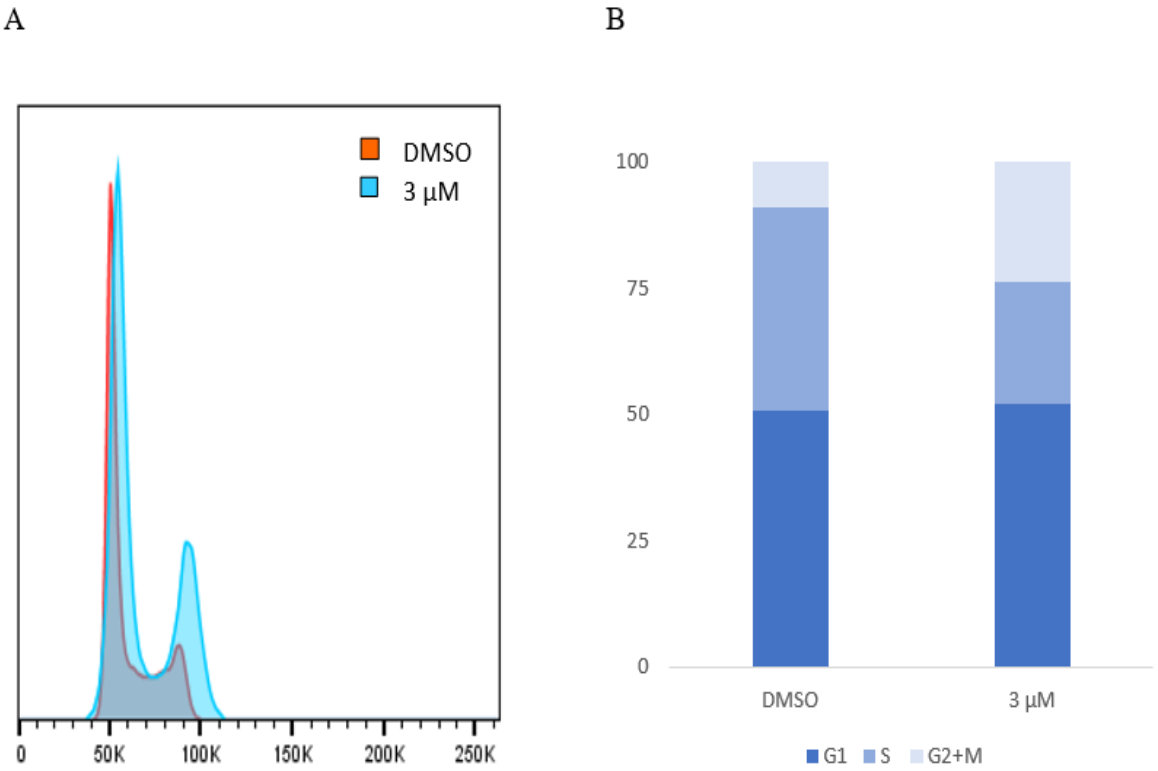

Figure 3.17 (A) Cell cycle analysis by FACS for 24 h SR-4835 treated cells. The figure illustrates the results obtained from the FACS experiment performed after treatment of G144 cells with SR-4835. The overlap Hoechst signal for DMSO and 3 µM treatment are shown, where 7876 and 7535 single cells were analysed, respectively. **(B) Quantification of cell cycle for 24 h SR-4835 treated cells.** The diagram depicts the distribution of the cell cycle for both DMSO and 3 µM treatment in percentage. The analysis was done by FlowJo analytical software.

4. Discussion

As previously discussed in this report, genetic diseases such as cancer are becoming more common among the global population, thus increasing the need to find new strategies to combat this condition. For instance, brain and nervous system cancer represent one of the deadliest forms of this diseases, with median overall survival of just over one year after diagnosis and accounting for 1.6 % of all fatalities in 2020 [60]. Moreover, Glioblastoma Multiforme (GBM) accounts for the most advanced and severe form of brain cancer, with less than 5-10 % of people surviving longer than five years after diagnosis [60].

Foregoing studies [64-66] indicate that genomic alternations leading to constitutive activation of CDK´s are a common factor for many cancer forms, including gliomas. For instance, brain cancer malignancies proliferate through the recruitment of several CDK´s early in G1 phase, and genomic instability in gliomas appears to be related to disturbances in S phase and in the transition between G2 and M phase [2]. For this reason, numerous synthetically created CDK Inhibitors (CKI´s) have been studied in relation to cancer, with some of them making their way to the clinics [68]. However, preclinical and clinical trials have generated mixed results over the past decades, giving a non-definite conclusion regarding the effectiveness of these therapeutics, especially on brain cancer [2].

In this study G-cells were exposed to several pharmacological tools targeting cell cycle and transcription at different levels, and the results compared against HeLa cells treated with the same set of inhibitors and/or degraders. Ideally, results showing a statistically significant difference between G-cells and HeLa, where G-cells respond “better” at a lower drug dosage than HeLa (HeLa survives), are of particular interest for our research group. Such findings may elucidate addictions in gliomas that are specific for this type of cancer, thus given better chance at developing tailored strategies to combat this disease.

4.1 Cell viability assays and colony formation experiments

In order to further elucidate the underlaying mechanisms that stimulate the aggressiveness (proliferation, invasion, resistance, etc) of GBM in higher eukaryotes, different type of pharmacological tools targeting both transcriptional and cell cycle related CDK´s (CDK 1, CDK 2, CDK 5, CDK 7, CDK 9 and CDK 12/13) as well as drugs targeting ATR protein, human topoisomerase I and II and NF-κB activator were tested on all cell lines studied in this project. For this, a set of molecular techniques including cell viability assays and colony formation assays together with fluorescence activated cell sorting were applied in order to characterize the effect of these pharmaceutics on glioma cells. Studying the effect of these drugs through such techniques could also shed light to the *in vivo* role of the above-mentioned proteins in relation to brain cancer proliferation, more specifically in GBM, and give an insight into their effect on the cell cycle.

For this purpose, all three cell lines used in the cell viability and clonogenic experiments were grown in their corresponding medium and seeded accordantly to section 2.2 and appendix B. The pharmacological tools, as described in Table 2.1, were employed in the experiments and IC_{50} curves were constructed for the cell viability experiments. On the other hand, only visual analysis was employed for the clonogenic assays, as illustrated through section 3.1, and no quantification was performed due to lack of time.

The cell viability experiments were conducted by taking advantage of the reducing capabilities of live cells in culture. For this, PrestoBlue reagents were employed as signalling dye compounds, hence making possible the construction of IC_{50} curves by using a multimode plate reader, where relative fluorescence signal was plotted against drug concentration (section 2.2.1 and 3.1). The collected data was processed with GraphPad Prism 9 software, normalizing the samples to the positive control (DMSO), and using a variable slope model as shown in section 3.1. Normalization was conducted in order to obtain the relative IC_{50}-values, thus showing how much concentration is required to lower the response by 50 % given the range of data acquired. On the other hand, the variable slope model was chosen after performing a series of statistical tests (F tests) comparing the available models in Prism 9 (data not shown).

The clonogenic assays were performed by treating HeLa cells for 7 days and G-cells for 14 days. During these periods, colonies were formed and consequently stained with crystal staining reagent, allowing an easier visual analysis of the dose-response effect in the different cell lines. It is important to remark that no parameters were changed during the 14/(7) days incubation period (section 2.3 and 3.1).

4.1.1 Cell cycle and transcriptional CDK inhibitors and degraders

A variety of cell cycle and transcriptional CDK inhibitors and degraders were studied in the first part of the project (section 3.1.1). Five different concentrations were employed on HeLa, G7 and G144 cells for the clonogenic assays, these being 2, 1, 0.5, 0.2 and 0.1 µM, while eight different concentrations were employed in the cell viability experiments, these being 10, 3, 1, 0.3, 0.1, 0.03, 0.01 and 0.003 µM.

Previous to results discussion, it is important to have in mind that several factors may have directly or indirectly affected the results obtained from the experiments. For example, the overall treatment effect on cells in culture may partially depend on the cell´s cellular stage and growth rate. For instance, HeLa, with a doubling rate of about 23 h [81] will undergo approximately three division rounds during the 72 h duration of the experiment, while G-cells, with a doubling rate of approximately 48 h [82], will at best undergo 1.5 divisions. This fact may also partially explain the differences in the IC_{50}-values between HeLa and G-cells. Hence, it can be hypothesized that these drugs do present a slightly "stronger" effect on HeLa as they undergo almost double as many divisions compared to G-cells in the

72 h treatment period. However, the differences in growth rate were taken into account by reducing the level of seeded HeLa cells in all experiments. Still, it is important to have this in mind as technical errors may occur during the experimental work.

Furthermore, the condition in which the cells were passed may also have influenced the results obtained. As with many other cells, G-cells are much dependent on having a thriving growth medium in order to proliferate optimally. If coating, growth medium or other parameters such as temperature were not to be ideally adjusted, the consequences could have resulted in improper cell division and eventually cellular death. These are also parameters that could have influenced the results of the experiments. In addition, cellular permeability is another major factor to be considered when performing pharmacological studies, and especially when simultaneously working with distinct cell lines. Factors such as molecular weight and lipophilicity may limit target exposure to the drug and thereby affect the treatment to be performed. Glioma cells tend to "group" and form spherical-like shapes when densely growing, and literature demonstrates [83] that GBM is characterized by histopathological heterogeneity. Moreover, high-resolution sequencing has shown that GBM also features significant inter-tumour molecular heterogeneity [84], thus making the treatment response vary between cells originating from different GBM tumours. This fact may explain why G7 and G144 respond slightly different to some drugs in the performed treatments (section 3.1).

As it can be observed from Figure 3.1 and table 3.1, the survival of HeLa cells appears to be more compromised than in G-cells after AUZ454 treatment. IC_{50}-values equivalent to 5.9×10^{-7}, 2.3×10^{-6} and 9.2×10^{-7} M for HeLa, G7 and G144, respectively, were measured for the experiment. Their correspondent R^2-values were calculated to be 0.918 for HeLa, 0.963 for G7 and 0.930 for G144. The R^2-values here are not meant to serve as direct measure of goodness-of-fit of the model, but more as a parameter indicating reproducibility of the results obtained from the cell viability experiments. In addition, Mann-Whitney test was employed in order to reveal any statistical significance between HeLa and G-cells. No significant results (≤ 0.05) were obtained, and the p-values for G7 and G144 were estimated to be 0.08 and 0.6, respectively. Figure 3.1 A also shows that HeLa proliferation is already affected during the 1 µM treatment, while G-cells appear to "survive" this level of toxicity. It is important to notice that in some of the wells in the colony formation experiment cells have detached from the central area of the surface. This problem occurred after the washing step following colony staining and may be caused by overgrowth of the cells or improper coating. The washing step could also have been further optimized, given the nature of G-cells. This is valid for the remaining clonogenic assays performed in the study that are affected in a similar manner.

On the other hand, from Figure 3.3 and table 3.1 it can be observed that treatment with CR-8 appears to slightly affect G144 more than HeLa, but the same is not true for G7. IC_{50}-values equivalent to 1.7×10^{-7}, 3.3×10^{-7} and 1.2×10^{-7} M for HeLa, G7 and G144, respectively, were measured for the experi-

ment. Their correspondent R^2-values were calculated to be 0.987 for HeLa, 0.990 for G7 and 0.941 for G144. The p-values for G7 and G144 were estimated to be 0.4 and 0.9, respectively, thus no statistical significance was found when comparing G7 against HeLa. Figure 3.3 A shows that CR-8 has a highly toxic effect on all cell lines in the studied concentration range, inhibiting the formation of colonies.

Figure 3.5 and table 3.1 also show that HeLa proliferation is inhibited at lower dosage than G-cells when treated with NVP-2. IC_{50}-values equivalent to 4.9×10^{-8}, 1.2×10^{-7} and 7.0×10^{-8} M for HeLa, G7 and G144, respectively, were measured for the experiment. Their correspondent R^2-values were calculated to be 0.994 for HeLa, 0.934 for G7 and 0.948 for G144. The p-values for G7 and G144 were estimated to be 0.08 and 0.1, respectively. Figure 3.5 A shows that HeLa proliferation as well as proliferation of G-cells is equally affected throughout all concentrations applied in the colony formation experiment.

Results from the treatment with RO-3306, as shown in Figure 3.7, depict that there is no significant difference between HeLa and G-cells. IC_{50}-values equivalent to 2.1×10^{-6}, 2.4×10^{-6} and 3.1×10^{-6} M for HeLa, G7 and G144, respectively, were measured for the experiment. Their correspondent R^2-values were calculated to be 0.871 for HeLa, 0.959 for G7 and 0.988 for G144. The p-values for G7 and G144 were estimated to be 0.2 and 0.4, respectively. Figure 3.7 A shows that G7 appears to be compromised at 2 µM while HeLa and G144 form small colonies on the plate at the same toxicity level. However, this should be further tested in order to verify the results.

Interestingly, a study on live cells performed by Wells et. al. [85] has shown that small pharmaceutical tools inhibiting CDK 1 and CDK 2 present poor selectivity, and in fact target other member of the CDK family as for example CDK 14-18, which in turn are not well defined. This phenomenon can be explained by the fact that most of the synthetically designed CDKI´s do target the ATP binding site of the CDK´s, which is highly conserved across the CDK enzyme family. Unspecific binding may lead to undesired side effects, increasing the cytotoxicity of these drugs, and making them potent killers of all types of cells, including cancer cells as well as healthy cells. Naturally, poorly specific inhibitors are usually not a good choice for the development of any type of pharmaceuticals but may still be useful in for example categorizing function and vitality of the target proteins in the light of cell survival. The fact that CDK inhibitors targeting CDK 1 and 2 are not target specific may partially explain the results obtained for treatments with AUZ454, CR-8, NVP-2 and RO-3306. As described above, both HeLa and G-cells were similarly affected, with no statistically significant differences in neither colony formation nor cell viability assays.

Once again, Figure 3.4 and table 3.1 illustrate that the survival of HeLa cells appears to be more compromised than in G-cells after LDC4297 treatment. IC_{50}-values equivalent to 2.0×10^{-7}, 6.0×10^{-7} and 9.7×10^{-7} M for HeLa, G7 and G144, respectively, were measured for the experiment. Their correspondent R^2-values were calculated to be 0.985 for HeLa, 0.950 for G7 and 0.881 for G144. The p-

values for G7 and G144 were estimated to be 0.4 for both cell lines. Figure 3.4 A also shows that HeLa proliferation is inhibited throughout all concentrations in the treatment, while G-cells appear to form small colonies at 0.1 µM.

Cell treatment with PROTAC CDK 9 Degrader-1 was problematic as signals obtained from the plate reader tended to vary greatly. Construction of IC_{50}-curves was achieved at the end, but the results did not fit well the chosen model. This can be observed from Figure 3.6 and table 3.1, especially when analysing the R^2-values. IC50-values equivalent to 4.2×10^{-6}, 1.4×10^{-6} and 4.4×10^{-6} M for HeLa, G7 and G144, respectively, were measured for the experiment. Their correspondent R^2-values were calculated to be 0.710 for HeLa, 0.990 for G7 and 0.893 for G144. The p-values for G7 and G144 were estimated to be 0.4 and 0.6, respectively. Figure 3.6 A also shows that the drug has no effect at all on the cells, or at least not a visual one. Interestingly, statistically significant results were achieved when analysing the effect of PROTAC CDK 9 Degrader-1 on the cell cycle of G-cells by FACS. This will be discussed further below in this section.

The previous mentioned study [85] has also demonstrated that many of the CDKI´s targeting CDK 4/6 as well as those targeting CDK 7 and 9 do present a high level of selectivity towards their target, with few examples presenting collateral inhibition of other members of this enzyme family. One such example is LDC4297, a highly selective CDK 7 inhibitor. Moreover, Wells et. al. [85] have shown that LDC4297 was actually less selective than previously reported, in addition presenting engagement with other members of the CDK family (CDK 1-6, for example). This, and the fact that CDK 7 inhibitors have an effect on both cell cycle and transcription makes them into highly potent toxic agents. The high levels of cytotoxicity may partially explain the results obtained after HeLa and G-cells treatment with LDC4297, as depicted above.

DRB, a CDK 9 inhibitor, was also among the tested drugs, but non-reliable results were obtained after treatment of HeLa and G-cells. A possible explanation may be short stability in DMSO and improper storage of the drug. In addition, the CDK 9 degrader-1 (PROTAC) studied in this project did also present complications, with no clear explanation for the obtained results. Theoretically, CDK 9 inhibitions should result in shut down of transcription and activation of apoptosis by p53, but no apparent effect resulted from the colony formation assays. Higher concentration may be needed for this drug in order to achieve a cytotoxic effect. Similarly, varying the concentration range for some of the pharmacological tools used in the study may have resulted in better results, especially when constructing the dosage-response curves.

From Figure 3.8 A it can be observed that the survival of G-cells appears to be more compromised than in HeLa cells after SR-4835 treatment. HeLa cells seem to survive the 0.1 µM treatment, while growth of G7 is inhibited at the same concentration. However, similar IC_{50}-values were obtained for both G7 and HeLa, these being 2.8×10^{-7} and 2.4×10^{-7} M for HeLa and G7, respectively. Their corre-

spondent R^2-values were calculated to be 0.993 for HeLa and 0.988 for G7. The p-value for G7 was estimated to be 0.8. Due to experimental complications, no valid results were obtained for G144 in regard to the cell viability experiment, hence no IC_{50}-curve was constructed for this cell line.

THZ531, a drug heavily studied in our research group, gave interesting findings when tested on G-cells and HeLa. Figure 3.9 A shows that the growth of G-cells is inhibited already at low concentrations (100 nm), while HeLa appears to be visually unaffected up to 500 nm treatment, when compared to the positive control DMSO. However, the IC_{50}-values were once again of no statistical significance, as they were measured to be 9.4×10^{-7}, 9.7×10^{-7} and 2.2×10^{-7} M for HeLa, G7 and G144, respectively. Their correspondent R^2-values were calculated to be 0.985 for HeLa, 0.914 for G7 and 0.962 for G144. The p-values for G7 and G144 were estimated to be 0.9 and 0.7, respectively.

Figure 3.2 and table 3.1 illustrate that the survival of HeLa cells is again more compromised than in G-cells after BSJ-4-116 treatment. IC_{50}-values equivalent to 6.8×10^{-8}, 4.1×10^{-7} and 2.3×10^{-7} M for HeLa, G7 and G144, respectively, were measured for the experiment. Their correspondent R^2-values were calculated to be 0.991 for HeLa, 0.970 for G7 and 0.989 for G144. The p-values for G7 and G144 were estimated to be 0.1 and 0.5, respectively. Figure 3.2 A also shows that HeLa proliferation is affected by all concentrations in the treatment, while G-cells show colony formation at already 0.2 µM and clear survival at 0.1 µM.

The CDK 12/13 inhibitors studied in this project, specially THZ531, did show a slightly higher effect on G-cells when compared to the control cell line. A study performed by Iniguez et. al. [86] did show that inhibition of proliferation after treatment with THZ531 in Ewing sarcoma was successful already at nanomolar concentration (100 nM). Similarly, here we have demonstrated that proliferation of G-cells is highly compromised, while the control cell line appears to be almost unaffected after 500 nM treatment. Moreover, a recent study by Fan et. al. [87] has shown that single inhibition of either CDK 12 or 13 does not compromise cell viability significantly, while dual inhibition, as in THZ531 and SR-4835, seems to severely affect viability and proliferation. However, here we have demonstrated that the same is not true when using a highly selective CDK 12 degrader, namely BSJ-4-116. This drug appears to inhibit proliferation in both HeLa and G-cells in a similar manner. A possible explanation may be that degraders do not compete for the active site of the CDK, as most of the inhibitors do, enhancing their overall efficiency and resulting in a better dosage effect. However, this theory should be tested in order to verify this statement.

4.1.2 ATR protein, human topoisomerase I & II and NF-κB activation inhibitors

In addition, drugs targeting ATR protein, human topoisomerase I and II and NF-κB activator were studied in the second part of the project (section 3.1.2). This included well characterized pharmaceuticals such as Doxorubicin, Etoposide and Triptolide.

As it can be observed from Figure 3.10 and table 3.2, the cytotoxicity of ATR inhibitor 2 appears to affect both HeLa and G-cells in a similar manner, with HeLa reacting at lower dosage. IC_{50}-values equivalent to 3.9 x 10^{-7}, 7.9 x 10^{-7} and 1.2 x 10^{-6} M for HeLa, G7 and G144, respectively, were measured for the experiment. Their correspondent R^2-values were calculated to be 0.985 for HeLa, 0.976 for G7 and 0.971 for G144. The p-values for G7 and G144 were both estimated to be 0.6. Figure 3.10 A also shows that HeLa proliferation is affected throughout all concentrations, while G144 appears to proliferate at 0.1 µM forming small colonies. However, these may not be of significance given their weak signal, and the experiment should be repeated in order to prove this fact. The cell response to AZ20 treatment was stronger for G7 compared to HeLa, and weaker for G144 compared to HeLa. IC_{50}-values equivalent to 8.2 x 10^{-7}, 5.6 x 10^{-7} and 1.2 x 10^{-6} M for HeLa, G7 and G144, respectively, were measured for the experiment. Their correspondent R^2-values were calculated to be 0.987 for HeLa, 0.974 for G7 and 0.963 for G144. The p-values for G7 and G144 were both estimated to be 0.8. However, Figure 3.11 A shows that HeLa proliferation is already totally inhibited during the 0.5 µM treatment, while G-cells appear to "survive" this level of toxicity, with a very weak staining signal.

It is previously reported [88] that high levels of endogenous ssDNA are found in many cancer forms, which in turn is the main activator of ATR kinase. ssDNA originating from double stranded DNA breaks or simply from replication stress are some examples of how this pathway is activated. However, not all cancers present high levels of ssDNA, and indeed, this fact may affect the cytotoxicity of some inhibitors targeting ATR. A study on pancreatic cancer [89] did show that AZ20 treatment did not result in significant tumour reduction, as growth inhibition was affected but cell death appeared to be limited. Here we have demonstrated that cell proliferation after AZ20 treatment is also compromised, with G7 responding slightly better to the drug compared with G144 and the control cell line. However, these results were not statistically significant. In addition, the colony formation experiment implies that both HeLa and G-cells proliferation are similarly affected by AZ20, which could be interpreted as both cell present comparable levels of endogenous ssDNA. However, this remains unclear and has to be verified in order to support this hypothesis. On the other hand, ATR inhibitor 2 did compromise both cell lines proliferation at lower concentration levels (already at 100 nM), but similarly to AZ20, no statistically significance was observed for neither G7 or G144.

Doxorubicin appears to affect HeLa proliferation in a much lower dosage compared to G-cells. This can be observed from Figure 3.12 B and table 3.2, where IC_{50}-values equivalent to 8.3 x 10^{-8}, 4.0 x 10^{-7} and 3.8 x 10^{-7} M for HeLa, G7 and G144, respectively, were measured for the experiment. Their correspondent R^2-values were calculated to be 0.994 for HeLa, 0.947 for G7 and 0.962 for G144. The p-values for G7 and G144 were estimated to be 0.3 and 0.2, respectively. Figure 3.12 A shows that both HeLa and G-cell proliferation is totally inhibited even at the lowest concentration of Doxorubicin.

On the other hand, Figure 3.13 B and table 3.2 illustrate that G7 reacts better to the Etoposide treatment, when compared to HeLa, with almost 50 % lower dosage needed to reach IC_{50}. The IC_{50}-values were measured to be 6.0×10^{-7}, 3.4×10^{-7} and 1.1×10^{-6} M for HeLa, G7 and G144, respectively. Their correspondent R^2-values were calculated to be 0.988 for HeLa, 0.975 for G7 and 0.955 for G144. The p-values for G7 and G144 were estimated to be 0.8 and 0.9, respectively, thus no statistical significance was found for G7 neither. Figure 3.13 A shows that proliferation is inhibited in all cell lines throughout all concentrations in the experiment. In addition, a weak signal for DMSO can be observed for G-cells, depicting a possible culturing problem (coating, seeding or medium issues) or improper passage of the cells.

Doxorubicin and Etoposide have been reported [90] to successfully penetrate the blood-brain barrier and induce cellular death by inhibiting topoisomerase activity. However, the study [90] argues that mixed results have been obtained by different authors, emphasizing the importance to further study this poisons and their effect on brain cancer. Here we have demonstrated that both Doxorubicin and Etoposide compromise colony formation in all cell lines throughout the selected range of concentrations and in fact Etoposide appears to have a better effect on G7 when compared with HeLa and G144. However, the same is not true for Doxorubicin, where HeLa responds better to the treatment than G-cells. This may be explained by the varying expression levels of topoisomerase I and II between cell lines as well as the permeability features of the different drugs, as mentioned above.

During the last decades, drugs targeting NF-κB activation have been attractive tools to study several diseases, including cancer. A study performed by Bredel et. al. [91] did demonstrate that certain mutations such as deletion of the *NFKBIA* gene (a natural repressor of NF-κB) in non-classical glioblastomas resulted in a similar effect as amplification of EGFR, hence augmenting glioblastoma pathogenesis and reducing survival. Triptolide, a naturally occurring anti-cancer compound, has been widely studied and associated to inhibit NF-κB activation. In addition, Titov et. al. [92] depicts that Triptolide has an important role as inhibitor of RNA polymerase II mediated transcription as it binds to the XPB subunit of TFIIH and inhibits its DNA-dependent ATPase activity. The latter mentioned features of Triptolide makes it a potent killer of any type of cells, and this is demonstrated in our study. Figure 3.14 and table 3.2 show the experiments involving Triptolide treatment. Again, HeLa seems to be more susceptible to this specific drug, when compared to G-cells. IC_{50}-values equivalent to 3.0×10^{-8}, 1.5×10^{-7} and 1.2×10^{-7} M for HeLa, G7 and G144, respectively, were measured for the experiment. Their correspondent R^2-values were calculated to be 0.999 for HeLa, 0.973 for G7 and 0.975 for G144. The p-values for G7 and G144 were both estimated to be 0.2. On the other hand, Figure 3.14 A shows that both HeLa and G-cell proliferation is totally inhibited throughout all concentrations applied in the assay.

4.2 Fluorescence-activated cell sorting analysis

In order to study the effect of the above discussed pharmacological tools on the cell cycle, fluorescence-activated cell sorting analysis was performed for glioma cells, more specifically for G144 cells. The choice to proceed with solely one G-cell line was made accordingly to the results obtained from the colony formation and cell viability experiments. Thus, given their similarity (no statistical difference) in responding to the employed drugs and the lack of time, it was easier to determine the effect on the cell cycle on one single cell line.

For this, G144 was grown in its corresponding medium and seeded accordantly to section 2.2 and appendix B, thus approximately 300 000 (24 h treatment) and 500 000 (6 h treatment) cells for treatments to be done in two-days' time or next day, respectively. Only nine of the pharmacological tools described in Table 2.1 were employed in the FACS experiment, these being BSJ-4-116, CR-8, DRB, LDC4297, NVP-2, PROTAC CDK9 Degrader-1, SR-4835, THZ531 and Triptolide.

LDC4297, SR-4835 and PROTAC CDK9 Degrader-1 were the only compounds found to exhibit a significant effect on the cell cycle of G144 cells, when compared to the vehicle. Results obtained for the remaining drugs did not present any significant difference between DMSO and treatment, and some of them were discarded as result of technical difficulties. Challenges such as obtaining enough number of cells in the final samples is one example of technical difficulties that were faced in the study. Due to lack of time, these treatments were not repeated. Interestingly, the 6 h treatment did not result in any significant difference between untreated and treated cells at any tested concentration (raw data not shown). This phenomenon may be explained by the fact that 6 h is a very promptly timepoint to expect a significant drug effect on cell cycle of G-cells, as these have a doubling time of around 48 h, as mentioned above. On the other hand, the 24 h treatment did show a significant difference in both 1 µM (not shown) and 3 µM treatments, when compared to the vehicle.

24 h treatment with 3 µM LDC4297 did result in a cell cycle distribution of 48, 28 and 23 % for G1, S and G2+M phase, respectively. On the other hand, the distribution for untreated G144 cells was calculated to be 55, 36 and 9 % for G1, S and G2+M phase, respectively. This is illustrated in Figure 3.15 B. As previously discussed, Wells et. al. [85] did demonstrate that inhibition of CDK 7 by LDC4297 is not as specific as previously though, and in fact collateral targeting of other CDK members were observed. The observed effect in this study can be explained by the fact that CDK 7 inhibition, as well as weaker unspecific inhibition of other CDK members (CDK 1-6), will eventually lead to cell cycle arrest at the G2/M phase and thereby inhibit cell proliferation. This was demonstrated in a study performed by Zhong et. al. [93]. Similarly, here we observe a decrease in number of cells found in G2/M phase after LDC4297, with 23 % for DMSO and 9 % for treated cells. Interestingly, despite the fact that no visible effect was observed after treatment with PROTAC CDK 9 Degrader-1 in the clonogenic assays, FACS analysis did demonstrate that cell cycle progression is being compromised following

treatment with the PROTAC. This may be explained by the fact that even though cell progression is being compromised, treatment with the drug does not lead to cell death, or at least not with the employed concentrations. It is also important to remark that the performed FACS analysis (live-dead and Hoechst staining) only gives a snapshot of the cell cycle, and in order to obtain information about, for example, amount of apoptotic cells and similar conditions the analysis should be extended to a wider number of biomarkers. As depicted in Figure 3.16 panel B, 24 h treatment with 3 µM PROTAC CDK9 Degrader-1 resulted in a cell cycle distribution of 73, 21 and 7 % for G1, S and G2+M phase, respectively. The distribution for the vehicle was calculated to be 50, 40 and 10 % for G1, S and G2+M phase, respectively. This results in a difference of 23 % for the G1 phase and 19 % for the S phase. These results imply that degradation of CDK 9 results in cell cycle arrest at G1 phase. This was also observed by Bettencourt et. al. [94] when studying kinases required for cell cycle progression. This phenomenon is explained by the fact that bromodomain protein 4 and jumonji C-domain-containing protein induce promoter-proximal pause release by interacting with positive TF-Eb and simultaneously activate the expression of key G1 phase genes. The latter mentioned are of crucial importance for G1/S phase progression, and when downregulated cell cycle arrest at G1 phase takes place.

3 µM SR-4835 treatment (24 h) resulted in a cell cycle distribution of 52, 24 and 24 % for G1, S and G2+M phase, respectively. On the other hand, control cells indicate a distribution of 51, 40 and 9 % for G1, S and G2+M phase, respectively. This is shown in Figure 3.17 panel B. As also mentioned earlier, disturbances in transcription through CDK 12/13 inhibition may lead to cell cycle progression inhibition due to the collateral interactions with other members of the CDK enzyme family. These results depict that the cells are being arrested in M/G1 phase check point (15 % difference between control and treated cells), a fact that may pin-point towards a possible effect of SR-4835 on M phase cyclins and/or CDK´s required for cell cycle progression.

4.3 Perspectives

These experimental results can be further considered concrete only through repetition of the experiments with robust reproducibility. This would ensure the credibility of the results and a confirmation of the resulted outcome. In addition, further experimental work focusing on more advanced cell viability assays as for example CellTiter-Glo or RealTime-Glo may enhance the construction of IC_{50}-curves and result in more precise determination of the dosage-response effect for the desired pharmaceuticals. Supplementary quantification of the clonogenic assays may also be beneficial, as IC_{50}-curves could be constructed and compared to the ones originating from the cell viability assays. Furthermore, targeting several other biomarkers in the FACS analysis (EdU/EU, for example), may be helpful in order to obtain a more detailed snapshot of the cell cycle and the correspondent cytotoxic effect of the treatments. Moreover, extending the analysis to other techniques as for example IF may give an insight into the physical changes occurring at single cell level. This may include studies on DNA replication and/or transcription, for example.

References

1 F. Mohammad, S. Weissmann, B. Leblanc, D.P. Pandey, J.W. Højfeldt, I. Comet, C. Zheng, J.V. Johansen, N. Rapin, B.T. Porse, A. Tvardovskiy, O.N. Jensen, N.G. Olaciregui, C. Lavarino, M. Suñol, C. de Torres, J. Mora, A.M. Carcaboso and K. Helin, Nat Med 23, 483-492 (2017) doi: 10.1038/nm.4293

2 D. Lubanska and L. Porter, Drugs R D 17, 255-263 (2017) doi: 10.1007/s40268-017-0180-1

3 G.M. Cooper, The Cell: A Molecular Approach, 2nd edn. (Sinauer Associates, 2000).

4 D.P. Clark, N.J. Pazdernik and M.R. McGehee, Molecular Biology, 3rd edn. (Elsevier, 2019).

5 M. Malumbres, Genome Biol 15, 122-122 (2014) doi: 10.1186/gb4184

6 M.C. Casimiro, M. Crosariol, E. Loro, Z. Li and R.G. Pestell, Genes Cancer 3, 649-657 (2012) doi: 10.1177/1947601913479022

7 D.K. Dimova and N.J. Dyson, Oncogene 24, 2810-2826 (2005) doi: 10.1038/sj.onc.1208612

8 C. Giacinti and A. Giordano, Oncogene 25, 5220-5227 (2006) doi: 10.1038/sj.onc.1209615

9 R.V. Lloyd, L.A. Erickson, L. Jin, E. Kulig, X. Qian, J.C. Cheville and B.W. Scheithauer, Am J Pathol 154, 313-323 (1999) doi: 10.1016/S0002-9440(10)65277-7

10 R.A. Sclafani and T.M. Holzen, Annu Rev Genet 41, 237-280 (2007) doi: 10.1146/annurev.genet.41.110306.130308

11 Z.A. Stewart and J.A. Pietenpol, Chemical Research in Toxicology 14, 243-263 (2001) doi: 10.1021/tx000199t

12 D. Deckbar, T. Stiff, B. Koch, C. Reis, M. Löbrich and P.A. Jeggo, Cancer Research 70, 4412 (2010) doi: 10.1158/0008-5472.CAN-09-3198

13 A.N. Kousholt, T. Menzel and C.S. Sørensen, Biomolecules 2, 579-607 (2012) doi: 10.3390/biom2040579

14 U. Kutay and M.W. Hetzer, Current Opinion in Cell Biology 20, 669-677 (2008) doi: https://doi.org/10.1016/j.ceb.2008.09.010

15 M.C. de Gooijer, A. van den Top, I. Bockaj, J.H. Beijnen, T. Würdinger and O. van Tellingen, FEBS Open Bio 7, 439-455 (2017) doi: 10.1002/2211-5463.12206

16 G.R. Stark and W.R. Taylor, in Checkpoint Controls and Cancer. Methods in Molecular Biology, (Human Press, 2004),

17 M.W. Parker, M.R. Botchan and J.M. Berger, Crit Rev Biochem Mol Biol 52, 107-144 (2017) doi: 10.1080/10409238.2016.1274717

18 S. Kang, M.-S. Kang, E. Ryu and K. Myung, Mutation Research/Fundamental and Molecular Mechanisms of Mutagenesis 809, 58-69 (2018) doi: https://doi.org/10.1016/j.mrfmmm.2017.04.002

19 M.L. DePamphilis, Cell Cycle 4, 70-79 (2005) doi: 10.4161/cc.4.1.1333

20 S. Tada, J.P. Chong, H.M. Mahbubani and J.J. Blow, Curr Biol 9, 211-214 (1999) doi: 10.1016/s0960-9822(99)80092-x

21 K. Labib, Genes Dev 24, 1208-1219 (2010) doi: 10.1101/gad.1933010

22 V.Q. Nguyen, C. Co and J.J. Li, Nature 411, 1068-1073 (2001) doi: 10.1038/35082600

23 Y. Kim and E.T. Kipreos, Cell Div 2, 18-18 (2007) doi: 10.1186/1747-1028-2-18

24 Ryan C. Heller, S. Kang, Wendy M. Lam, S. Chen, Clara S. Chan and Stephen P. Bell, Cell 146, 80-91 (2011) doi: https://doi.org/10.1016/j.cell.2011.06.012

25 D. Duzdevich, Megan D. Warner, S. Ticau, Nikola A. Ivica, Stephen P. Bell and Eric C. Greene, Molecular Cell 58, 483-494 (2015) doi: https://doi.org/10.1016/j.molcel.2015.03.017

26 S. Sengupta, F. van Deursen, G. de Piccoli and K. Labib, Current Biology 23, 543-552 (2013) doi: https://doi.org/10.1016/j.cub.2013.02.011

27 Y. Quan, Y. Xia, L. Liu, J. Cui, Z. Li, Q. Cao, Xiaojiang S. Chen, Judith L. Campbell and H. Lou, Cell Reports 13, 2576-2586 (2015) doi: https://doi.org/10.1016/j.celrep.2015.11.018

28 J.H. Lee and J.M. Berger, Genes (Basel) 10, (2019) doi: 10.3390/genes10110859

29 W. Goedecke, in xPharm: The Comprehensive Pharmacology Reference, ed. by S.J. Enna and D.B. Bylund (Elsevier, New York, 2007), p. 1-2

30 J.J. Champoux, Annual Review of Biochemistry 70, 369-413 (2001) doi: 10.1146/annurev.biochem.70.1.369

31 J.V. Walker and J.L. Nitiss, Cancer Invest 20, 570-589 (2002) doi: 10.1081/cnv-120002156
32 T. Brown, in Genomes 4, (Garland Science, New York, 2018),
33 G.A.C. Singer, J. Wu, P. Yan, C. Plass, T.H.M. Huang and R.V. Davuluri, BMC Genomics 9, 349 (2008) doi: 10.1186/1471-2164-9-349
34 R. Carter and G. Drouin, Genomics 94, 388-396 (2009) doi: https://doi.org/10.1016/j.ygeno.2009.08.011
35 A.C. Schier and D.J. Taatjes, Genes Dev 34, 465-488 (2020) doi: 10.1101/gad.335679.119
36 R.D. Martin, T.E. Hébert and J.C. Tanny, Int J Mol Sci 21, 3354 (2020) doi: 10.3390/ijms21093354
37 N. Linzer, A. Trumbull, R. Nar, M.D. Gibbons, D.T. Yu, J. Strouboulis and J. Bungert, Frontiers in Molecular Biosciences 8, (2021) doi: 10.3389/fmolb.2021.681550
38 S.F. Tolić-Nørrelykke, M.B. Rasmussen, F.S. Pavone, K. Berg-Sørensen and L.B. Oddershede, Biophys J 90, 3694-3703 (2006) doi: 10.1529/biophysj.105.074856
39 X. Liu, D.A. Bushnell and R.D. Kornberg, Biochim Biophys Acta 1829, 2-8 (2013) doi: 10.1016/j.bbagrm.2012.09.003
40 K. Kamada, G. Roeder Robert and K. Burley Stephen, Proceedings of the National Academy of Sciences 100, 2296-2299 (2003) doi: 10.1073/pnas.262798199
41 N. Petrenko, Y. Jin, L. Dong, K.H. Wong and K. Struhl, eLife 8, e43654 (2019) doi: 10.7554/eLife.43654
42 F.C. Holstege, U. Fiedler and H.T. Timmers, EMBO J 16, 7468-7480 (1997) doi: 10.1093/emboj/16.24.7468
43 J.K. Rimel and D.J. Taatjes, Protein Sci 27, 1018-1037 (2018) doi: 10.1002/pro.3424
44 B.J. Greber and E. Nogales, Subcell Biochem 93, 143-192 (2019) doi: 10.1007/978-3-030-28151-9_5
45 Z. Zhang and R. Tjian, Transcription 9, 159-165 (2018) doi: 10.1080/21541264.2017.1363017
46 I. Jonkers and J.T. Lis, Nature Reviews Molecular Cell Biology 16, 167-177 (2015) doi: 10.1038/nrm3953
47 C.-H. Wu, Y. Yamaguchi, L.R. Benjamin, M. Horvat-Gordon, J. Washinsky, E. Enerly, J. Larsson, A. Lambertsson, H. Handa and D. Gilmour, Genes & development 17, 1402-1414 (2003) doi: 10.1101/gad.1091403
48 G. Napolitano and A. Ballabio, J Cell Sci 129, 2475-2481 (2016) doi: 10.1242/jcs.146365
49 J.A. Martina, Y. Chen, M. Gucek and R. Puertollano, Autophagy 8, 903-914 (2012) doi: 10.4161/auto.19653
50 B. Kim, I. Nesvizhskii Alexey, P.G. Rani, S. Hahn, R. Aebersold and A. Ranish Jeffrey, Proceedings of the National Academy of Sciences 104, 16068-16073 (2007) doi: 10.1073/pnas.0704573104
51 T. Ishibashi, M. Dangkulwanich, Y. Coello, A. Lionberger Troy, L. Lubkowska, S. Ponticelli Alfred, M. Kashlev and C. Bustamante, Proceedings of the National Academy of Sciences 111, 3419-3424 (2014) doi: 10.1073/pnas.1401611111
52 J.B. Crickard, J. Lee, T.H. Lee and J.C. Reese, Nucleic Acids Res 45, 6362-6374 (2017) doi: 10.1093/nar/gkx220
53 A. Ramanathan, G.B. Robb and S.-H. Chan, Nucleic acids research 44, 7511-7526 (2016) doi: 10.1093/nar/gkw551
54 R. Worch, A. Niedzwiecka, J. Stepinski, C. Mazza, M. Jankowska-Anyszka, E. Darzynkiewicz, S. Cusack and R. Stolarski, RNA 11, 1355-1363 (2005) doi: 10.1261/rna.2850705
55 J.N. Kuehner, E.L. Pearson and C. Moore, Nat Rev Mol Cell Biol 12, 283-294 (2011) doi: 10.1038/nrm3098
56 N.J. Proudfoot, Science 352, aad9926-aad9926 (2016) doi: 10.1126/science.aad9926
57 U. Kühn and E. Wahle, Biochim Biophys Acta 1678, 67-84 (2004) doi: 10.1016/j.bbaexp.2004.03.008
58 P.P. Sarma, D. Dutta, Z. Mirza, K.K. Saikia and B.K. Baishya, Molecular Biology 51, 293-299 (2017) doi: 10.1134/S0026893317020182

59 A.A. Morley and D.R. Turner, Mutat Res 428, 11-15 (1999) doi: 10.1016/s1383-5742(99)00026-5
60 H. Sung, J. Ferlay, R.L. Siegel, M. Laversanne, I. Soerjomataram, A. Jemal and F. Bray, CA: A Cancer Journal for Clinicians 71, 209-249 (2021) doi: https://doi.org/10.3322/caac.21660
61 A.B. Lassman, Current Neurology and Neuroscience Reports 4, 228-233 (2004) doi: 10.1007/s11910-004-0043-3
62 M. Ghosh, S. Shubham, K. Mandal, V. Trivedi, R. Chauhan and S. Naseera, Indian J Cancer 54, 362-367 (2017) doi: 10.4103/ijc.IJC_157_17
63 N. Scholz, K.M. Kurian, F.A. Siebzehnrubl and J.D.F. Licchesi, Frontiers in Oncology 10, (2020) doi: 10.3389/fonc.2020.574011
64 M. Malumbres and M. Barbacid, Nat Rev Cancer 9, 153-166 (2009) doi: 10.1038/nrc2602
65 A. Deshpande, P. Sicinski and P.W. Hinds, Oncogene 24, 2909-2915 (2005) doi: 10.1038/sj.onc.1208618
66 T.J. Gonda and R.G. Ramsay, Nat Rev Cancer 15, 686-694 (2015) doi: 10.1038/nrc4018
67 A. Besson, S.F. Dowdy and J.M. Roberts, Dev Cell 14, 159-169 (2008) doi: 10.1016/j.devcel.2008.01.013
68 S. Vijayaraghavan, S. Moulder, K. Keyomarsi and R.M. Layman, Target Oncol 13, 21-38 (2018) doi: 10.1007/s11523-017-0541-2
69 V. Juric and B. Murphy, Cancer Drug Resistance 3, 48-62 (2020) doi: 10.20517/cdr.2019.105
70 S.A. Greenall, Y.C. Lim, C.B. Mitchell, K.S. Ensbey, B.W. Stringer, A.L. Wilding, G.M. O'Neill, K.L. McDonald, D.J. Gough, B.W. Day and T.G. Johns, Oncogenesis 6, e336 (2017) doi: 10.1038/oncsis.2017.33
71 K. Tamura, Jpn J Clin Oncol 49, 993-998 (2019) doi: 10.1093/jjco/hyz151
72 K.M. Sakamoto, K.B. Kim, A. Kumagai, F. Mercurio, C.M. Crews and R.J. Deshaies, Proceedings of the National Academy of Sciences 98, 8554-8559 (2001) doi: doi:10.1073/pnas.141230798
73 X. Qiu, Y. Li, B. Yu, J. Ren, H. Huang, M. Wang, H. Ding, Z. Li, J. Wang and J. Bian, Eur J Med Chem 211, 113091 (2021) doi: 10.1016/j.ejmech.2020.113091
74 R. Mandal, S. Becker and K. Strebhardt, Cancers 13, (2021) doi: 10.3390/cancers13092181
75 M. Zhang, K. Zhao, X. Xu, Y. Yang, S. Yan, P. Wei, H. Liu, J. Xu, F. Xiao, H. Zhou, X. Yang, N. Huang, J. Liu, K. He, K. Xie, G. Zhang, S. Huang and N. Zhang, Nature Communications 9, 4475 (2018) doi: 10.1038/s41467-018-06862-2
76 T. Fujisawa and P. Filippakopoulos, Nature Reviews Molecular Cell Biology 18, 246-262 (2017) doi: 10.1038/nrm.2016.143
77 H. Yang, L. Wei, Y. Xun, A. Yang and H. You, Mol Ther Oncolytics 21, 1-14 (2021) doi: 10.1016/j.omto.2021.03.005
78 B.P. Lucey, W.A. Nelson-Rees and G.M. Hutchins, Archives of Pathology & Laboratory Medicine 133, 1463-1467 (2009) doi: 10.5858/133.9.1463
79 S.M. Pollard, K. Yoshikawa, I.D. Clarke, D. Danovi, S. Stricker, R. Russell, J. Bayani, R. Head, M. Lee, M. Bernstein, J.A. Squire, A. Smith and P. Dirks, Cell Stem Cell 4, 568-580 (2009) doi: https://doi.org/10.1016/j.stem.2009.03.014
80 D. Guldager Kring Rasmussen and M.A. Karsdal, in Biochemistry of Collagens, Laminins and Elastin, ed. by M.A. Karsdal (Academic Press, 2016), p. 163-196
81 R.A. Meck, A.L. Carsten and J.J. Kelsch, Cancer Res 36, 2317-2320 (1976)
82 O. Alexandru, A. Georgescu, L. Ene, S. Purcaru, F. Serban, A. Popescu, C. Brindusa, L. Tataranu, V. Ciubotaru and A. Dricu, Journal of Cancer Research and Therapeutics 12, 1025-1032 (2016) doi: 10.4103/0973-1482.167609
83 A. Comba, S.M. Faisal, M.L. Varela, T. Hollon, W.N. Al-Holou, Y. Umemura, F.J. Nunez, S. Motsch, M.G. Castro and P.R. Lowenstein, Frontiers in Oncology 11, (2021) doi: 10.3389/fonc.2021.703764
84 N.R. Parker, P. Khong, J.F. Parkinson, V.M. Howell and H.R. Wheeler, Frontiers in Oncology 5, (2015) doi: 10.3389/fonc.2015.00055

85 C.I. Wells, J.D. Vasta, C.R. Corona, J. Wilkinson, C.A. Zimprich, M.R. Ingold, J.E. Pickett, D.H. Drewry, K.M. Pugh, M.K. Schwinn, B. Hwang, H. Zegzouti, K.V.M. Huber, M. Cong, P.L. Meisenheimer, T.M. Willson and M.B. Robers, Nature Communications 11, 2743 (2020) doi: 10.1038/s41467-020-16559-0
86 A.B. Iniguez, B. Stolte, E.J. Wang, A.S. Conway, G. Alexe, N.V. Dharia, N. Kwiatkowski, T. Zhang, B.J. Abraham, J. Mora, P. Kalev, A. Leggett, D. Chowdhury, C.H. Benes, R.A. Young, N.S. Gray and K. Stegmaier, Cancer Cell 33, 202-216.e206 (2018) doi: 10.1016/j.ccell.2017.12.009
87 Z. Fan, R. Devlin Jennifer, J. Hogg Simon, A. Doyle Maria, F. Harrison Paul, I. Todorovski, A. Cluse Leonie, A. Knight Deborah, J. Sandow Jarrod, G. Gregory, A. Fox, H. Beilharz Traude, N. Kwiatkowski, E. Scott Nichollas, T. Vidakovic Ana, P. Kelly Gavin, Q. Svejstrup Jesper, M. Geyer, S. Gray Nathanael, J. Vervoort Stephin and W. Johnstone Ricky, Science Advances 6, eaaz5041 doi: 10.1126/sciadv.aaz5041
88 L.I. Toledo, M. Murga and O. Fernandez-Capetillo, Molecular Oncology 5, 368-373 (2011) doi: https://doi.org/10.1016/j.molonc.2011.07.002
89 S. Liu, Y. Ge, T. Wang, H. Edwards, Q. Ren, Y. Jiang, C. Quan and G. Wang, Oncol Rep 37, 3377-3386 (2017) doi: 10.3892/or.2017.5580
90 A. Mehta, C.U. Awah and A.M. Sonabend, Frontiers in Neurology 9, (2018) doi: 10.3389/fneur.2018.00459
91 M. Bredel, D.M. Scholtens, A.K. Yadav, A.A. Alvarez, J.J. Renfrow, J.P. Chandler, I.L.Y. Yu, M.S. Carro, F. Dai, M.J. Tagge, R. Ferrarese, C. Bredel, H.S. Phillips, P.J. Lukac, P.A. Robe, A. Weyerbrock, H. Vogel, S. Dubner, B. Mobley, X. He, A.C. Scheck, B.I. Sikic, K.D. Aldape, A. Chakravarti and G.R.t. Harsh, N Engl J Med 364, 627-637 (2011) doi: 10.1056/NEJMoa1006312
92 D.V. Titov, B. Gilman, Q.L. He, S. Bhat, W.K. Low, Y. Dang, M. Smeaton, A.L. Demain, P.S. Miller, J.F. Kugel, J.A. Goodrich and J.O. Liu, Nat Chem Biol 7, 182-188 (2011) doi: 10.1038/nchembio.522
93 S. Zhong, Y. Zhang, X. Yin and W. Di, Onco Targets Ther 12, 2137-2147 (2019) doi: 10.2147/OTT.S195655
94 M. Bettencourt-Dias, R. Giet, R. Sinka, A. Mazumdar, W.G. Lock, F. Balloux, P.J. Zafiropoulos, S. Yamaguchi, S. Winter, R.W. Carthew, M. Cooper, D. Jones, L. Frenz and D.M. Glover, Nature 432, 980-987 (2004) doi: 10.1038/nature03160

Appendices

Appendix A; Categorization of human CDK´s and their activators

Table A.1 categorizes the different type of human CDK´s involved in cell cycle regulation and their corresponding cyclin partners. The table is an adaptation from [5].

CDK Type	Cyclin Partner
CDK 1	Cyc A
CDK 2	Cyc B
CDK 3	Cyc E
	Cyc C
CDK 4	Cyc D
CDK 6	
CDK 5	CDK 5R1
CDK 14	CDK 5R2
CDK 15	Cyc D
CDK 16	Cyc Y
CDK 17	
CDK 18	

Table A.2 categorizes the different type of human CDK´s involved in transcription and their corresponding cyclin partners. The table is an adaptation from [5].

CDK Type	Cyclin Partner
CDK 7	Cyc H
CDK 20	Cyc H
CDK 8	Cyc C
CDK 19	
CDK 11	Cyc L
CDK 10	CDK M
CDK 9	CDK T
CDK 12	Cyc K
CDK 13	

Appendix B; Cell cultivation medium and cultivation parameters

Preparation of N2B27 medium

250 ml	1X Dulbecco´s Modified Eagle Medium/nutrient mixture F-12 (DMEM/F-12)	Gibco
250 ml	1X neurobasal medium	Gibco
1 vial	N2 supplement (16 µg putricine dihydrochloride, 6.25 µg insulin, 50 µg apotransferrin, 21.6 ng progesterone in EtOH, 15 nM sodium selenite)	*
1 vial	B27 supplement	*
5 ml	100X penicillin/streptomycin glutamine	Gibco
5 ml	100X glutaMAX	Gibco
5 ml	100X Minimum Essential Medium-Non-Essential Amino Acids	Gibco
5 ml	100 mM sodium pyruvate	Gibco
500 µl	50 mM β-mercaptoethanol	Gibco
5 ml	1 M Hepes	Fisher BioReagents
50 µg	Bovine Serum Albumin (BSA)	Saween&Werner
4 µg	Heparin	Merck Life Science

**Both N2 and B27 were internally elaborated.*

Preparation of NSC medium

The preparation of the NSC medium was performed by the addition of Epidermal Growth Factor (EGF, Preprotech) and Fibroblast Growth Factor-basic (FGFb, Preprotech) to the N2B27 medium to a final concentration of 10 ng/ml. Both growth factors were at initial stock concentration of 50 µg/ml.

Preparation of HeLa medium

The preparation of the HeLa medium, used for HeLa cultivation, was performed by the addition of Foetal Bovine Serum (FBS, SigmaAdrich®) at final concentration of 10 % and 1 % final concentration penicillin-streptomycin (Thermo Fisher Scientific) to high glucose DMEM medium.

Table B.1 shows the parameters used in the cultivation and expansion of G7, G144 and HeLa cells. The volumetric quantities for the coating procedure as well as the addition of the corresponding medium and usage of TrypLE and PBS+TI are defined regarding the size of the plate being employed. Note! Coating does not apply for HeLa cells.

Size	**Coating, ml**	**Medium, ml**	**TrypLE, ml**	**PBS+TI, ml**	**Cells seeded, 10^6**
Tray	50	80-120	8	40	10-20
15 cm	8-12	16-25	1.5	8-12	2-10
10 cm	4-6	7-12	1	4-9	1-5
6 cm	1.5-3	3-5	0.35	1-4	0.2-1
6-well*	0.8-1.5	1.5-3	0.2	1	0.05-0.5
12-well*	0.5-1	0.5-2	0.1	1	0.02-0.2
24-well*	0.3-1	0.5-1.2	0.050	1	0.01-0.1
96-well*	0.05	0.05	NA	NA	0.003-0.01

**The volumes described apply per well.*

Appendix C; Parameters for the pharmacological treatments

Table C.1 illustrates the first set up for the drug treatments performed in the study. Three different drugs were tested in one 96-well plate containing the same cell culture, thus either G7, G144 or HeLa. The final volume per well was set up to 100 µl, thus 50 µl cell culture and 50 µl drug solution. Eight dilutions with three replicates per dilution were tested, with the highest (H) being 10 µM and the lowest (L) being 0.005 µM. 0.1 % DMSO was used as control (C) and pure medium as blank (B).

Drug / Dilution	Drug A			C	Drug B			C	Drug C			B
1 (H)												
2												
3												
4												
5												
6												
7												
8 (L)												

Table C.2 illustrates the second set up for the drug treatments performed in the study. Each drug was tested in two 6-well plates containing the same cell culture, thus either G7, G144 or HeLa. The final volume per well was set up to 2 ml, thus 1 ml cell culture and 1 ml drug solution. Five dilutions with two replicates per dilution were tested, with the highest being 2 µM and the lowest being 0.1 µM. 0.04 % DMSO was used as control (C).

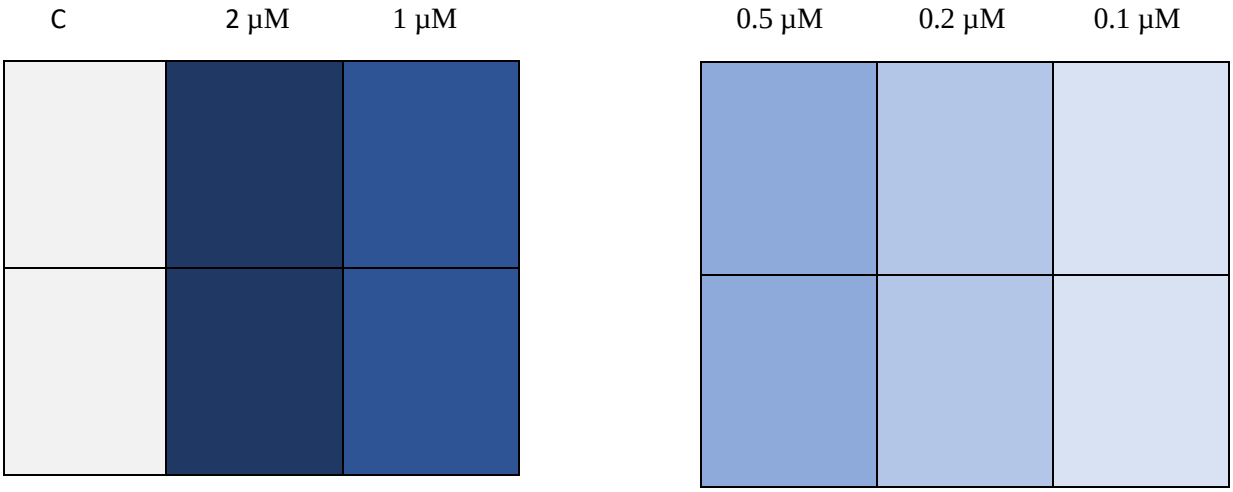

Table C.3 illustrates the third set up for the drug treatments performed in the study. Each drug was tested in two 6-well plates containing the same cell culture with different treatment times, these being 6 and 24 h. Only G144 cells were tested in this experiment. The final volume per well was set up to 2 ml, thus 1 ml cell culture and 1 ml drug solution. Two dilutions with two replicates per dilution were tested, with the highest being 3 µM and the lowest being 1 µM. 0.06 % DMSO was used as control (C).

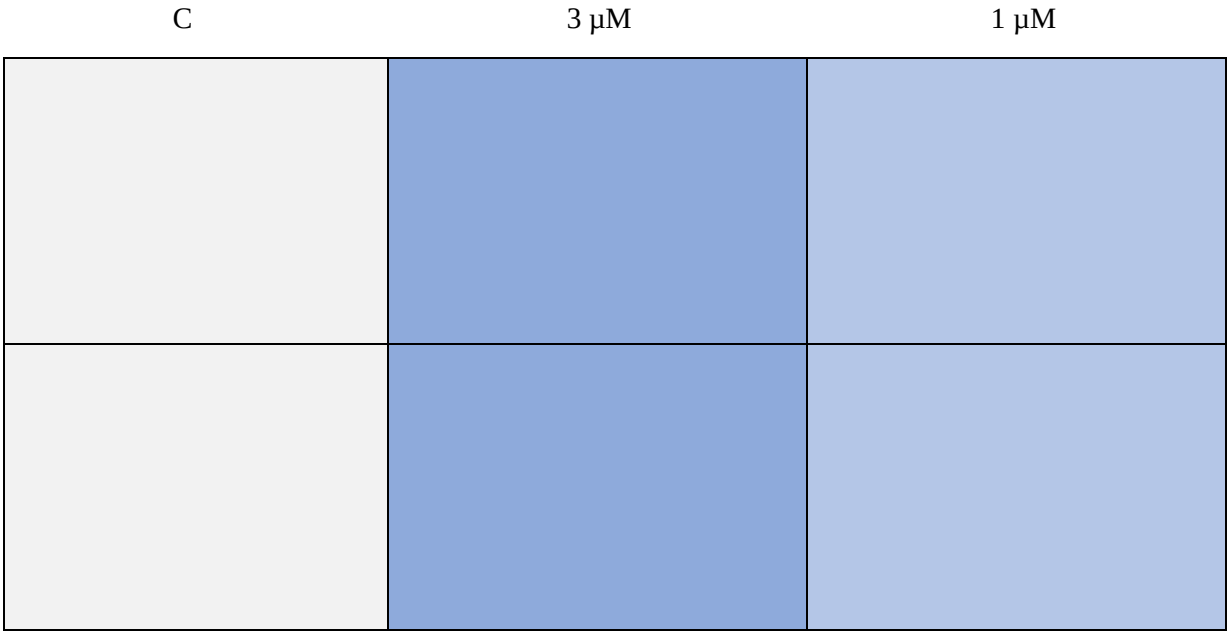

Norges miljø- og biovitenskapelige universitet
Noregs miljø- og biovitskapelege universitet
Norwegian University of Life Sciences

Postboks 5003
NO-1432 Ås
Norway